Model-based Active Control of Thermoacoustic Instability in Continuous Combustion Processes

by

Jennifer Weerts Rumsey

B.S., Mechanical Engineering
Purdue University, 1996

Submitted to the Department of Mechanical Engineering
in partial fulfillment of the requirements for the degree of

Master of Science in Mechanical Engineering

at the

Massachusetts Institute of Technology

June 1998

Author .....
Department of Mechanical Engineering
May 14, 1998

Certified by .....
Anuradha M. Annaswamy
Associate Professor of Mechanical Engineering
Thesis Supervisor

Accepted by ..
Ain A. Sonin
Chairman, Department Committee on Graduate Students

Model-based Active Control of Thermoacoustic Instability in Continuous Combustion Processes

by

Jennifer Weerts Rumsey

Submitted to the Department of Mechanical Engineering
on May 14, 1998, in partial fulfillment of the
requirements for the degree of
Master of Science in Mechanical Engineering

Abstract

Thermoacoustic instability is frequently found in continuous combustion processes in propulsion, power generation, and heating. Active control has been increasingly pursued in recent years to suppress the pressure oscillations which result from this instability, while maintaining performance objectives such as low NO_x emission and high efficiency. This thesis considers the physics behind the thermoacoustic instability and utilizes a model based on the physics to understand the problem and design an active controller to suppress the instability. A one-dimensional, laminar combustor is modeled and a 1 kW bench-top combustor rig constructed for experimental validation of simulation results. The model considers the linear acoustic and flame dynamics, acoustic mode coupling, and actuator dynamics. Several model-based control designs including proportional, phase-lead, and LQG are presented and tested on the bench-top combustor using a 0.2 W loudspeaker as an actuator. Results show that the model-based controllers are effective in suppressing the instability, and that the simulation results accurately predict the response of the real system. Using the LQG controller, a settling time of as low as 23 milliseconds was obtained, significantly faster than those reported on similar setups. The nonlinear dynamics which leads to the limit-cycle behavior in real systems are investigated by looking at several "black-box" type models of nonlinear behavior. The performance of the linear controllers on the nonlinear models is investigated and an explanation for their success given.

Thesis Supervisor: Anuradha M. Annaswamy
Title: Associate Professor of Mechanical Engineering

Acknowledgments

There are many people who have touched my life, who have helped shape me into the person I have become and will become. The foundation of my life is Jesus Christ and I thank God for the many blessing he has given me.

This work would not be possible without Professor Anu Annaswamy's guidance and support. I thank her for allowing me to be a part of this exciting project and for her advice on both my graduate work and personal development. Thank you also to the National Science Foundation for their financial support of my master's work through a graduate fellowship. A special thanks goes to the rest of the thermoacoustic instability group here at MIT - Professor Ahmed Ghoniem, Mahmoud Fleifil, and Jean-Pierre Hathout for their contributions to this work and advice through the many challenges I faced.

I would like to express my gratidue to all the Professors both here at MIT and at Purdue for the knowledge they have passed on to me and for their inspiration in the classroom, especially Dr. Amar Bose, Professor Jim Jones, and Professor H. Doyle Thompson. I would also like to thank Mike, Travis, and Pat for being the best study partners anyone could ask for. You not only forced me to perform at my highest level while at Purdue, but you made it fun (most of the time). I would not be where I am today without the mentorship of John Wall. Thank you John for your professional and personal advice. Your encouragement to pursue mechanical engineering, come to MIT, and believe in myself has had more influence in my life than you could possibly know.

Last, but not least I would like to thank my family for their love and support. Thanks Mom for raising me to know no limits on what I can do and for being the best mother anyone could ask for. I would especially like to thank my husband Jim for moving to Boston so I could come to MIT, for putting up with my complaints and cheering me up when I was down, and for encouraging me to pursue my dreams.

Contents

List of Figures

List of Tables

Chapter 1

Introduction

Thermoacoustic instability is a common problem in continuous combustion processes. Applications in which it can be found include gas turbine engines, boilers, and waste incinerators. This instability, which results from the interaction between the acoustic process and the combustion process, appears as large amplitude pressure oscillations. These pressure oscillations are detrimental to many of the systems in which they occur, causing high levels of acoustic noise, high burn rates, and mechanical failures. Efforts to combat the instability have increased in recent years as a result of the growing desire to lower NO_x formation, decrease thermal output and improve efficiency. Attempts to achieve these goals inevitably exacerbate the instability.

Thermoacoustic instability was first discovered in the 19^{th} century when several independent studies revealed that sound could be generated by a flame placed inside a large tube. This came to be known as the "dancing" or "singing" flame. The theory that this growing pressure oscillation was caused by an interaction between the heat release rate and the pressure was originally hypothesized by Rayleigh [1]. Rayleigh's criterion is the basis for many explanations of thermoacoustic instability .

Most of the past attempts to suppress the oscillations involved the use of hardware. Methods such as changing the fuel delivery system, changing the fuel injection distribution pattern, modifications to the combustor or the geometry of the combustor, acoustic damping liners, and baffles have all been attempted. These methods are costly and time consuming, however, and there is no guarantee that they will

work under changing operating conditions. Recently, the focus has shifted towards active control or the continuous perturbation of combustion parameters to interrupt the pressure growth and eliminate the instability [2]. Active control has become more feasible in recent years due to the fact that actuators and sensors which are fast, accurate, reliable, and cost effective have become prevalent. Actuators including acoustic drivers such as loudspeakers and air- or fuel- modulators for fuel injectors that introduce secondary fuel streams are utilized. Microphones, flow meters, and photomultipliers are used as sensors to collect information on the pressure, velocity, and heat release [3]. An additional advantage of active control is that it consumes only a small fraction of the power generated by the system. The control objectives include pressure stabilization, high efficiency operation, increased thermal output, and low NO_x formation.

Active controllers generally fall into one of two categories: those based on experimental control strategies and those based on theoretical models. Examples of the first category include [4]-[10], all of which successfully suppress the dominant pressure instability. These approaches typically involve the use of an analog circuit comprised of a filter and a phase-shifter. The parameters are tuned by trial and error until the dominant instability is suppressed. This often results in the excitation of other pressure instabilities at different frequencies. These secondary peaks are due to the controller design, which considers only the dominant unstable mode in the system, and occur at frequencies other than the natural modes of the system [19]. For example, in [7], two experimental controllers are used in an attempt to stabilize the thermoacoustic instability in a one-dimensional premixed methane-air combustor. The first controller consists of an amplifier, a phase-shifter, and an 8^{th} order butterworth filter. The second controller combines the first controller with a notch filter and a lead compensater. Both result in a reduction of the dominant instability, however, an instability is excited at two new frequencies. Another problem with these controllers is that the dominant instability can only be reduced for flow rates in the range of 200 to 330 milliliters per second.

Examples of the second category include [5, 9], [12]-[15]. For this category, the fun-

damental laws that govern the behavior of the thermal acoustics in the combustor are utilized. Using this method, the combustor behavior can be analyzed and predicted as parameters change. In [5], while a model-based controller is discussed, the analysis was limited to only one frequency, the unstable one. In [12], an input-output system identification approach is used to determine the model and the μ-synthesis method is employed for control. In [13] -[15], the authors have used physical law-based models and a control design based on this model and drawn from modern control theory.

Until recently, a model which represents the combustion process and the interaction of all of the subsystems present did not exist. A physically-based finite-dimensional model of a continuous combustion process has been developed at MIT in [19],[16]-[11]. This model is based on one-dimensional laminar flow, an anchored flame with a concentrated heat release zone, and a loudspeaker as an actuator. In [11], a dynamic model is derived for the flame relating the unsteady heat release rate and the unsteady velocity components. In [16], it is shown that the modal amplitudes of the unforced wave equation become coupled when a heat source and an active control source are present, and affect each other. This coupling is shown to have an impact on a successful active control design in that when it is neglected in the model for certain actuator-sensor locations, the controller fails to suppress the thermoacoustic instability. In [19], an analytical explanation for the secondary peaks that occur in the experimental investigations of active control is given. In particular, it is shown that the peaks arise due to the interaction between subsystems in combustors and controllers at frequencies other than the range where thermoacoustic resonance occurs. In [18], the same dynamic model developed under nominal conditions is used to design a model-based control using an LQG-strategy and leads to an improved performance in simulation over existing experimental and model-based results. The goal in this thesis is to not only develop a model which accurately represents the combustion process, but also to show that using a model-based approach for control design will lead to a more robust controller with superior performance and a wider operating range than those designed using experimental control strategies. This will be shown both theoretically through simulations and experimentally with a bench-top

combustor rig.

The MIT model for premixed laminar combustion considers only the linear dynamics of the flame and the acoustics. Clearly, in real systems nonlinearities are present, and these nonlinearities result in the limit-cycle behavior which is observed. Mechanisms in the combustion process that may be responsible for the nonlinear behavior are numerous, highly coupled, and difficult to model analytically using low-order dynamic models. The flame dynamics appears to be the dominant factor in producing the limit-cycle effect, although nonlinearities occur in the acoustic subsystem as well. Even the nonlinearities in the heat-release dynamics are complex, however, given the multiple scales of fluctuations due to the convective pressure and velocity fields, vortex-shedding mechanisms, and the coupling present between the acoustics and heat-release.

Nonlinear models of limit-cycles in thermoacoustic instability have been discussed in [20]-[23]. In [20], the complete partial differential equations describing the acoustics as well as the heat release dynamics with the flame anchored using a perforated disk are shown to result in limit-cycles through numerical studies. In [21], nonlinear acoustic components are included in the model, and are shown to lead to limit-cycles using numerical studies of the time-averaged dynamics of the combustion dynamics. In [22], limit-cycles are shown to occur by including a saturation-type nonlinearity in the heat release dynamics. In [23], the linear heat release dynamic model from [17] is expanded to include mixing dynamics and convective time-delay and is shown numerically to exhibit limit-cycles.

In this thesis, a class of low-order, "black-box" finite dimensional nonlinear models of thermoacoustic instability that are capable of exhibiting limit-cycles are developed and their behavior verified through analytical, numerical, and experimental investigations. The advantage of the approach taken here is that it results in a relatively low-order, simple nonlinear model which not only predicts the limit-cycle behavior, but allows straight-forward control design to be carried out. The class of nonlinear models proposed in this thesis is constructed by the inclusion of a single nonlinearity in the linear model suggested in [24]. This nonlinearity is incorporated in the heat re-

lease dynamics and can belong to one of three different types, (i) a phase change, (ii) a gain-change, or (iii) a combination of phase and gain changes, between the input and output. The resulting finite-dimensional nonlinear model is analyzed using describing functions and show that all three types of nonlinearities result in limit-cycles. Class (i) arises due to changes in the flame kinematics (as suggested in [20]), class (ii) may occur due to saturation effects (as proposed in [22]), where as class (iii) may be due to mixing and time-delay (as shown in [23]). The model predictions using a two-mode acoustic model are shown to match experimental results of a bench-top combustor rig, as well as simulations of the complete partial differential equation (PDE) model, quite well.

It is also shown in this thesis that a linear controller designed based solely on the linear dynamics can still be successful in suppressing the thermoacoustic instability even in the presence of these nonlinearities, under certain conditions. Linear control of pressure oscillations with limit-cycles has been addressed in [14], where numerical studies of the time-averaged combustion dynamics are presented. The result in [14], however, does not address whether the proposed linear controller will succeed or fail in suppressing the limit-cycle behavior. In contrast, the stability properties of a linear controller will be discussed in this thesis. The analysis presented is verified by the linear-model based control design which is successfully implemented in simulations of the nonlinear models and experimentally on a bench-top combustor rig.

In this work, the model-based approach of suppressing the thermoacoustic instability will be verified. Chapter 2 describes the theory behind this model-based approach. The model of the combustion process which was developed at MIT will be outlined. The modern control theory which was utilized in the controller design will also be discussed. In chapter 3 the experimental setup which is used to verify the model capabilities will be described. This includes a detailed description of the combustor, the actuator, and the data aquisition system. Chapter 4 will outline the simulation results obtained using the model and the corresponding results of the experiments on the bench-top combustor at MIT. The robustness of the model to uncertainties will also be presented and the effect of considering multiple acoustic

modes and mode coupling in the model will be analyzed. Low-order "black-box" type nonlinear models which give the limit-cycle behavior will be presented in Chapter 5. These models will be used to show that a linear controller designed based on only linear dynamics can still be successful in suppressing the thermoacoustic instability in the presence of the nonlinearities which lead to the limit-cycle behavior and an explanation for this will be given. A discussion of results, including the implications of the results and a comparison to other work will be completed in Chapter 6.

Chapter 2

Theoretical Framework

2.1 A Finite-Dimension Model of the Combustor

A dynamic, finite dimensional model has been developed which represents the dominant characteristics of the combustion instability. This model was used as the basis for designing control strategies for the experimental combustor. A summary of the model is given in this section. See References [11][16]-[19]. for details of the model derivation.

Two subprocesses, acoustics and combustion, couple with each other through feedback and result in the thermoacoustic instability. The total heat release rate at the flame location affects the acoustic dynamics and thus the unsteady pressure. At the same time, the flow velocity affects the flame dynamics and thus the heat release rate, leading to coupling of the two subprocesses. The governing equations of the system are partial differential equations.

The acoustic dynamics of the combustion system can be derived starting from the conservation equations. Assuming negligible transport processes and one dimensional flow, the conservation equations of the mass, momentum, and energy can be written as

$$\frac{\partial p}{\partial t} + \frac{\partial (\rho u)}{\partial x} = 0 \tag{2.1}$$

$$\rho\frac{\partial u}{\partial t}+\rho u\frac{\partial u}{\partial x}+\frac{\partial p}{\partial t} = 0 \quad (2.2)$$

$$\frac{\partial p}{\partial t}+u\frac{\partial p}{\partial x}+\gamma p\frac{\partial u}{\partial x} = (\gamma-1)q \quad (2.3)$$

where ρ, u, p, and q refer to the density, velocity, pressure, and heat release rate, respectively, and γ is the specific heat ratio.

These conservation equations are further simplified by assuming that the gases on both sides of the combustion zone behave as an ideal gas, separating the variables into their mean and perturbed components, and assuming that the flame zone is localized spatially at $x = x_f$. Mean heat was considered in the model of the system, but the average values of u, p, ρ, and M, the Mach number, were used in the calculations for simplification. A side-mounted loudspeaker was considered as an actuator and introduces a dynamic effect on the acoustic field. A schematic of the combustor with a side-mounted loudspeaker is shown in Figure 2-1. Including the effect of the loudspeaker with x_a the location of the loudspeaker, and v_c the velocity of the diaphragm of the loudspeaker, the representation of the acoustic dynamics was the following:

$$\left(\frac{\partial^2 p'}{\partial t^2}+2\overline{M}\bar{c}\frac{\partial^2 p'}{\partial x\partial t}-\bar{c}^2\frac{\partial^2 p'}{\partial x^2}\right) = (\gamma-1)\left(\frac{\partial q'_f}{\partial t}+\overline{M}\bar{c}\frac{\partial q'_f}{\partial x}\right)+\gamma\bar{p}\left(\alpha_r\frac{\partial v_c}{\partial t}\right) \quad (2.4)$$

$$\frac{\partial p'}{\partial t}+\overline{M}\bar{c}\frac{\partial p'}{\partial x}+\gamma\bar{p}\frac{\partial u'}{\partial x} = (\gamma-1)q'_f+\gamma\bar{p}\alpha_r v_c. \quad (2.5)$$

where p', u', and q'_f denote the unsteady components of the pressure, velocity, and heat release rate, respectively, $\bar{p}$ is the mean pressure, $\bar{c}$ is the average speed of sound in air, γ is the specific heat ratio, and α_r is the ratio of cross-sectional areas of the loudspeaker and the combustor (see [16, 19] for details).

A model of the premixed laminar flame was derived considering the flame as a surface across which reactants are converted into products. The flame responds to changes in velocity. If $\xi(r,t)$ is the axial displacement of the flame surface, its dynamic

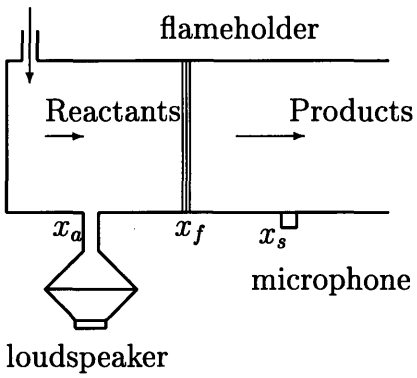

Figure 2-1: Schematic of the combustor with a side-mounted loudspeaker.

response can be characterized as

$$\frac{\partial \xi}{\partial t} = u - v\frac{\partial \xi}{\partial r} - S_u\sqrt{\left(\frac{\partial \xi}{\partial r}\right)^2 + 1}, \qquad A_f = 2\pi \int_0^R \left(r\sqrt{\left(\frac{\partial \xi}{\partial r}\right)^2 + 1} \right) dr \quad (2.6)$$

where u and v are fluid velocities in the axial and radial directions, respectively, S_u is the laminar burning velocity with respect to reactants, and A_f is the flame surface area. Assuming that the heat release rate is proportional to the area of the flame surface, a linearized form of (2.6) can be derived when the heat release zone is localized at $x = x_f$, as described in [11]

$$\dot{q}'_f = -w_f\left(q'_f + g_f u'_f\right) \quad (2.7)$$

$$\omega_f = \left(\frac{4S_u}{\epsilon d_p}\right) \qquad \text{and} \qquad g_f = \left(\frac{\epsilon d_p}{D}\right)^2 n_f \rho_u \Delta q_r,$$

where q'_f and u'_f are the heat release rate and flow velocity at $x = x_f$, respectively, Δq_r is the heat release rate per unit mass of the mixture, ρ_u is the density of the premixed reactants, D is the diameter of the flameholder, n_f is the number of perforations in the flameholder, and ϵd_p is the diameter of the flame with d_p representing the diameter of the perforation and ϵ representing the increase in the flame base from the hole diameter due to entrainment from the neighboring holes.

The distributed system defined by Eqs. (2.4), (2.5), and (2.7) can be approximated

using a Rayleigh-Ritz modal expansion

$$p'(x,t) = \overline{p}\sum_{i=1}^{n}\psi_i(x)\eta_i(t) \tag{2.8}$$

where $\psi_i(x) = \sin(k_i x + \phi_{i0})$ and k_i and ϕ_{i0} are determined by the boundary conditions, and correspond to the spatial mode shapes, and k_i are the wave numbers.

The analysis of the combustion system leads to the following finite-dimensional model for a side-mounted loudspeaker and a microphone as the actuator-sensor pair:

$$\ddot{\eta}_i + \overline{M}\zeta\omega_i\,\dot{\eta}_i + \omega_i^2\eta_i = b_i\,\dot{q}'_f - b_i\overline{M}\omega_i R_o q'_f + b_{c_i}\,\dot{v}_c, \tag{2.9}$$

$$\tilde{u}'_f = \sum_{i=1}^{n}(c_i\,\dot{\eta}_i - c_{ui}\eta_i) + k_{ao}\alpha_r v_c, \tag{2.10}$$

$$\dot{q}'_f + b_f q'_f = \omega_f g_f \tilde{u}'_f, \tag{2.11}$$

$$y = \sum_{i=1}^{n} c_{c_i}\eta_i \tag{2.12}$$

where $b_f = \omega_f(1 - \theta a_0 g_f)$ is the effective flame bandwidth,

$$b_i = \frac{\gamma a_0}{E}\psi_i(x_f), \quad c_i = \frac{1}{\gamma k_i^2}\frac{d\psi_i}{dx}(x_f),$$

$$b_{c_i} = \frac{\gamma}{E}\alpha_r\psi_i(x_a), \quad c_{c_i} = \psi_i(x_s),$$

$$E = \int_0^L \psi_i^2 dx, \quad \omega_f = \frac{4S_u}{d_p}, \quad g_f = \left(\frac{\epsilon d_p}{D}\right)^2 n_f\rho_u\Delta q_r, \quad b_f = \omega_f(1-\theta a_0 g_f),$$

$$a_o = \frac{\gamma - 1}{\gamma\overline{p}}, \quad c_u i = \frac{d\psi_i}{dx}(x_f)(\lambda k_i^2)^{-1}\overline{M}r_1,$$

$$R_o = \frac{\frac{d\psi_i}{dx}(x_f)}{k\psi(x_f)}, \quad R_1 = \frac{1}{R_o},$$

$k_{ao} = 1$ if $x_a < x_f$ and 0 otherwise, x_s and x_a are the location of the microphone and loudspeaker, and y denotes the normalized unsteady pressure, i.e., $y = p'(x_s,t)/\overline{p}$. In transfer function format, this system of equations can be written as

$$y = W(s)\,\dot{v}_c, \qquad W(s) = \frac{n(s)}{d(s)} \tag{2.13}$$

where $W(s)$ is the open-loop transfer function which represents the complete com-

bustor, including laminar flame kinematics and multiple acoustic modes.

An examination of $W(s)$ reveals that it is a $(2n+1)$th order system, where n is the number of acoustic modes included in the model, and can be unstable and nonminimum phase. The system responds over a wide range of frequencies, due to the flame dynamics at low frequencies and due to the acoustics at higher frequencies. The nature of the feedback interaction between acoustics and the heat release rate results in a tight coupling between the flame dynamics and acoustics as well as among the various acoustic modes themselves. The relative degree of $W(s)$, for a side-mounted loudspeaker, is two. The pole-zero locations depend on a number of system parameters including the locations of the actuator, the sensor, as well as the flame. This can be seen from the structure of $d(s)$ and $n(s)$ which are given below for $n = 2$:

$$\begin{aligned} n(s) &= c_{c1}\left\{b_{c1}\left[(s+b_f)(s^2+{\omega_2}^2)-\beta'_{22}s^2\right]+\tilde{b}_{c2}\beta'_{12}s^2+\omega_f g_f k_{a0}k_a A_r\tilde{b}_1(s^2+{\omega_2}^2)\right\} \\ &\quad +c_{c2}\left\{b_{c2}\left[(s+b_f)(s^2+{\omega_1}^2)-\beta'_{11}s^2\right]+\tilde{b}_{c1}\beta'_{21}s^2+\omega_f g_f k_{a0}k_a A_r\tilde{b}_2(s^2+{\omega_1}^2)\right\} \\ d(s) &= (s+b_f)(s^2+{\omega_1}^2)(s^2+{\omega_2}^2)-\beta'_{11}s^2(s^2+{\omega_2}^2)-\beta'_{22}s^2(s^2+{\omega_1}^2). \end{aligned}$$

where

$$\beta_{ii} = \frac{\psi_i(x_f)\dfrac{d\psi_i}{dx}(x_f)}{k_i^2\displaystyle\int_0^L \psi_i^2(\xi)d\xi}, \qquad \beta'_{ii} = g_f\beta_{ii}.$$

This model can be utilized to determine the stability of a given combustion system. It also serves as the tool for using a model-based approach to the control design.

2.2 Actuator and Sensor Dynamics

One can characterize the dynamic relation between the voltage into the loudspeaker, v, and the diaphragm acceleration as

$$\dot{v}_c = G_l(s)v, \qquad G_l(s) = \frac{k_1 s^2}{m_l s^2 + b_l s + k_l}, \tag{2.14}$$

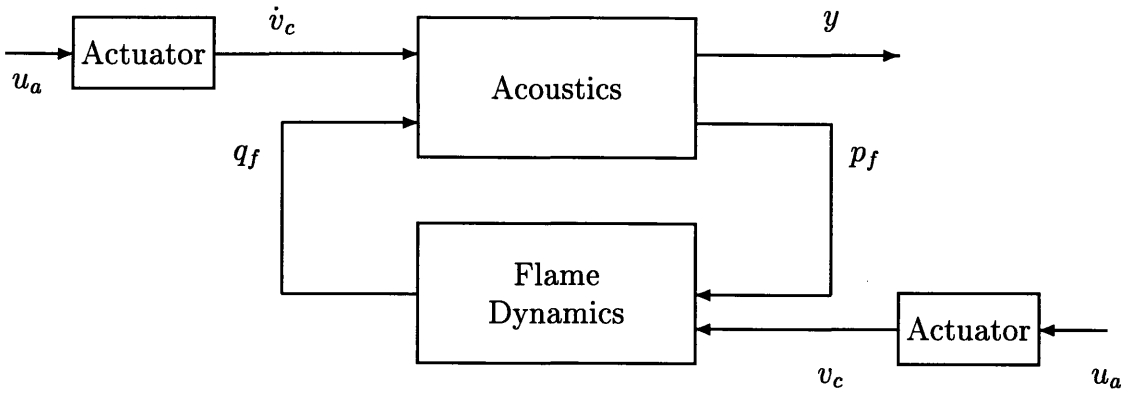

Figure 2-2: A schematic of the input-output model.

where m_l, b_l, and k_l represent the mass, friction, and stiffness properties, respectively, of the loudspeaker, and k_1 is a calibration gain. Additional dynamics can arise from the housing used to focus the acoustics of the loudspeaker onto the combustor, such as a funnel or a waveguide [10]. This housing typically encloses some volume and can act as a Helmholtz resonator with a certain damping and resonant frequency which could overlap with the acoustic range of the combustor, making the task of designing a controller more difficult. It may be important to design this housing so as to ensure minimal attenuation and minimize the introduction of additional dynamics. If the frequency of the loudspeaker dynamics is of the order of the acoustic modes, then the dynamics are significant enough that they must be taken into account in the model. If the frequency is not on the order of the acoustic modes, then the loudspeaker can be modeled simply as a gain.

Including the effect of the actuator dynamics into the combustor model, the open-loop transfer function is of the form

$$y = G_l(s)W(s)i \tag{2.15}$$

which is of order $2n+3$, is unstable and possibly nonminimum phase, and needs to be stabilized using an active controller. A schematic of the complete combustion system is shown in Figure 2-2.

The microphone, which was used as a sensor, typically exhibits a linear output

over a large range of frequencies. For this reason, the microphone could be modeled as a simple gain.

2.3 A Linear Quadratic Gaussian Controller

The linear quadratic gaussian (LQG) is a form of optimal control whose goal is to minimize some performance index. This controller determines the control input into the finite-dimensional linear system while optimizing a cost function which is quadratic in the system states and control inputs. The LQG control design has been analyzed and successfully used in a range of applications for decades. A brief summary of this optimal controller will be given below. For more details refer to [25]-[26].

The goal of the LQG is to determine the control input u into a system in state-space format:

$$\dot{x} = Ax + Bu, \qquad y = Cx$$

where x represents the states of the system and y represents the outputs of the system that can be measured. LQG varies from a linear quadratic regulator (LQR) in that no all states of the system can be measured, and the design of a state estimator of the following form is required

$$\begin{aligned} \dot{\hat{x}} &= A\hat{x} + Bu + H\left(y - C\hat{x}\right) \\ u &= -K\hat{x} \end{aligned}$$

with $(A-BK)$ controllable and $(A-HC)$ observable. Once the eigenvalues of $A-BK$ and $A-HC$ of the closed-loop system are specified, K and H can be designed easily. The LQG is an optimal control strategy which leads to a natural specification of K and H. K can be determined using a cost function

$$J = \int_0^\infty (y^T Q y + u^T R u) dt \tag{2.16}$$

where Q and R represent matrices that weight the various outputs and inputs appropriately. One choice is to set $Q = I$ and $R = \lambda I$ so that λ is a scaling factor that determines the trade-off between fast transients and magnitude of the control input. This yields a solution

$$K = R^{-1}B^T P$$

where P is the solution of the Riccati equation

$$A^T P + PA + C^T C - PBR^{-1}B^T P = 0.$$

The choice of H in (i) can also be made in a similar manner, by posing the problem as the design of a Kalman filter which ensures that $\hat{x}$ converges to x as efficiently as possible. By introducing a fictitious input noise with a variance I and an output noise with a variance R_f, the solution is of the form [25, 26]

$$H = {R_f}^{-1}C^T P_f$$

where

$$P_f A^T + AP_f + BB^T - P_f C^T {R_f}^{-1} C = 0.$$

One can use the MATLAB Control Systems Toolbox to compute G and H efficiently, by choosing $R_f = \mu I$ and fine-tuning λ and μ to allow fast transients to be achieved without unrealistic or undesirable cost. The added benefit of the LQG controller is that it will not only suppress the oscillations at the unstable frequency, but is designed to suppress oscillations over the entire range of frequencies which are considered in the model.

Chapter 3

Experimental Setup

Given that a continuous combustion process is exceedingly complex and the result of several interacting subprocesses, the experimental setup had to be carefully designed so that it duplicated the specific combustion process which the model represents. At the same time, the setup had to be complex enough to exhibit a sufficiently high degree of instability for a number of operating conditions and also represent a premixed laminar combustor with a concentrated heat release zone. First, the geometry had to be selected so that the flow was predominantly one-dimensional and laminar. The geometry was chosen similar to that of combustors tested by Poinsot [6] and Gulati and Mani [8], so that comparisons could be made. Second, it had to be ensured that a premixed flame with good mixing was present. To accomplish this, fuel and air were mixed in a sudden expansion pipe before entering the combustion chamber and a nozzle was used for enhancing mixing between fuel and air. A mechanism had to be chosen for stabilizing the flame and to provide a range of operation where there is no flame extinction or separation. The material for the combustion chamber had to be appropriately chosen so that it could withstand heat and accommodate input/output ports for monitoring and control. A cooling system had to be integrated into the setup. The experimental design also needed to include supplies of air and fuel that could be regulated.

Another factor that had to be addressed was the issue of safety. Given the use of flammable liquids and an open flame, it had to be ensured that both ignition and

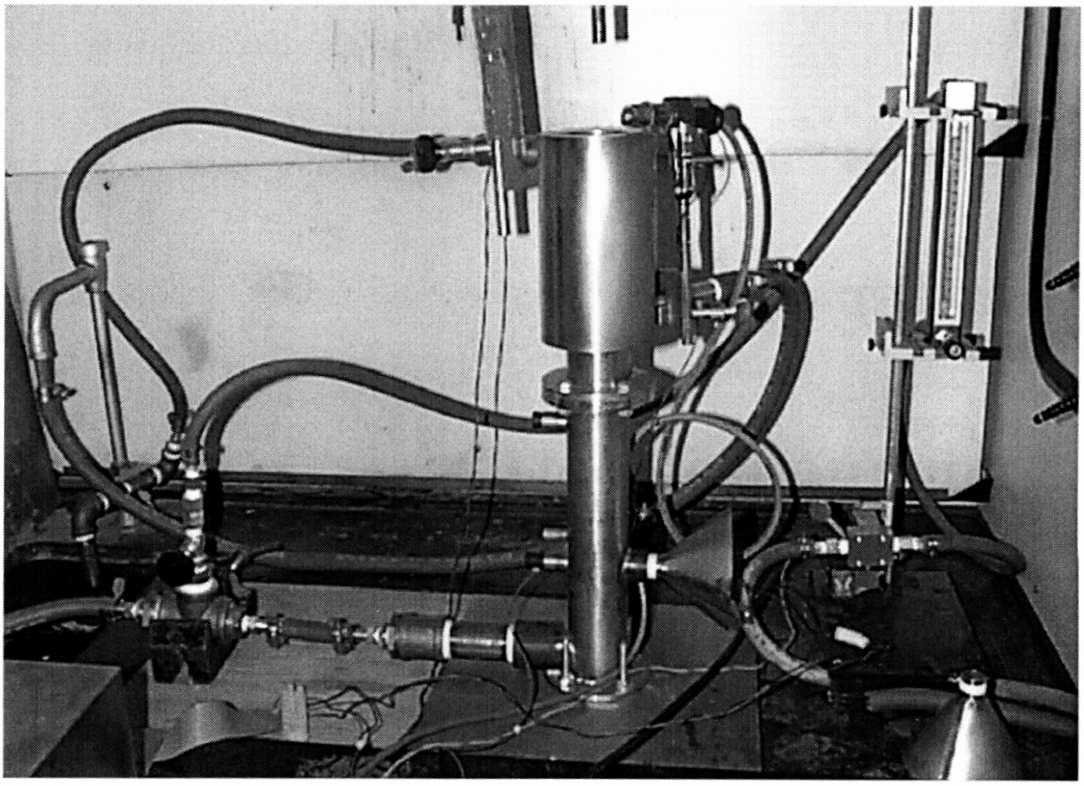

Figure 3-1: The Bench-top combustor rig.

extinction of the flame did not pose any hazards.

A bench-top combustor which met the above requirements was constructed to verify experimentally the simulation results for the combustion model. The experimental setup consists of a test-rig for the combustion process, a calibrated microphone for measuring the pressure, a 0.2 W Radio Shack loudspeaker driver to use as an actuator, two type K Omega thermocouples, a Keithley MetraByte data acquisition and control board, and a Pentium PC. A circuit that includes a spark plug and a battery is used to ensure automatic ignition and another which includes a photo-sensor and a relay was designed to shut off fuel supply in the face of flame extinction. A photograph and a schematic of the system are shown in Figures 3-1 and 3-2.

3.1 The Combustor

The combustion test-rig provides one-dimensional, laminar, premixed flow, as considered in the model. Air is supplied through a low-noise blower and is dehumidified by

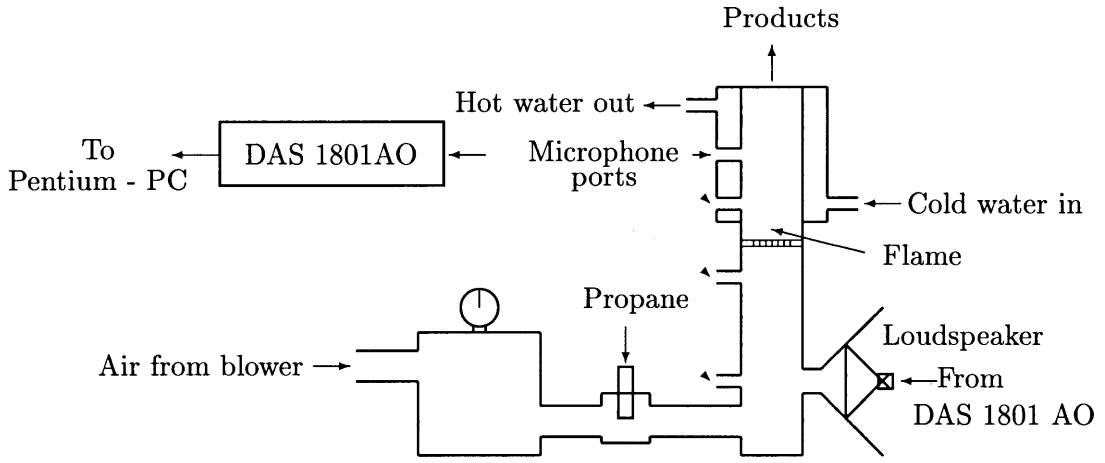

Figure 3-2: Schematic of the combustor test-rig, data-acquisition, and control.

passing it through a desiccant. This may be necessary in humid conditions to prevent the failure of the microphone, depending on the type of microphone being used. The air is then passed through a settling chamber and the flow rate is regulated using an Omega flowmeter. Propane is utilized as a fuel and is supplied through a pressure regulator and a rotameter used for adjusting the fuel flow rate. A nozzle enhances mixing between the fuel and air. The combustion chamber is a 5.3-cm diameter, 47-cm long tube closed at the upstream end and open at the downstream end. The flame is anchored on a perforated disc with 80 holes fixed 26-cm from the upstream end. A cooling jacket around the hot section of the combustor prevents the walls of the combustor from increasing in temperature. Several ports are included for mounting actuators and sensors.

3.2 The Measurement and Control System

The choice of the actuator and sensor for the measurement and control system proved to be a challenging one. A microphone was chosen as a pressure sensor due to its fast response and ability to accurately measure low pressures. This was desirable, since the goal was to suppress the thermoacoustic instability. The microphone did have several limitations, however. Initially, a Radio Shack condenser microphone ele-

ment was chosen as the sensor. This element had little protection from the humidity in the air and from possible flame flash-back, leading to frequent failure and unreliable measurements. Instead, a protected PC microphone was used to measure the pressure. Additionally, while the microphones could be used to accurately measure low level pressures, at higher pressure levels their measurements became nonlinear. This occurred at approximately ± 160 Pa for the microphone chosen for testing. Another option for pressure measurement is a piezoelectric sensor. While these can be used to accurately measure higher pressure levels, the sensitivity at low pressures is compromised.

The microphone is placed in a selected port to measure the pressure at the desired location in the combustor. It is then connected to an input channel on the data acquisition board through a screw terminal accessory. The Keithly MetraByte DAS1801-AO data acquisition board was chosen because of its speed and versatility. The board is capable of sampling at up to 312 kHz on its input channels. This speed was desirable in order to allow sampling to occur fast enough to prevent aliasing. The board has 16 single-ended or 8 differential inputs and 2 waveform-quality analog outputs. Experiments were conducted using differential inputs to minimize the effect of noise, which is especially important when the voltage being measured is small. In this case the input range was ± 5 volts. The output range on the board was ± 10 volts. The board was mounted in a 166 MHz Pentium PC.

In order to utilize the information about the pressure from the microphone to determine the control input needed, it was necessary to write code to both send commands to the data acquisition board and calculate the control input based on the pressure signal and the controller to be implemented. This was one of the most important and challenging aspects of setting up the data acquisition system. The task required that the user be able to specify the sampling rate and the number of samples to be taken. Additionally, it was necessary that the sampling occur quickly and accurately. This required that the execution of all code be fast and written in a way that minimized the time delay between the reading of the pressure signal and the control input signal being sent to the loudspeaker by the board. Pre-written functions for the

DAS1801-AO board could not be utilized because of their slow execution and inability to allow the input value at each sampling instant to be accessed real-time. Therefore, register-level programming was used to performed such tasks as setting the data acquisition board to the desired setting (differential input, desired gain, input channels and sampling order), programming the clock to sample at the sampling rate specified by the user, collecting the information on the pressure amplitude at each sampling instant, calculating the control effort based on a controller algorithm, outputting this control input, and clearing the board at the end of each test. The sampling rate was specified using timers on the data acquisition board. These timers were given an initial count value based on the sampling rate desired and, once triggered, began counting down to zero. When zero was reached, a flag was sent to the status register and the program signaled for the board to take data. This timer was immediately reset and began counting down to zero once again. This method of timing will be accurate as long as the time required to complete calculations in the control loop is less than the time between samples. The computer must also be dedicated to the sampling and control processes so that other processes and commands do not interfere with acquiring data. The data was stored in an array during the program execution and saved to a file at the end of each test. Memory allocation had to be done in a way that allowed a large number of data points to be stored during the program execution. This required the variables which stored the pressure and control input to be declared as global variables rather than local ones to prevent stack overflow from occurring during data acquisition. The output of the data acquisition board was sent through a potentiometer which allowed the amplitude of the voltage to be modified before it reached the loudspeaker. An example of the C code used in the testing and control can be found in Appendix A.

The model for the combustion system was developed in continuous time and thus all controllers were designed in continuous time. Implementation on the data acquisition board required that these controller transfer functions be converted to algorithms in discrete time. This was done using two methods: (1) the backward difference method [27], and (2) Matlab's Control System Toolbox continuous to discrete time

conversion assuming a zero order hold.

Two type K Omega thermocouples were used to measure the temperature in the cold (upstream from the flame) and hot (downstream from the flame) sections of the combustor. These thermocouples were connected to the data acquisition board through a screw terminal panel with a built in cold junction, which served as a reference point.

3.3 Experimental Conditions

To develop an accurate model of the experimental system, it was necessary not only to use the geometry of the combustor itself in the model, but also the operating conditions for the tests. Most experiments were conducted with an equivalence ratio between 0.68 and 0.74 and an air flow rate of 333 mL/s (0.38 g/s), which corresponded to an unstable operating condition without control (Equivalence ratios of less than 0.67 corresponded to a stable operating point). The flow rate was varied between 267 mL/s and 400 mL/s and the power of the combustor was approximately 1 kW. A sampling rate of 10 kHz was found to be more than sufficient to prevent aliasing.

Chapter 4

Validation of Model-Based Active Controllers

The first step in validating the model-based approach to designing controllers for the suppression of a thermoacoustic instability was to develop a model to represent the bench-top combustor. Controllers were then designed based on this model and their ability to suppress the instability simulated. Control design and simulations were conducted considering two different actuator/sensor configurations. The first case was for the actuator and sensor collocated at D. See Figure 4-1 for the actuator-sensor-flame locations in the combustor. For the second case, the actuator remained at D, but the sensor was moved to C. The performance of these simulated controllers could be compared to controllers implemented on other similar combustion systems. Once the model had been developed and the model-based controllers designed and simulated, the controllers were implemented on the actual bench-top combustor rig. This allowed the performance of the control strategy in simulation and experiment to be compared.

4.1 The Uncontrolled Combustor Model

The combustor model as in Eqs. (2.9) - (2.12) was simulated using the following parameters: $L = 0.62m$, $\gamma = 1.4$, $\bar{p} = 1atm$, $\bar{c}_1 = 347m/s$, $c_2 = 485m/s$,$\bar{M} =$

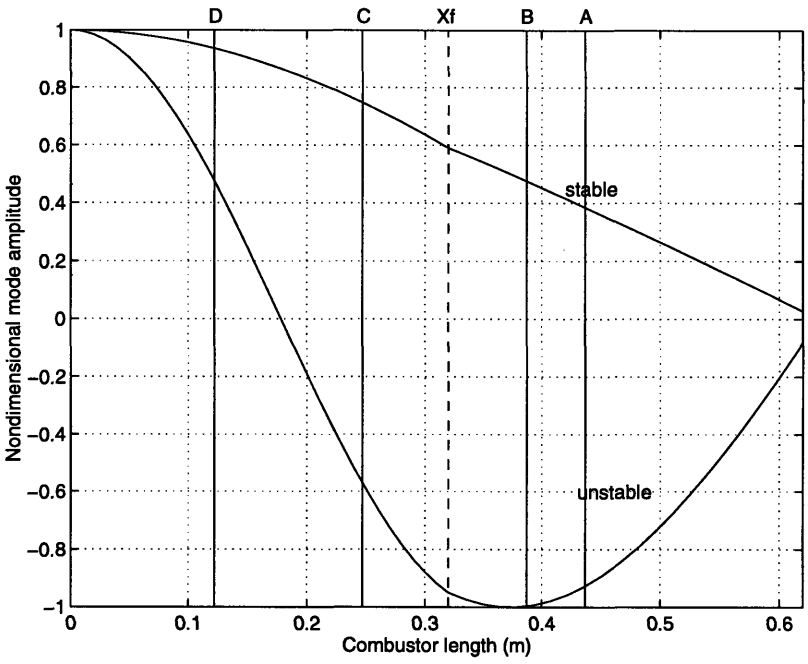

Figure 4-1: Mode shapes for closed-open combustor boundary conditions and actuator-sensor-flame locations.

3.612×10^{-4}, $\rho_u = 1.163 kg/m^3$, $L_{eff} = 0.535$, $\Delta q_r = 2.26 \times 10^6 J/kg$ based on an equivalence ratio of 0.74, $S_u = 0.3 m/s$, $\theta = 0.5$, $\epsilon = 2.0$, $d_p = 1.5 \times 10^{-3} m$, $D = 0.053 m$, and $n_f = 80$. These were chosen to match the geometry and fuel properties of the combustor as closely as possible. For example, S_u was chosen based on the burning velocity for propane and accounting for heat losses at the walls of the combustor. The heat of reaction Δq_r was found using the following equation:

$$\Delta q_r = C_v \frac{\phi}{\phi + 15.6}, \tag{4.1}$$

where C_v is the calorific value of propane, and 15.6 is the stoichiometric ratio between air and the fuel. θ and ϵ, which also affect the flame parameters, were lumped approximations to account for the effect of the velocity behind and ahead of the flame and the increase in flame diameter beyond the perforation diameter, respectively. The length of the combustor required two corrections from the actual geometric length. The length, L, under consideration was the acoustic length which was effected by

the unsteady pressure oscillations. An end-correction was required to account for the fact that a column of air beyond the exit of the combustion chamber was a part of the acoustic system. The length of this end correction could be found by locating the pressure null (where the oscillation amplitude became zero) with a microphone. and was found to be 0.09 m. For the bench-top combustor chosen, the length of the air/fuel feed tube, which was 0.06 m, also affected the acoustics of the combustor and was added to the total acoustic length. The effect of mean heat, which results in a significant change in the velocity, density, and temperature of the hot gases in the combustor, was to shrink the effective length of the combustor. The acoustic mode shapes are sinusoidal in this effective combustor, thus L_{eff} was utilized to calculate the frequency of the first and second acoustic modes. L_{eff} could be found using the following equation:

$$L_{eff} = L - (1 - \theta_1)(L - x_0), \tag{4.2}$$

where $\theta = \overline{c}_1/\overline{c}_2$ and is less than one. A damping ratio $\zeta = 0.0033$ was added at all frequencies to account for passive damping in the system, the effects of which were not included in the model. The choice of ζ was therefore arbitrary, and was selected so as to match the experimental growth rates over as wide a range of equivalence ratios as possible. A closed-open boundary condition was chosen due to the structure of the flow conditions, and the fact that the loudspeaker to be used for control was side-mounted. The first two acoustic modes were considered in the model. The corresponding mode shapes, k_i, were computed using L_{eff}, and ω_i was found to be 162 Hz and 488 Hz for $i = 1, 2$. The mode shapes for the entire length of the combustor,L, are shown in Figure 4-1 and are not perfectly sinusoidal. There is a slight discontinuity at x_f due to mean heat effects. Denoting $W_{\mathrm{C/D}}(s)$ as a transfer function with the sensor at C and the actuator at D, the resulting plant transfer functions are of the form

$$W_{\mathrm{D/D}}(s) = 2.15 \times 10^5 \frac{(s + 440)(s^2 - 83s + 7.70 \times 10^6)}{(s + 14.9)(s^2 + 407s + 1.03 \times 10^6)(s^2 - 63s + 9.41 \times 10^6)},$$

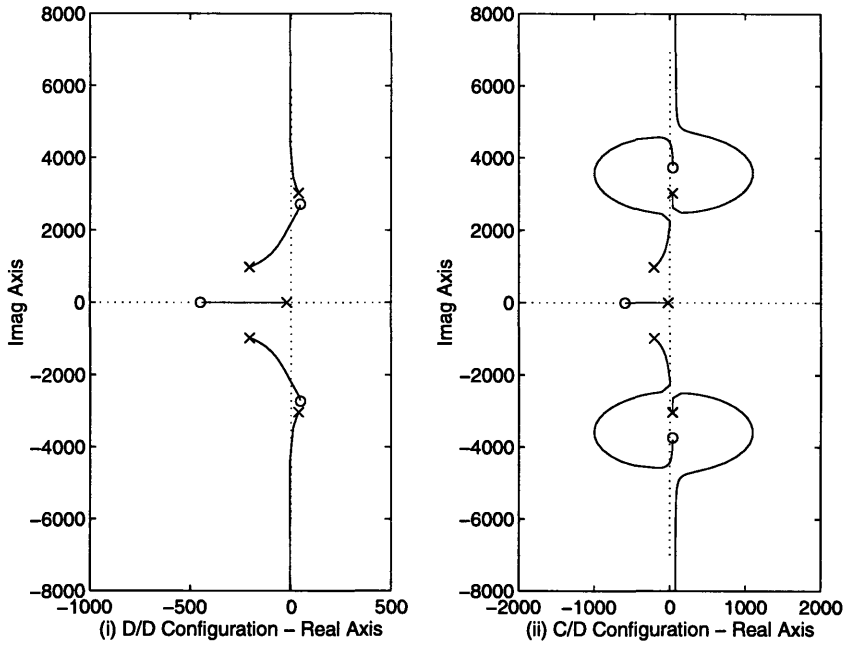

Figure 4-2: Root locus of combustion system with (i) D/D actuator-sensor configuration and (ii) C/D actuator-sensor configuration - without actuator dynamics.

$$W_{\mathrm{C/D}}(s) = 8.38 \times 10^4 \frac{(s+589)(s^2-26s+1.47\times 10^7)}{(s+14.9)(s^2+407s+1.03\times 10^6)(s^2-63s+9.41\times 10^6)},$$

assuming that only the first two modes are present. The root loci showing the pole and zero locations for each actuator-sensor location are shown in Figure 4-2. For both the D/D and C/D cases, the system has an unstable pair of poles and zeros. The zeros for the C/D case, however, move farther away from the origin. The fact that they are no longer interlaced between the stable and unstable poles implies that a low-order phase-lead controller will not be sufficient to stabilize the system. This is due to the fact that the centroid of the root locus no longer lies in the left-half plane.

The performance of the uncontrolled combustor for both the simulation and experiment with the D/D configuration is shown in Figure 4-3. Over the first 100 milliseconds the simulation and experimental growth rates match closely (approximately 32 milliseconds). Beyond this point, the pressure level continues to grow in the linear model, as expected, while nonlinearities begin to dominate in the ex-

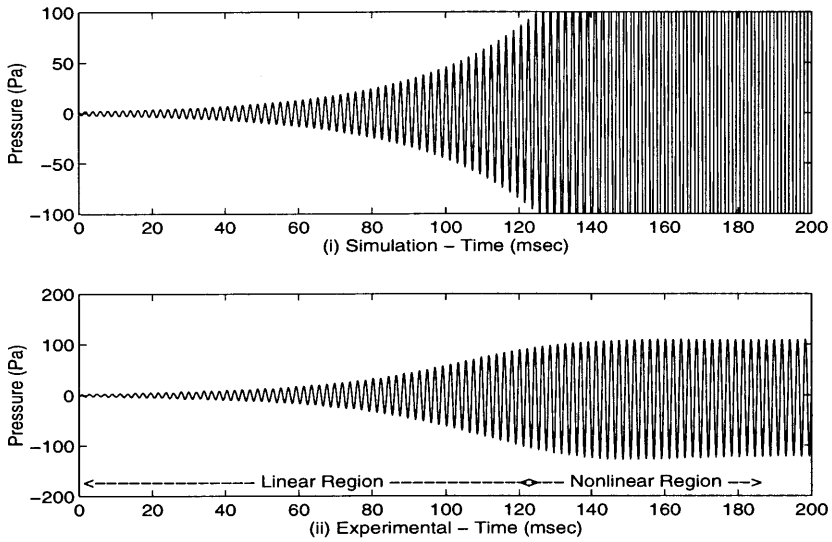

Figure 4-3: Pressure oscillations for uncontrolled combustor (i) Simulation results using the two mode model and (ii) Experimental results.

perimental combustor and a limit-cycle is reached. The experimental and predicted behavior of the combustor differ more drastically for $\phi < 0.67$. The former led to a stable system while the latter yielded an unstable system with a smaller growth rate. This may be due to the modeling error in the passive damping mechanism, which may in fact be nonlinear and depend on ϕ. The unstable frequency predicted by the simulation of 488 Hz was close to that observed experimentally at 470 Hz.

4.2 The Complete Combustor Model

To complete the model of the experimental system, the actuator and sensor dynamics also had to be explicitly taken into account before designing the controllers. Using a function generator and a photo sensor for measuring the displacement of the loudspeaker diaphragm, a frequency analysis was carried out. This analysis was used to determine the transfer function relating the voltage into the loudspeaker to the

acceleration of the loudspeaker diaphragm. The approach taken was to obtain an experimental frequency response of the loudspeaker by exciting it at various frequencies and calculating the gain and phase. A curve was then fit to this data by comparing the experimental gain and phase information to the Bode plot of a transfer function of the form of Eq. (2.14) with varying k_l, m_l, and b_l. It was found that the dynamics of the 0.2W loudspeaker used in experimental investigations could best be expressed as:

$$G_l(s) = \frac{35.5s^2}{s^2 + 364s + 3.320 \times 10^6} \tag{4.3}$$

The Bode plot of this transfer function along with the experimental data points are shown in Figure 4-4. The natural frequency of the loudspeaker, which was 290 Hz, is on the order of the first acoustic mode, indicating the necessity of including the actuator dynamics in the control design process. To complete the model of the experimental system, a sensor gain of 45.3 Pa/Volt was included in the simulation. This gain was calculated using a Rriual-Kejar piston phone. The code used to develop a complete model of the uncontrolled combustor in MATLAB, which was then utilized for control design is shown in Appendix B. The root loci of the complete system, including the actuator and sensor dynamics is shown in Figure 4-5 (i) and (ii) for the D/D and C/D actuator-sensor configurations, respectively. A schematic of the system components included in the model is shown in Figure 4-6.

In addition to the combustion dynamics, loudspeaker dynamics, and sensor gain, the limitations of the loudspeaker were considered when designing a controller. Beyond a known input voltage, the diaphragm motion of the loudspeaker became nonlinear. To ensure that this region was avoided, the potentiometer in the loudspeaker circuit was adjusted so that with a maximum voltage of ± 10 volts into it (the limit of the data acquisition board's output), the voltage signal sent to the loudspeaker would remain within the loudspeaker's linear range. The maximum acceleration the loudspeaker could provide in the linear range at the unstable frequency was $600 m/s^2$. This limitation on the maximum control effort was taken into account when designing the controllers, the details of which are described below.

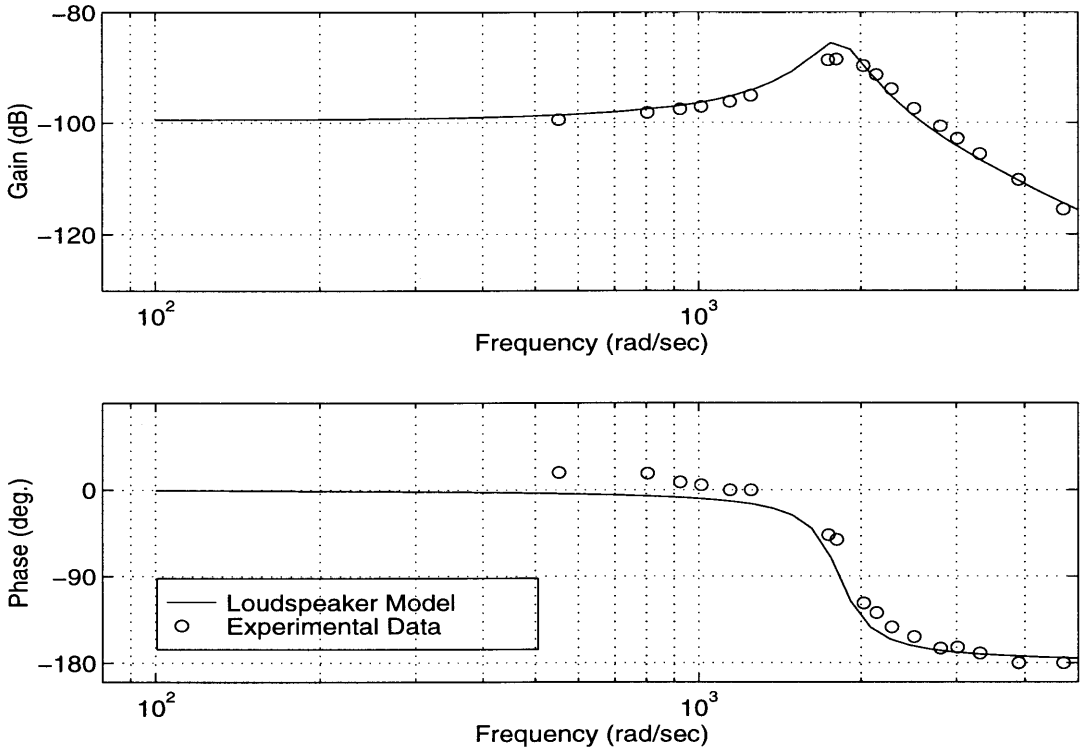

Figure 4-4: Bode plot for the 0.2 W loudspeaker dynamics and experimental gain and phase information.

4.3 Active Control of the Instability

4.3.1 The D/D Actuator-Sensor Configuration

Low-order controllers were designed first using the combustor model. The D/D actuator-sensor configuration exemplified the importance the loudspeaker dynamics could play in the system. As can seen by to root locus shown in Figure 4-5(i) for the D/D configuration, the addition of the actuator dynamics implies that a proportional controller will be sufficient to suppress the instability. The model indicated that a proportional controller with a gain K_p between 8.5 and 54.0 could stabilize the system. Higher gains would lead to the excitation of a new frequency. A first-order phase-lead controller of the form

$$G_c(s) = k_c \frac{s + z_c}{s + p_c} \tag{4.4}$$

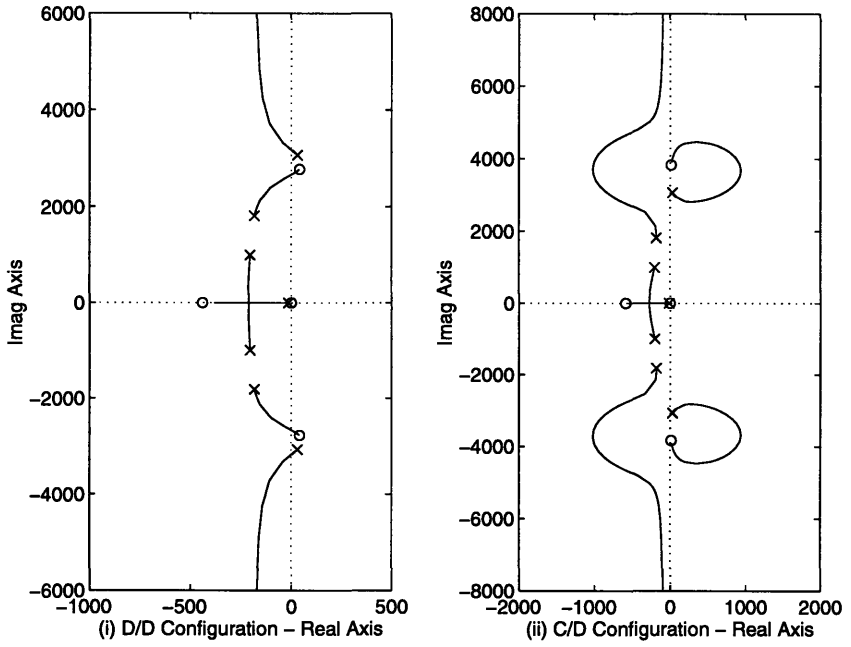

Figure 4-5: Root locus of combustion system with (i) D/D actuator-sensor configuration and (ii) C/D actuator-sensor configuration - with actuator dynamics.

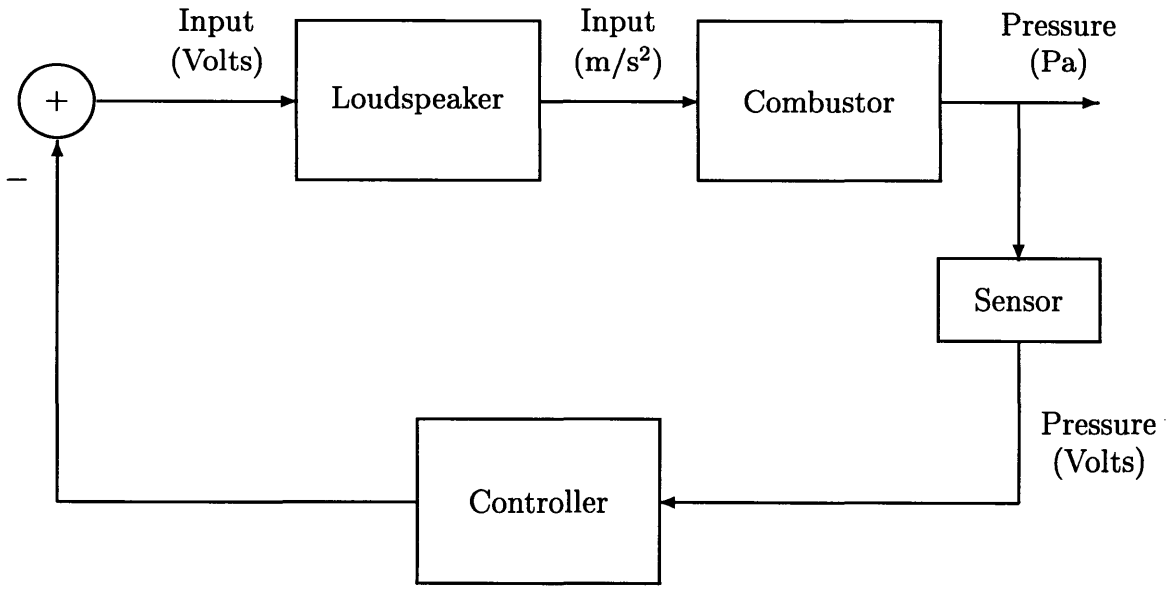

Figure 4-6: A model of the experimental system components.

could also be utilized to stabilize the system with this configuration. A phase-lead controller with $z_c = 1400$ and $p_c = 1900$ was designed and found to stabilize the two-mode model of the system for k_c between 6.6 and 77.0. The gain that was implemented experimentally was chosen so that the corresponding control effort did not exceed the maximum allowable limit, considering the limitations of the loudspeaker. The gain values which led to the smallest settling time for the two controllers and still met the control effort limitation are given by $K_p = 13.0$ and $k_c = 12.0$. The power limitations also reduced the range of equivalence ratios for the success of both of these controllers to $(0.68, 0.7)$. If the equivalence ratio was increased beyond this region, the unsteady pressure level increased to a point which required more control effort than could be provided by the system.

Once the low-order controllers had been chosen, the LQG controller was designed with the system model as in $W_{\mathrm{D/D}}(s)G_l(s)$. The two design parameters μ and ρ were chosen so that the maximum loudspeaker acceleration was close to $600m/s^2$, and were given by $\mu = 0.001$, and $\rho = 0.01$. The code used to design the LQG controller in MATLAB is shown in Appendix C. The resulting LQG controller was evaluated using MATLAB's Control Systems Toolbox as

$$G_{\mathrm{D/D}}(s) = \frac{3.68 \times 10^4 (s - n_1)(s + n_2)(s^2 - n_3 s + n_4)(s^2 + n_5 s + n_6)}{(s + d_1)(s^2 + d_2 s + d_3)(s^2 + d_4 s + d_5)(s^2 + d_6 s + d_7)},$$

where

$$\begin{aligned} n_1 &= 525 \\ n_2 &= 14.9 \\ n_3 &= 212 \\ n_4 &= 7.66 \times 10^6 \\ n_5 &= 665 \\ n_6 &= 1.68 \times 10^6 \\ d_1 &= 14.9 \\ d_2 &= 3695 \\ d_3 &= 1.26 \times 10^7 \\ d_4 &= 210 \end{aligned}$$

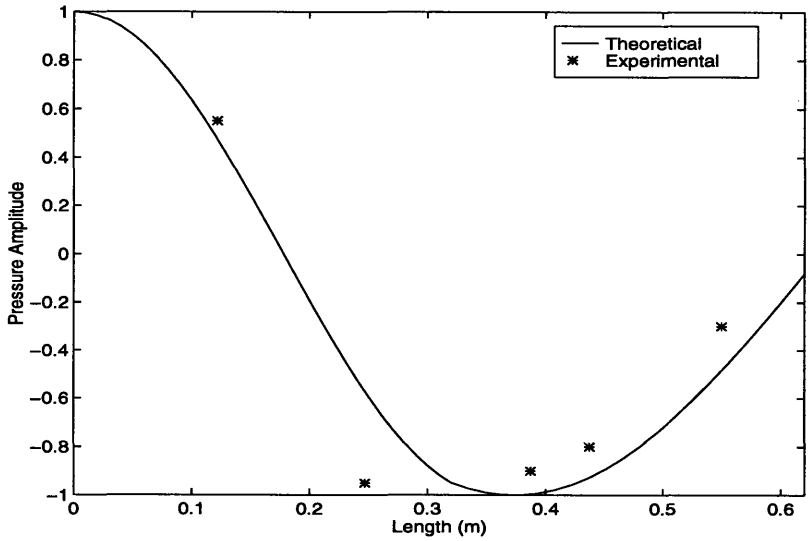

Figure 4-7: Theoretical and experimental mode shape in combustor

$$d_5 = 7.78 \times 10^6$$

$$d_6 = 746$$

$$d_7 = 3.27 \times 10^5$$

The three controllers designed based on the two mode model were implemented on the bench-top combustor discussed in Chapter 3 to test their performance experimentally. Although simulation results indicated that the controllers could be successfully used to suppress the thermoacoustic instability, to gain confidence in the model and method used to design the controllers, it was clearly necessary to test them on the actual system. The first verification of the model was to test the unstable mode shape in the combustor. This was done by measuring the pressure amplitude at each of the four ports along the combustor (see Figure 3-2) and at the exit of the combustor. Results closely corresponded with the pressure amplitude calculated theoretically at these points as shown in Figure 4-7.

The simulated controllers were implemented directly in the experiment using the

discretization of the controller by the backward-difference method for the phase-lead controller and using the MATLAB Control Systems Toolbox and a zero-order-hold method for the LQG controller. The experimental and simulation results for the pressure response and control effort are shown in Figures 4-8, 4-9, and 4-10 for proportional control, phase-lead control and LQG control, respectively. The proportional and phase-lead results correspond to an equivalence ratio of 0.70, while the LQG controller had an equivalence ratio of 0.72. The initial conditions were chosen for the simulation assuming that they corresponded to a case when only the second mode (the unstable one) was excited. As the complexity of the controller increased, the settling time and control effort required decreased. The settling time for the proportional controller was 161 milliseconds in the simulation and 179 milliseconds experimentally. For the phase-lead controller, the corresponding settling times were 99 milliseconds and 154 milliseconds respectively. If the equivalence ratio was increased beyond 0.70, the proportional and phase-lead controllers were not able to suppress the thermoacoustic instability, indicating that the control effort required had exceeded the system's limits, as predicted by the simulations. The discrepancy between the theoretical and experimental control efforts may be explained by passive damping in the experimental system, which aided more in the suppression of the instability at lower equivalence ratios.

The most dramatic pressure suppression was seen with the LQG controller as shown in Figure 4-10. For the D/D actuator-sensor configuration, the LQG controller had a settling time of 35 milliseconds in the simulation and 36 milliseconds experimentally. It can be observed from Figure 4-10 that both the settling time and control effort predicted by the simulation match that from the experiment quite well. Higher equivalence ratios could be controlled using the LQG controller than with the low-order controllers due to the fact that less control effort was required. For example, simulation results using the proportional and phase-lead controller for an equivalence ratio of 0.72 showed that the maximum control effort required was approximately $2500 m/s^2$ and $1800 m/s^2$, respectively. While the low-order controllers could only suppress the instability up to $\phi = 0.70$ in the experiments, the LQG controller could

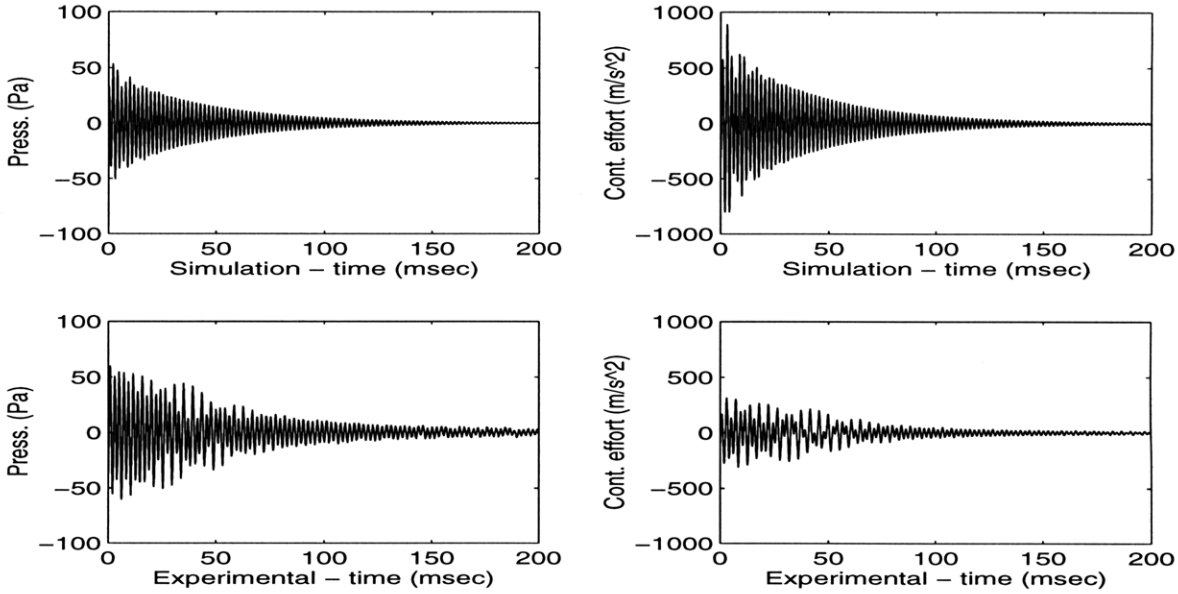

Figure 4-8: Pressure response and control input for a side-mounted loudspeaker with D/D configuration and proportional control: Simulation results using the two-mode model and experimental results.

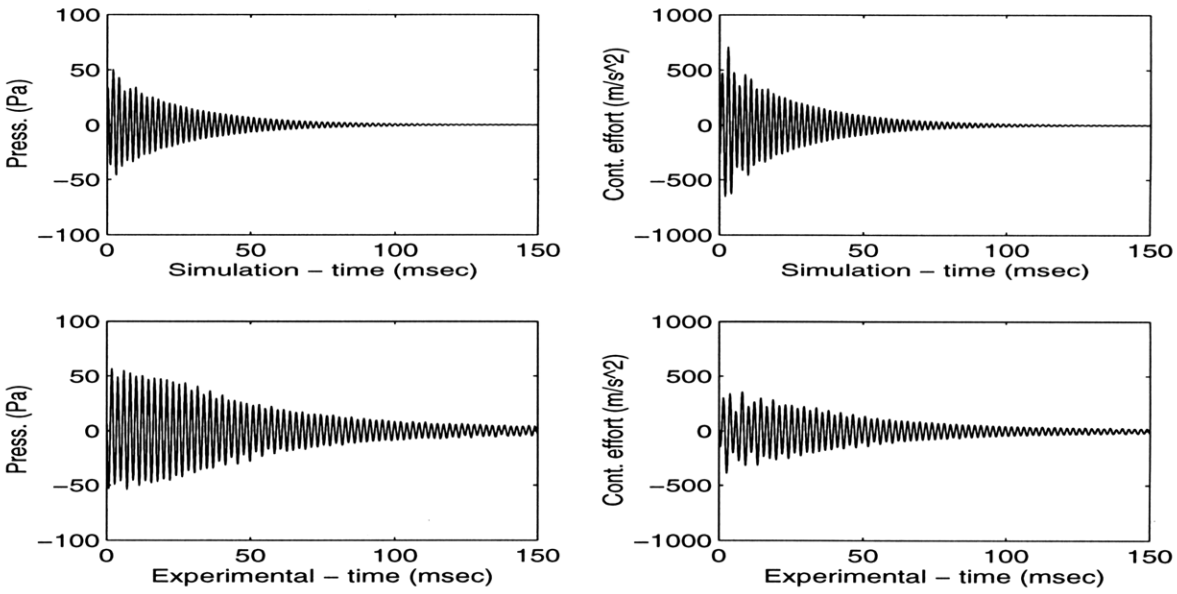

Figure 4-9: Pressure response and control input for a side-mounted loudspeaker with D/D configuration and phase-lead control: Simulation results using the two-mode model and experimental results.

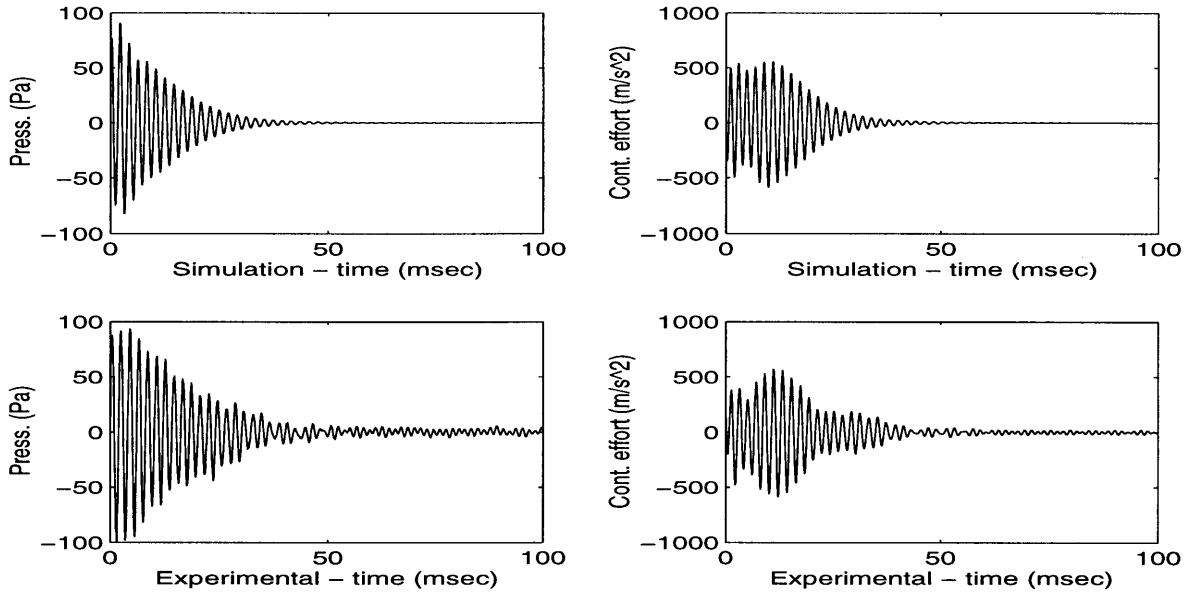

Figure 4-10: Pressure response and control input for a side-mounted loudspeaker with D/D configuration and LQG control: Simulation results using the two-mode model and experimental results.

successfully suppress the instability for all ϕ's up to 0.74. As ϕ increased, however, a slight increase in settling time occurred, as shown in Figure 4-11, which gives the settling time versus equivalence ratio for the LQG controller. The increase in settling time with ϕ is due to the fact that the pressure levels and therefore the required control effort increase with ϕ whereas the loudspeaker has limited control authority. Interestingly, the average settling time obtained using the LQG controller is more than twice as fast as that reported in [4], which was for a similar combustor with the same power and pressure levels.

Using the LQG controller, the pressure level was suppressed from a level of 210 Pa (at B) to an ambient noise level of 1.5 Pa, which corresponds to a reduction of 44 dB. The residual noise is mostly due to the blower, which accounts for the small amplitude of the pressure oscillations in steady-state that can be seen in Figure 4-10. A power spectrum of the combustor with and without control is shown in Figure 4-12 along with the power spectrum of the system with no combustion for reference. Changes in the flow rate while maintaining the same equivalence ratio did not affect

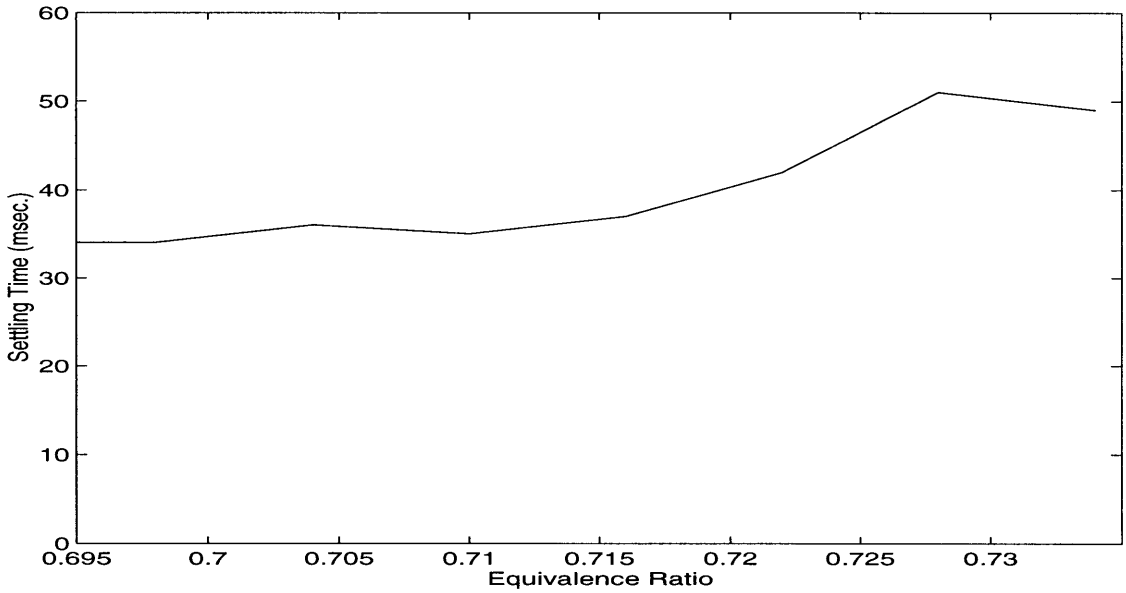

Figure 4-11: 2%-settling time achieved using the LQG controller as a function of the equivalence ratio for D/D configuration.

the ability of the controller to stabilize the thermoacoustic instability, in contrast to Ref. [8].

4.3.2 The C/D Actuator-Sensor Configuration

For the C/D case, a proportional or phase-lead controller was not sufficient to suppress the thermoacoustic instability, due to the fact that the unstable zeros are not longer interlaced between the stable and unstable poles, as discussed in Section 4.1. The root locus of the combustion system, including the loudspeaker dynamics, with the C/D configuration is shown in Figure 4-5(ii). An LQG controller was designed using MATLAB's Control System Toolbox, for comparison to the D/D configuration. The transfer function was evaluated as

$$G_{\mathrm{C/D}}(s) = \frac{1.13 \times 10^4 (s - n_1)(s + n_2)(s^2 - n_3 s + n_4)(s^2 + n_5 s + n_6)}{(s + d_1)(s^2 + d_2 s + d_3)(s^2 + d_4 s + d_5)(s^2 + d_6 s + d_7)},$$

where $n_1 = 3945$

$n_2 = 14.9$

$n_3 = 1341$

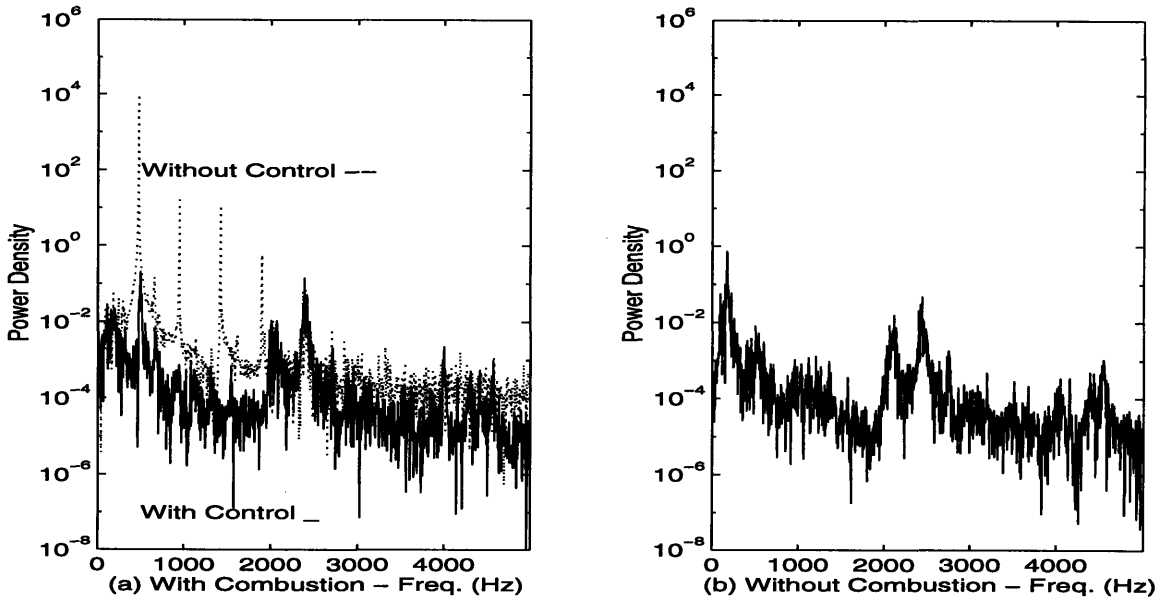

Figure 4-12: Power spectrum of the pressure response (a) with and without control and (b) with blower noise (without combustion).

$$
\begin{aligned}
n_4 &= 77.86 \times 10^6 \\
n_5 &= 436 \\
n_6 &= 1.43 \times 10^6 \\
d_1 &= 15 \\
d_2 &= 584 \\
d_3 &= 1.15 \times 10^7 \\
d_4 &= 3329 \\
d_5 &= 7.79 \times 10^6 \\
d_6 &= 781 \\
d_7 &= 3.59 \times 10^5
\end{aligned}
$$

Simulation and experimental results are shown in Figure 4-13. The settling time for this controller was 31 milliseconds theoretically and 23 milliseconds experimentally. Once again, the settling time and control effort in the simulation and the experiment were in close agreement. As expected, the pressure amplitude was higher at the C/D

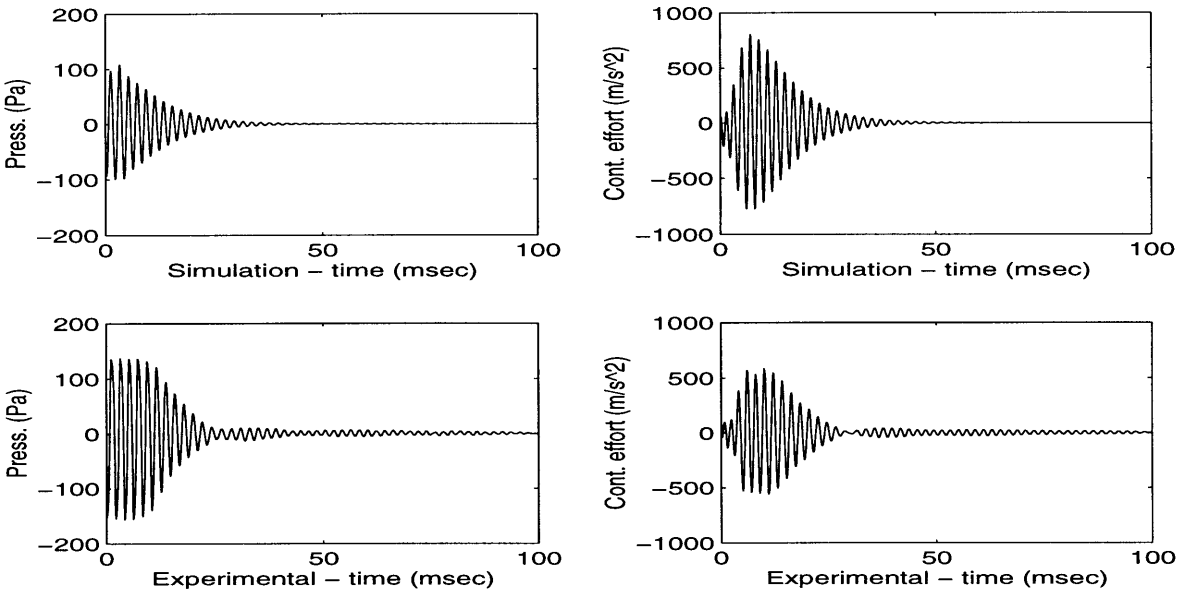

Figure 4-13: Pressure response and control input for a side-mounted loudspeaker with C/D configuration and LQG control: Simulation results using the two-mode model and experimental results.

location for the same equivalence ratio than the D/D case, due to the fact that the sensor is closer to the anti-node when placed at C. The instability once again could be suppressed for equivalence between 0.68 and 0.74. Increasing ϕ beyond this point resulted in two problems with the C/D configuration. The first problem was that the pressure measurements by the microphone became nonlinear, while the second was that pressure levels and therefore the required control effort increased to a point which exceeded that which could be provided by the system. A plot of settling time versus ϕ for the C/D configuration is shown in Figure 4-14 and exhibits a similar trend to that observed for the D/D configuration.

The model-based LQG controller with the C/D configuration proved to be the most successful in suppressing the thermoacoustic instability both in simulation and experiment. The experimental settling time of 23 milliseconds is almost four times faster than that reported in [4], and the controller was successful for all flow rates tested.

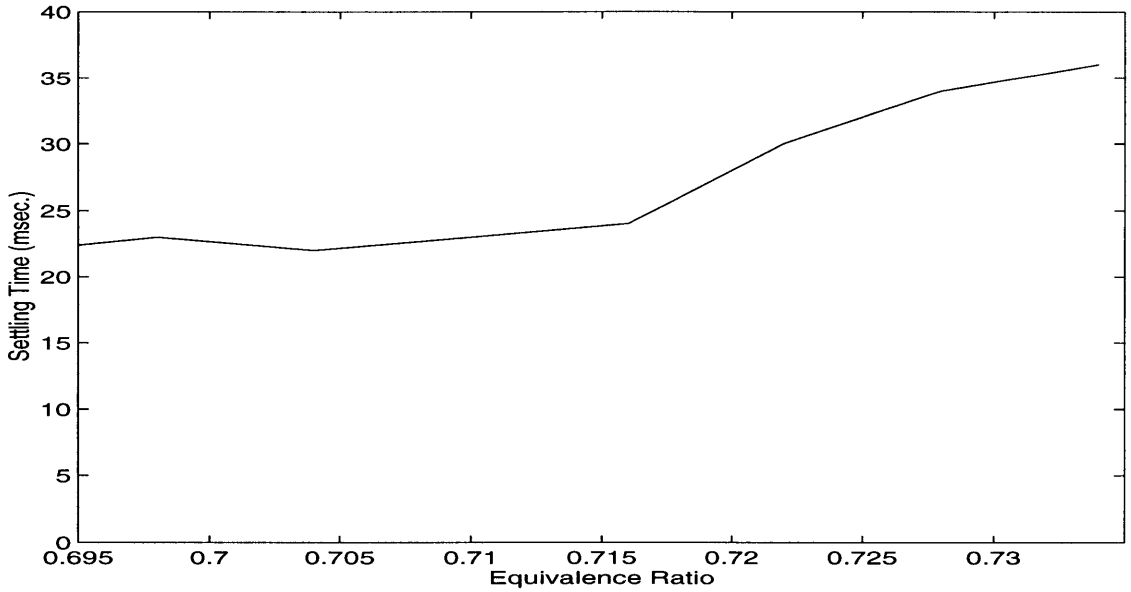

Figure 4-14: 2%-settling time achieved using the LQG controller as a function of the equivalence ratio for C/D configuration.

4.3.3 Effect of Model Changes on LQG Control Design

An LQG control design was chosen because of the ability to optimize the controller based on a weighting of the performance of the controller versus the control effort required using ρ and μ. Even with the use of these two parameters, however, numerous controllers could be chosen. The following paragraphs will discuss how the choice of ρ and μ were made and also how changes in the model affected the LQG's performance.

In Section 4.2 the limitations of the loudspeaker which was used as an actuator for the bench-top combustor were discussed. These limitations placed a restriction on the values of ρ and μ that could be chosen. As their values were decreased, the settling time of the controlled system also decreased, but the control effort required to suppress the instability increased. If ρ and μ were chosen in the LQG control design such that the control effort required was significantly larger than that which could be achieved by the experimental system, the simulations indicated a fast settling time, but the experimental controller was not able to achieve the same performance due to loudspeaker saturation, and the actual settling time was much larger. At the same time, as ρ and μ were increased, the settling time in both simulation and

experiment increased and the control effort required decreased. The goal, therefore, was to optimize the controller by having ρ and μ small enough to achieve as fast a settling time as possible while considering the limitation on the control effort and avoiding actuator saturation.

Several iterations on the model were made in developing the model-based control strategy. "Model a" considered the physical length of the combustor as the acoustic length, neglected mean heat, contained an incorrect definition of Δq_r, and ignored the increase in diameter of each flamelet over the perforation diameter of the plate. "Model b" corrected the definition of Δq_r and the values of several parameters, including the addition of ϵ to account for the increase in the flamelet diameter beyond the perforation diameter, a phenomena which had been observed experimentally. "Model c" was developed based on a detailed study of the acoustics in the combustor. Length corrections were made to both the hot and cold sections of the combustor. The average temperature in the hot section was adjusted to reflect the fact that the acoustic hot section extended beyond the physical exit of the combustor. In addition, mean heat was included in this model. In summary, "Model a" is an "incorrect" model (the reason for its inclusion will become apparent below), "Model b" is an approximate model, while "Model c" is the most accurate finite-dimensional model, derived entirely using calculations based on acoustical properties, geometry, and boundary conditions. The parameters for each model are given in Table 4.1.

The variation of the model had an interesting effect in the LQG control design and the resulting settling time for the experimental system. The pole-zero plots for each of the three controllers is shown in Figure 4-15(i), (ii), and (iii) for "Models a, b, and c," respectively, for the D/D configuration and in Figure 4-16(i), (ii), and (iii) for the C/D configuration. Note the locations of the zeros in each case. For each model, the controller was designed considering the limitation imposed by the loudspeaker. When the controllers were tested on the combustor for the D/D configuration, a settling time of 20 milliseconds was obtained for "Model a" as shown in Figure 4-17, 41 milliseconds for "Model b" (see Figure 4-18), and 36 milliseconds for "Model c" as shown previously in Figure 4-10. For the C/D configuration, the settling times

	"Model a"	"Model b"	"Model c"
T_{hot}	600 K	600 K	550 K
L	0.495	0.487	0.62
d_f	0.0015	0.003	0.003
D	0.0382	0.053	0.053
S_u	0.28	0.3	0.3
Δq_r	4.3×10^6	2.26×10^6	2.26×10^6
b_1	747	400	400
b_2	90.2	14.8	14.8
b_3	90.2	65.1	65.1
f_2	526	535	487
Growth Rate	114	65.1	31.3

Table 4.1: Summary of parameters for "Model a", "Model b", and "Model c".

were 32 milliseconds, 42 milliseconds, and 23 milliseconds for "Models a, b, and c," respectively as shown in Figures 4-19, 4-20, and in Section 4.3.2 in Figure 4-13. The performance for the C/D configuration indicates that the better the model accuracy, the better the control performance. The question that arises is why at D/D, the inaccurate model ("Model a") resulted in the fastest settling time (20 milliseconds) while the most accurate model ("Model c") led to a slower performance.

There appears to be two factors which affect the performance of the LQG controllers developed using these three models and may lead to an explanation for the performance of each controller. The first factor is the accurateness of the model in representing the actual combustion system, and the second is the location of the right-most zero pair for the controller. For the C/D actuator and sensor configuration the controller is quite sensitive to modeling errors, as seen in Section 4.4. The LQG controller designed based on "Model c", where the unstable frequency in the model is the closest to that observed experimentally, has the fastest settling time. The location of the controller zeros will have some effect on performance, but is not as critical as the accurateness of the model. The trend is for the performance to improve with model accuracy. The question that remains is why the performance of the LQG controller based on "Model a" is the fastest for the D/D configuration.

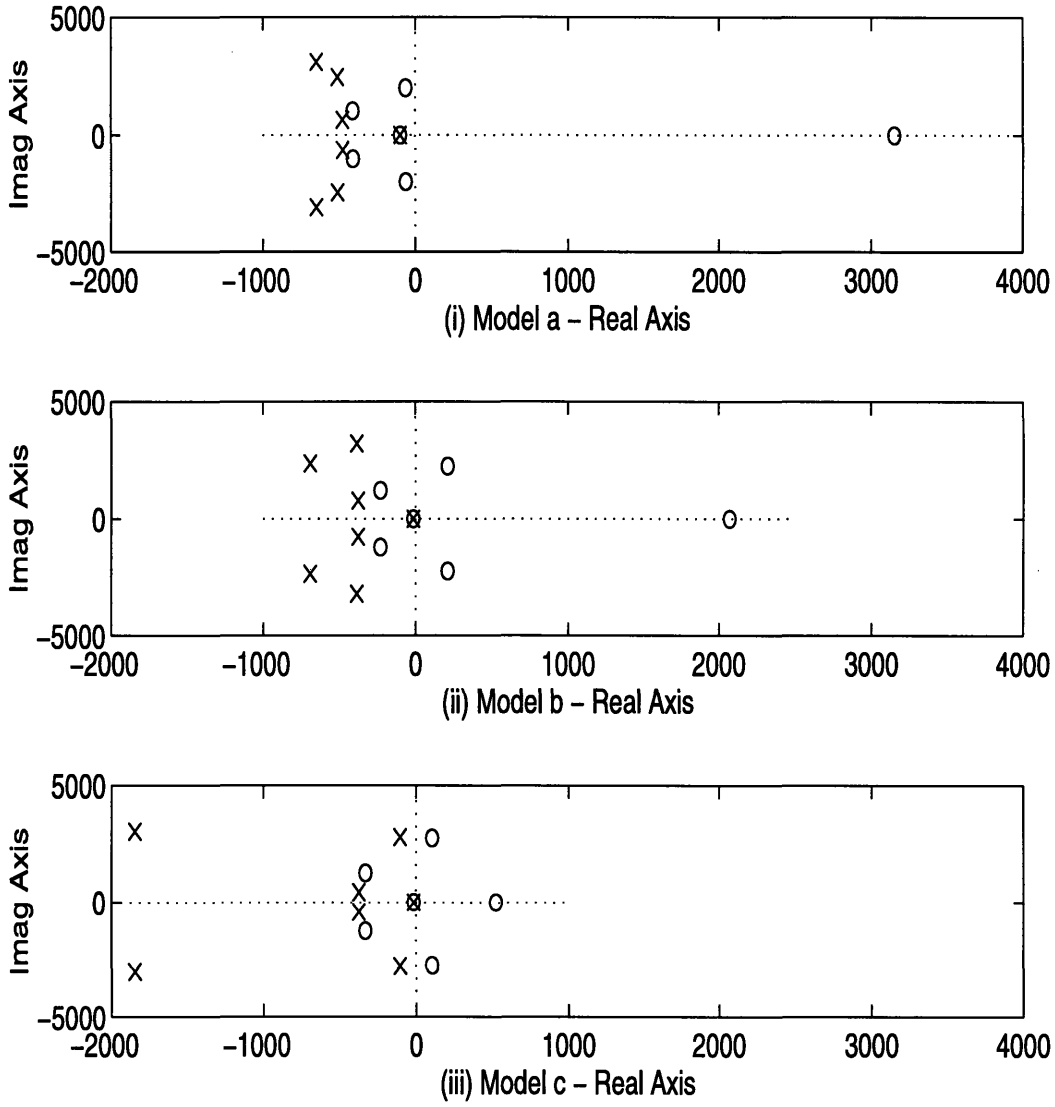

Figure 4-15: Pole-zero plots of the LQG controller designed using (i) "Model a", (ii) "Model b", and (iii) "Model c" with D/D configuration.

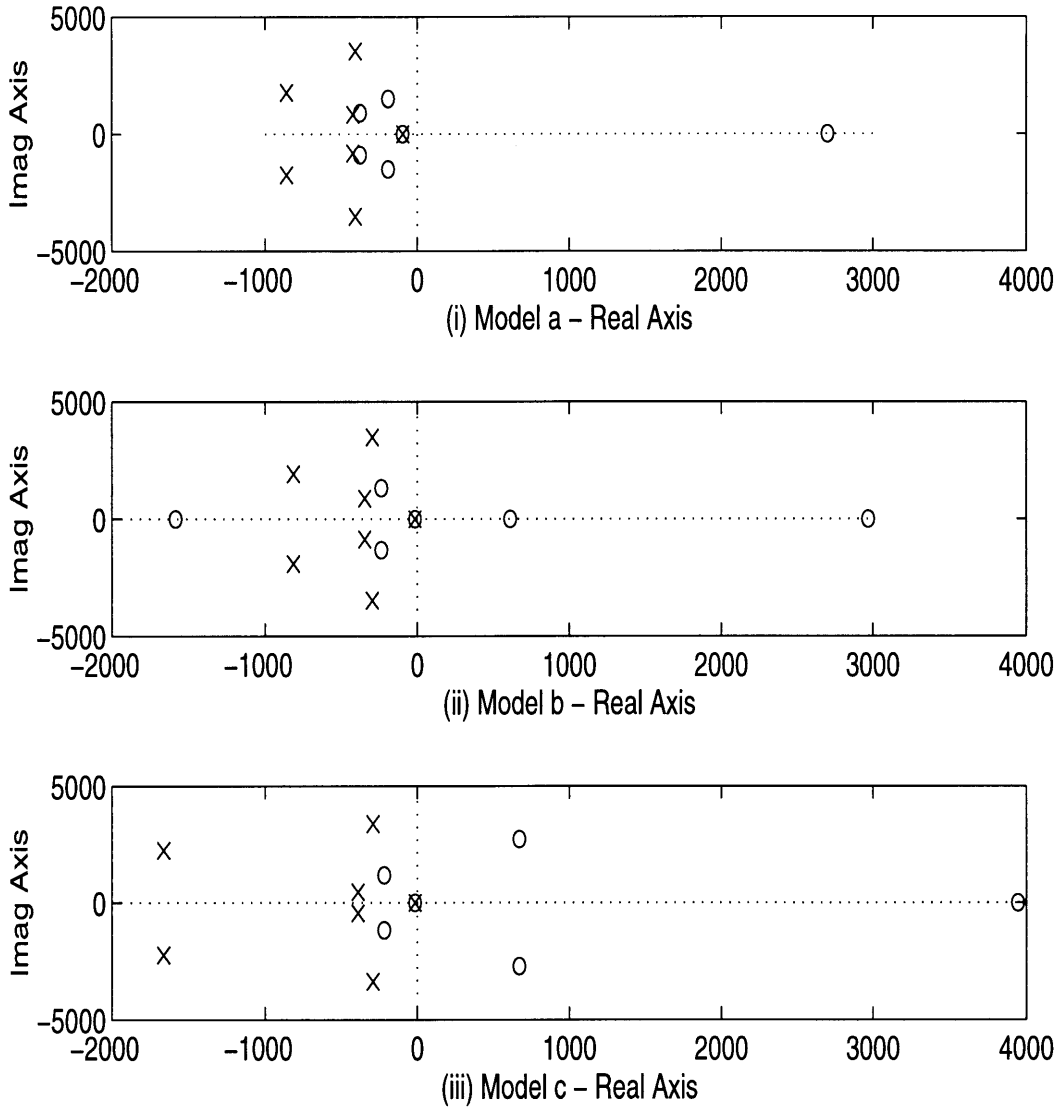

Figure 4-16: Pole-zero plots of the LQG controller designed using (i) "Model a", (ii) "Model b", and (iii) "Model c" with C/D configuration.

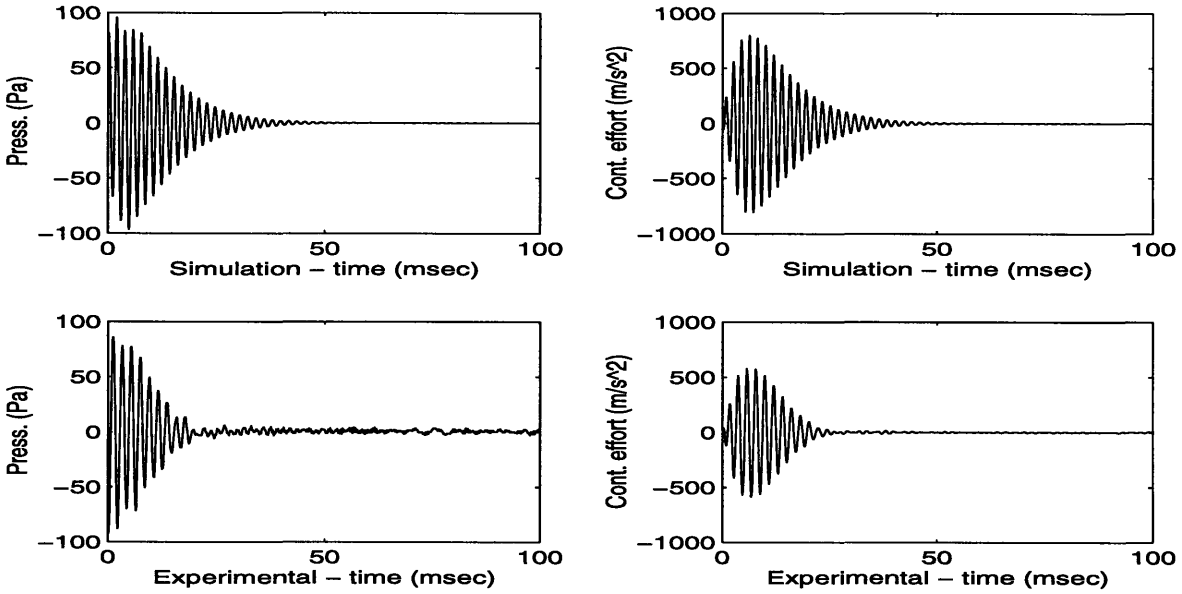

Figure 4-17: Pressure response and control input for a side-mounted loudspeaker with D/D configuration and LQG control: Simulation and experimental results for controller designed using "Model a"

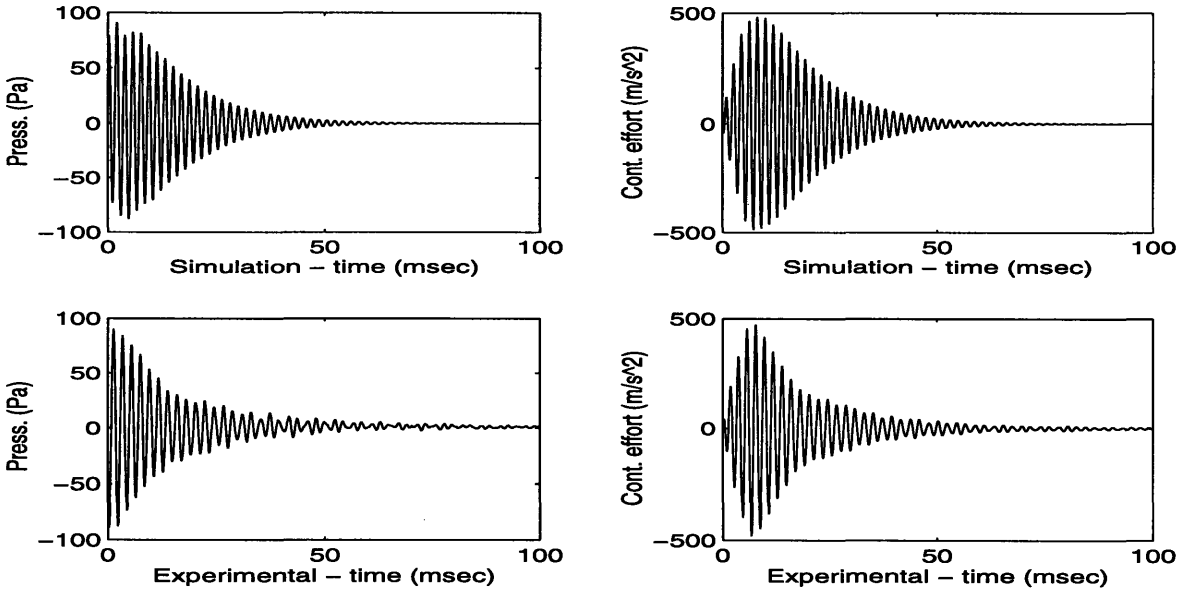

Figure 4-18: Pressure response and control input for a side-mounted loudspeaker with D/D configuration and LQG control: Simulation and experimental results for controller designed using "Model b"

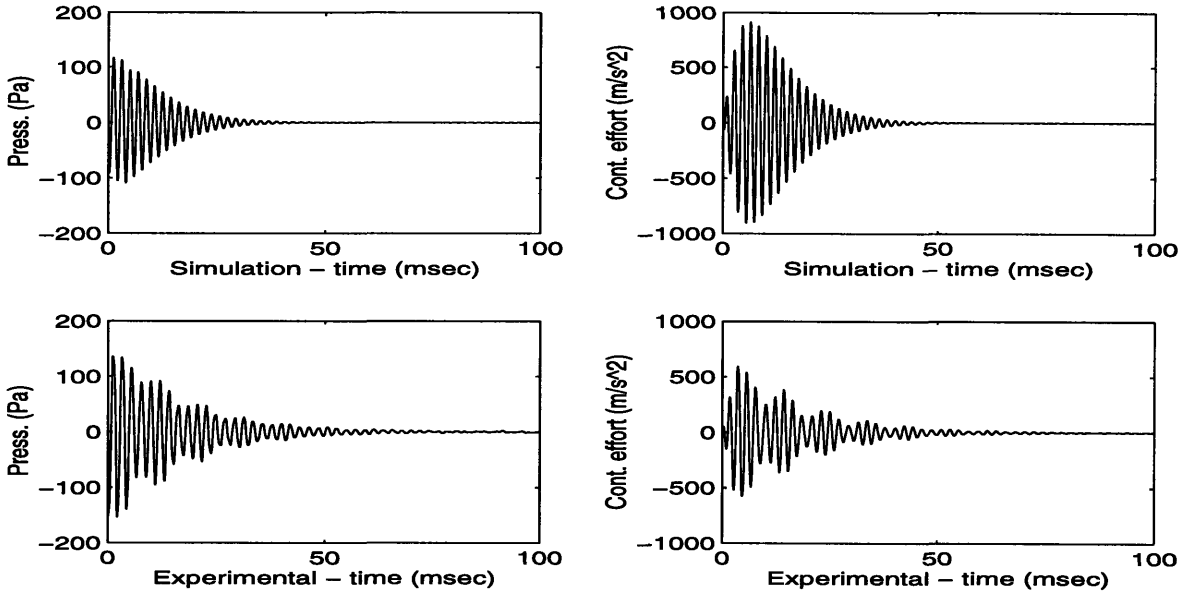

Figure 4-19: Pressure response and control input for a side-mounted loudspeaker with C/D configuration and LQG control: Simulation and experimental results for controller designed using "Model a"

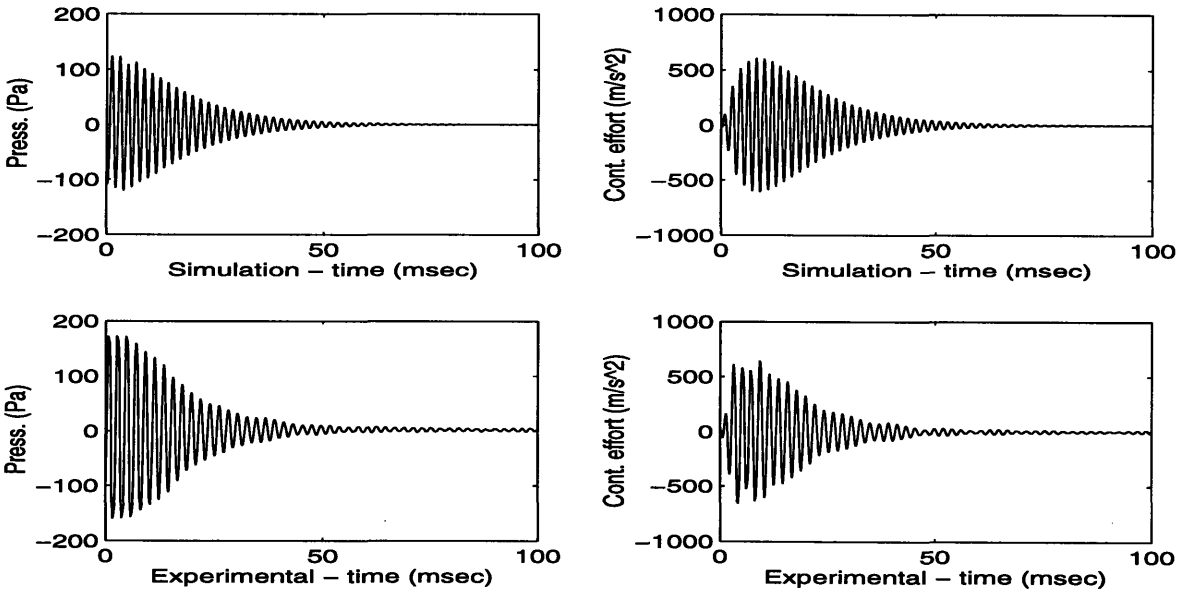

Figure 4-20: Pressure response and control input for a side-mounted loudspeaker with C/D configuration and LQG control: Simulation and experimental results for controller designed using "Model b"

Perhaps an explanation is that when the actuator and sensor are collocated at D/D, the controller is robust to modeling errors, an observation which is further verified in Section 4.4, and the dominant influence comes from the location of this zero pair. As this zero pair becomes less nonminimum phase, the settling time becomes faster. The best performance occurs for "Model a", where this zero pair is actually minimum phase.

The location of the actuator and sensor plays a critical roll in the performance of the controllers for various models. When the actuator and sensor are both at D, the controllers are much more robust to modeling errors than if the sensor were placed at C. I speculate that the reason for this is two-fold. The first factor is if the actuator and sensor are collocated or not. When the actuator and sensor are not collocated, modeling errors are compounded by the fact that control is not applied at the same location where the pressure is measured. The second factor is how nonminimum phase the zero pair for the uncontrolled combustion system is. For configurations where this zero pair is more nonminimum phase (such as C/D), the task of controlling the system become more challanging and dependent on the accurateness of the model. These factors explain why the performance of the controller for the C/D configuration is a function of model accurateness, while for the D/D configuration it is dependent on the location of the controller zeros.

4.4 Robustness of the LQG Controller

4.4.1 One Acoustic Mode Model

For the combustion system under consideration, it is the second acoustic mode which is the unstable one. One question which should be asked is how important is the consideration of other acoustic modes in the model. The flame dynamics are such that the flame acts like a low pass filter, reducing the importance of acoustic modes higher than the unstable one. The importance of including the first mode may be significant, however. The goal is to eliminate the thermoacoustic instability in the

combustion system. This implies that not only should the unstable frequency be stabilized, but the controller should be such that no new frequencies are excited. The LQG control design requires accurate information about the system to accomplish this task.

The effect of neglecting the first mode was studied for both the C/D and D/D configurations. The approach taken was to design an LQG controller as before, but with a model considering only the unstable mode. This controller was then simulation on the one-mode model, the two-model model, and tested experimentally on the bench-top combustor rig.

For the D/D configuration, the LQG controller designed based on the one mode model with $\rho = 0.01$ and $\mu = 0.001$ suppressed the instability on this model with a settling time of 28 milliseconds as shown in Figure 4-21(i). When simulated on the two mode model, the settling time was approximately the same, but the control effort required increased slightly as shown in Figure 4-21(ii). The results of this controller on the experimental combustor are shown in Figure 4-21(iii), which indicates that the settling time increases to 65 milliseconds This increase in settling time is due to the fact that the control effort required exceeds the limitations of the system (observe the saturation of the control effort at $600m/s^2$ for the first 20 milliseconds in Figure 4-21(iii)). Simulations were also done by decreasing ρ and μ with similar results. The one mode LQG controller resulted in a similar settling time on both the one mode model and the two mode model, but the control effort required increased for the two mode model. These controllers were not be tested experimentally because of the amount of control effort which they required.

The inclusion of the first acoustic mode proved to be more significant for the non-collocated actuator a sensor configuration, C/D. The LQG controller designed based on the one mode model with $\rho = 0.01$ and $\mu = 0.001$ predicted a settling time of 23 milliseconds when simulated on the one mode model as shown in Figure 4-22(i). Figure 4-22(ii) shows that when the controller was simulated on the two mode model, the settling time increased to 65 milliseconds Experimentally the controller resulted in a settling time of 79 milliseconds as shown in Figure 4-22(iii). Simulations

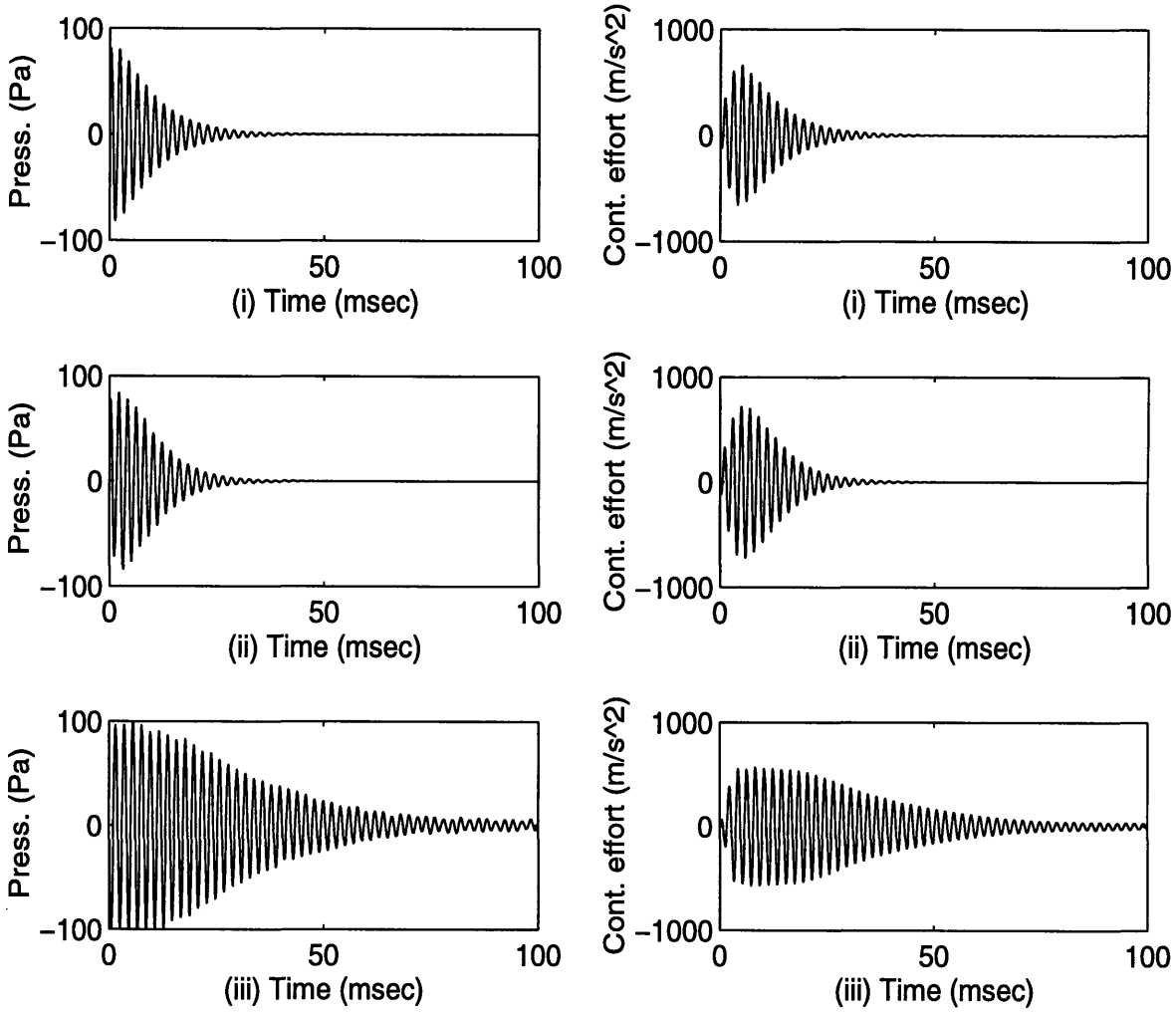

Figure 4-21: Pressure response and control input for one mode LQG controller with D/D configuration, $\rho = 0.01$ and $\mu = 0.001$: (i)Simulation results on one mode model, (ii) Simulation results on the two mode model, and (iii) Experimental results

completed with the LQG controller designed using smaller ρ and μ indicated that the discrepancy between the settling times on the one and two mode models increased as the values of ρ and μ decreased. While the controller on the one mode model became faster, on the two mode model the settling time increased until the controller was unable to suppress the instability. Figures 4-23(i) and 4-23(ii) show simulation results of an LQG controller designed based on the one mode model with $\rho = 0.002$ and $\mu = 0.0002$ on the one mode and two mode models, respectively. While the settling time is 10 milliseconds for the one-mode model, the pressure oscillations blow up on the two mode model, with a new frequency of 130 Hz being excited. This controller could not be tested experimentally because of the amount of control effort required. Close agreement between the two mode model and the experiment in other tests, however, builds confidence in its ability to predict the experimental results.

Simulation and experimental results indicate the importance of including both the first acoustic mode as well as the unstable one in the combustion system model. Implications of neglecting the first acoustic mode will vary from decreased controller performance (longer settling time or larger control effort) to the excitation of a new resonant frequency in the system, depending on the actuator and sensor configuration. Including the first two acoustic modes in the model allows the LQG controller to be optimized to achieve higher performance at less cost than if the first mode was neglected.

4.4.2 Acoustic Mode Coupling

One advantage of the MIT model is that it includes the linear coupling between the acoustic modes. Traditional analysis of combustion instability has been based on the assumption that this coupling is insignificant. In [16] it is shown theoretically that neglecting linear coupling in active control design can lead to serious errors, depending on the actuator and sensor location. The effect of the linear coupling on the control design for the two actuator sensor configurations used in testing on the bench-top combustor is illustrated in this Section.

An LQG controller was designed based on a model which neglected linear coupling

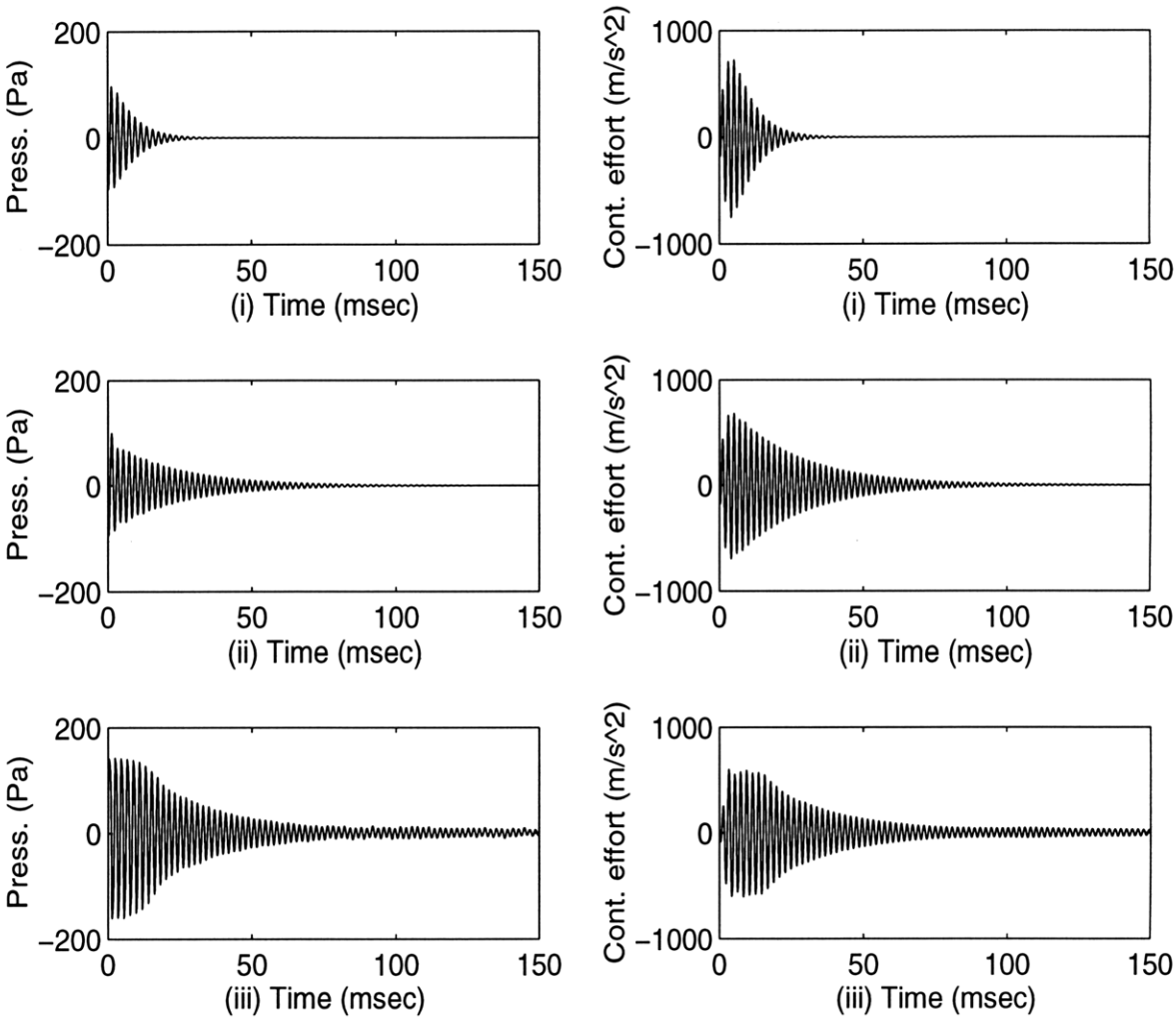

Figure 4-22: Pressure response and control input for one mode LQG controller with C/D configuration, $\rho = 0.01$ and $\mu = 0.001$: (i)Simulation results on one mode model, (ii) Simulation results on the two mode model, and (iii) Experimental results

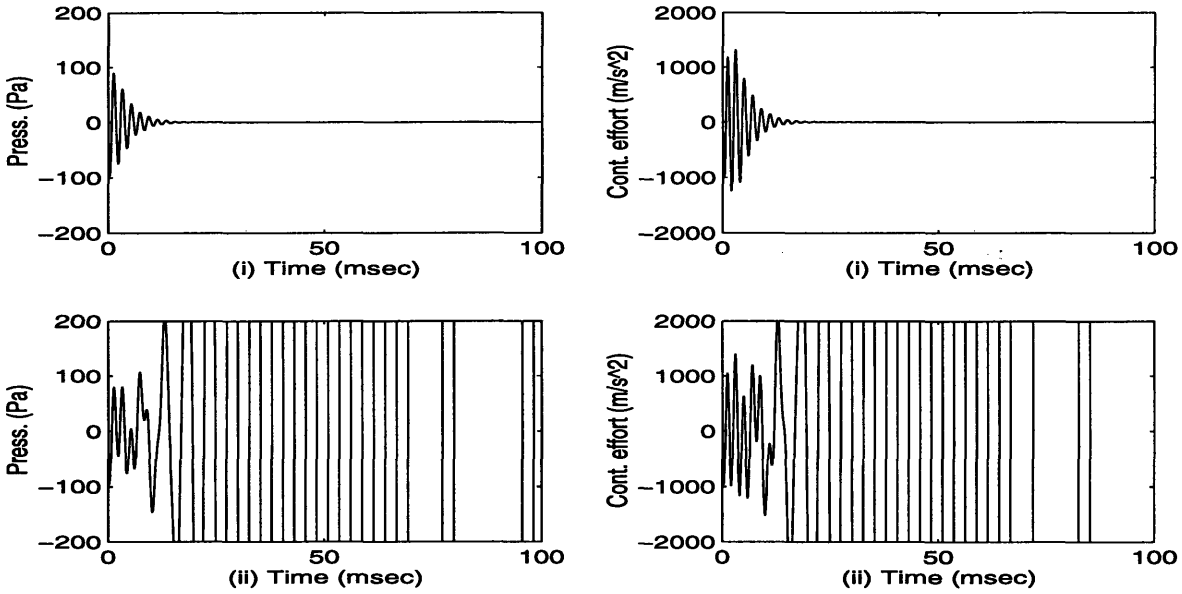

Figure 4-23: Pressure response and control input for one mode LQG controller with C/D configuration, $\rho = 0.002$ and $\mu = 0.0002$: (i) Simulation results on one mode model and (ii) Simulation results on two mode model

and simulated on the model without coupling, the model with coupling, and tested on the bench-top combustor. For the D/D configuration, an LQG controller with $\rho = 0.01$ and $\mu = 0.001$ resulted in a settling time of 27 milliseconds on the model without coupling, as shown in Figure 4-24(i). When this controller was simulated on the model with linear coupling, the settling time increased to 36 milliseconds and the control effort required also increased as seen in Figure 4-24(ii). Experimentally, however, it was observed that the settling time for this controller increased to 72 milliseconds, as seen in Figure 4-24(iii). This additional increase in settling time is due to the limitation on the control effort in the experimental system as the saturation of the control effort over the first 20 milliseconds in Figure 4-24(iii) illustrates.

The effect of mode coupling on the control design with the C/D configuration was also analyzed. An LQG controller was designed based on the combustion model which neglected coupling with $\rho = 0.015$ and $\mu = 0.0015$. Simulation on the model with no coupling predicted a settling time of 30 milliseconds as seen in Figure 4-25(i). When the controller was simulated on the model with linear mode coupling, the settling

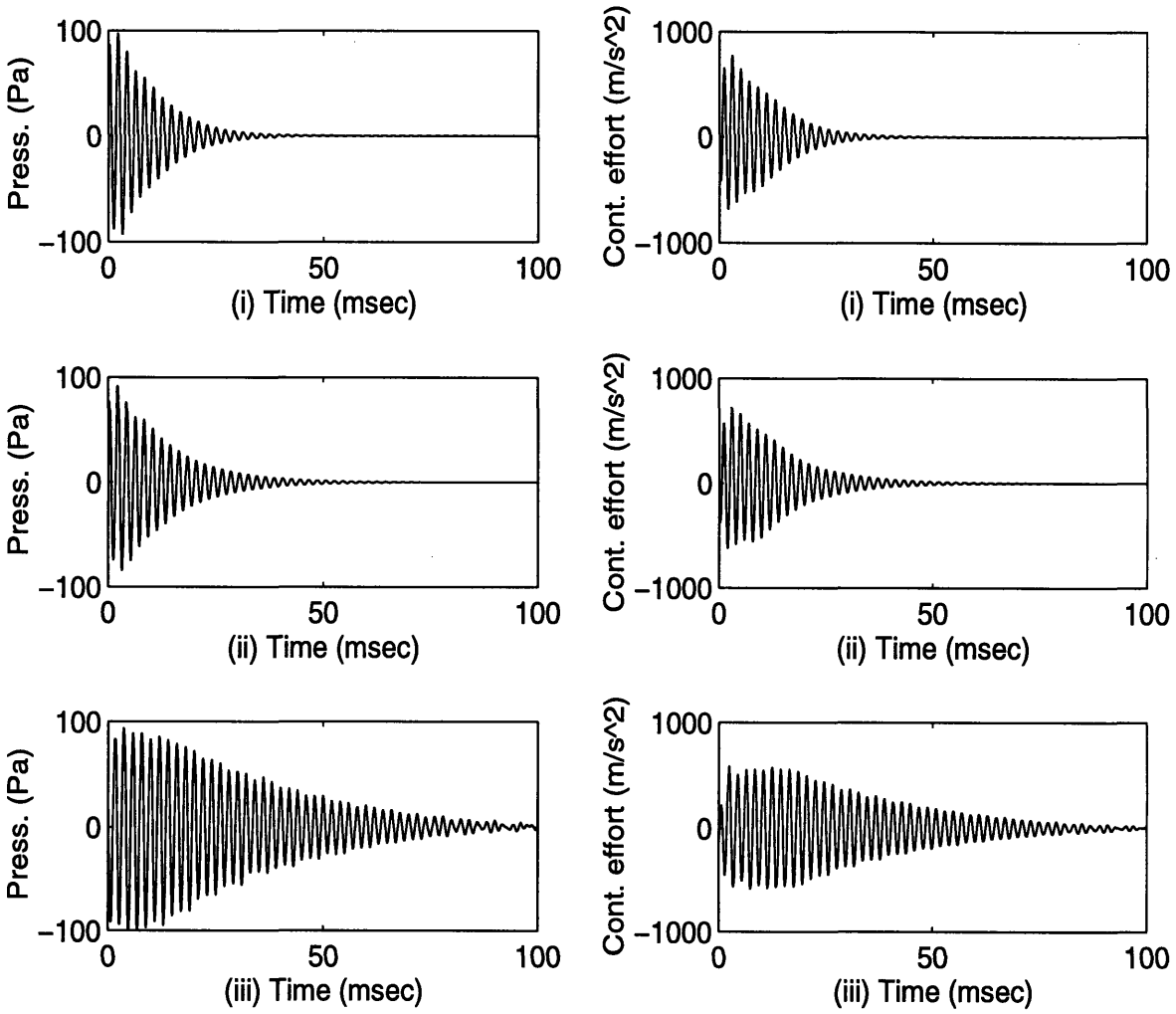

Figure 4-24: Pressure response and control input for LQG controller designed based on model with no coupling and D/D configuration, $\rho = 0.01$ and $\mu = 0.001$: (i) Simulation results on model with no coupling, (ii) Simulation results on model with coupling, and (iii) Experimental results

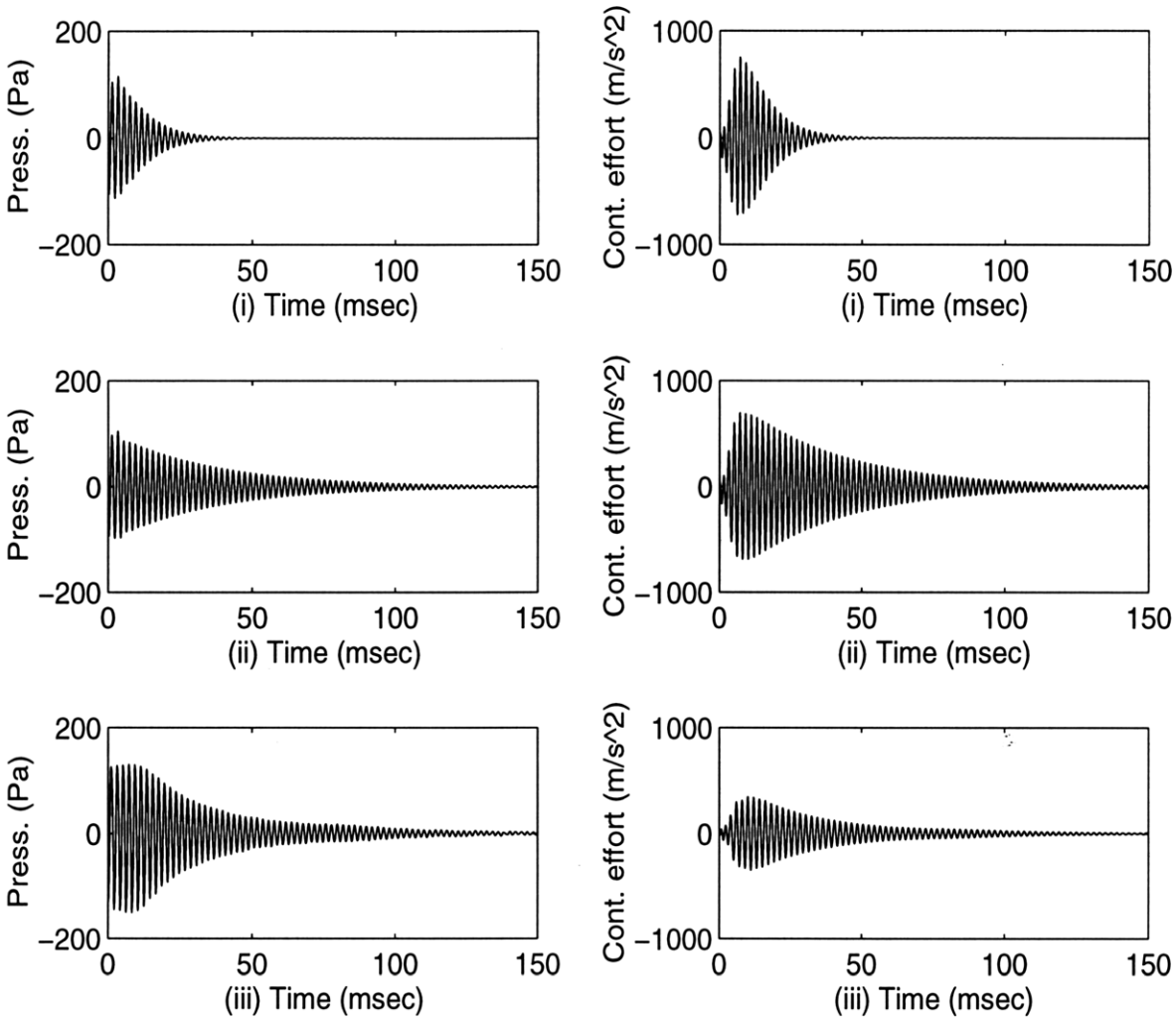

Figure 4-25: Pressure response and control input for LQG controller designed based on model with no coupling and C/D configuration, $\rho = 0.015$ and $\mu = 0.0015$: (i) Simulation results on model with no coupling, (ii) Simulation results on model with coupling, and (iii) Experimental results

time increased to 108 milliseconds (see Figure 4-25(ii)). Experimental results for the controller, shown in Figure 4-25(iii), agreed closely with the simulation on the model with coupling and resulted in a settling time of 95 milliseconds Simulations were also completed with varying ρ and μ for the LQG control design. For the C/D configuration, decreasing ρ and μ below a certain value resulted in a controller that stabilized the system modeled without coupling, but was unable to stabilize the system with coupling. Figures 4-26(i) and (ii) show simulation results on the model without coupling and with coupling, respectively, for an LQG controller designed neglecting coupling with $\rho = 0.002$ and $\mu = 0.0002$.

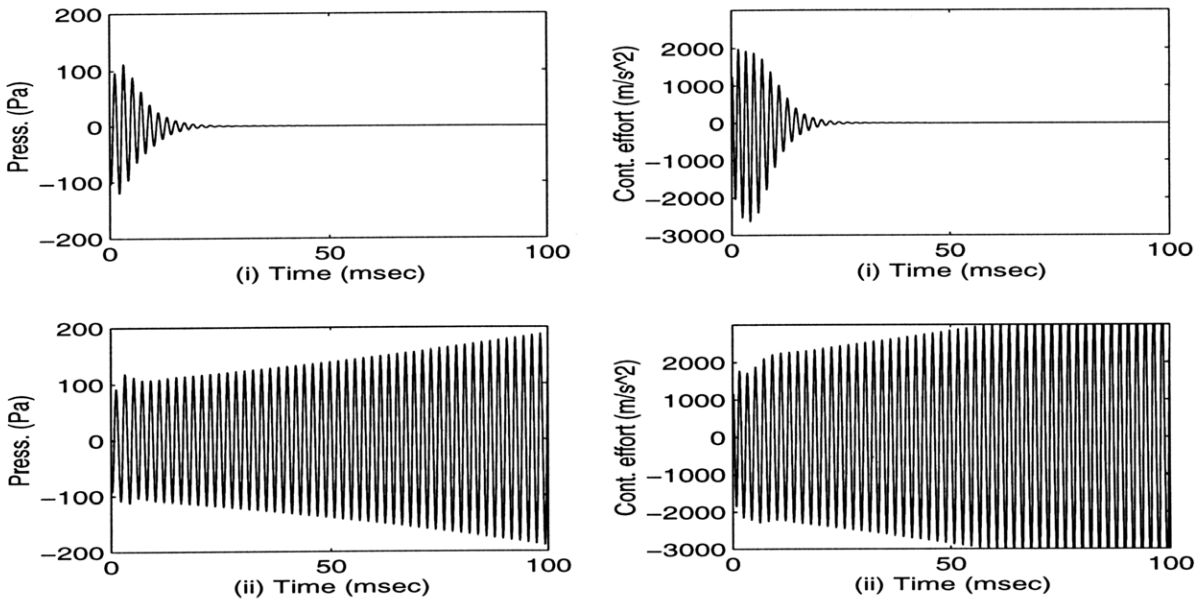

Figure 4-26: Pressure response and control input for LQG controller designed based on model with no coupling and C/D configuration, $\rho = 0.002$ and $\mu = 0.0002$: (i) Simulation results on model with no coupling and (ii) Simulation results on model with coupling

These results indicate that the inclusion of acoustic mode coupling is important in model development and control design. While neglecting this coupling may have minimal impact on the model of the uncontrolled system, it can have a significant effect on the LQG control design. For certain actuator-sensor configurations, the ability of the LQG controller designed using a model which neglects mode coupling to suppress the unstable frequency cannot be guaranteed. Even for actuator-sensor configurations in which the controller designed based on the model neglecting coupling suppresses the instability, such as for D/D, the performance of the controller is decreased over that predicted by the simulation.

4.4.3 Parameter Perturbation

Several assumptions were made in developing the model of the continuous combustion process. In addition, parameters such as θ, which accounts for the effect of the velocity behind and ahead of the flame, ϵ, which accounts for the increase in the flame diameter beyond the perforation diameter, S_u, the laminar burning velocity,

T_h, the temperature in the hot section which effected the effective length of the combustor, ζ, used to account for passive damping in the combustion system, and even the acoustic length, L, are uncertain. For this reason, a parametric study which perturbed these parameters was conducted in order to determine the effect on the model-based LQG controller. Perturbations of these parameters by 20% were made and the effect on the ability of the model-based LQG controller to suppress the instability experimentally studied. The most critical parameter appears to be T_h, the temperature in the hot section. When this value was increased by 20%, the settling time for the LQG controller with C/D configuration increased to 120 milliseconds Changing T_h had a more significant effect than changing L directly. Changing T_h has a direct effect on both the unstable frequency and also on the growth rate because the position of the flame relative to the length of the combustor shifts. Changing L would have a similar, but not as dramatic an effect because the variation is in the entirely length, not just the hot section, and the shift in the flame position is smaller. Cases in which T_h cannot be measured with reasonable accuracy may call for an adaptive control strategy. All other parameter perturbations led to a settling time of between 23 and 36 milliseconds, close to that observed with the original model.

The robustness of the LQG controller to the equivalence ratio was tested by changing ϕ on-line in the experiment by varying the fuel flow rate. The controller provides a robust performance over all values of $\phi \in [0.55, 0.74]$ even though the uncontrolled model and the experiment differed in the stability behavior for $\phi < 0.68$.

Chapter 5

Nonlinearities in Thermoacoustic Instabilities and Linear Control

5.1 A Low-order Nonlinear Model of Thermoacoustic Instability

Experimental observations of thermoacoustic instability clearly indicate the strong presence of nonlinearities, whose effect is a stabilizing one. The dynamic behavior in these problems are typically of the form of exponentially diverging oscillations which transition to a limit-cycle behavior. The linear model of Chapter 2 has been shown to capture the divergent aspects, and obviously not the latter effect. In this section, extensions to this linear model that capture nonlinear mechanisms that may be responsible for the limit-cycle are proposed.

Nonlinearities can occur in both the acoustic and heat release subsystems of the combustion process. The dominant nonlinearities which lead to the limit-cycle behavior, however, occur in the heat release dynamics. The focus, therefore, is on the heat release dynamic model in Eq. (2.12) which implies that the heat release rate changes linearly with velocity. In actual flames, however, as the velocity increases there appears to be different mechanisms that introduce a nonlinear effect on the heat release [22, 29, 20]. Three different, hypothetical, low-order nonlinear models

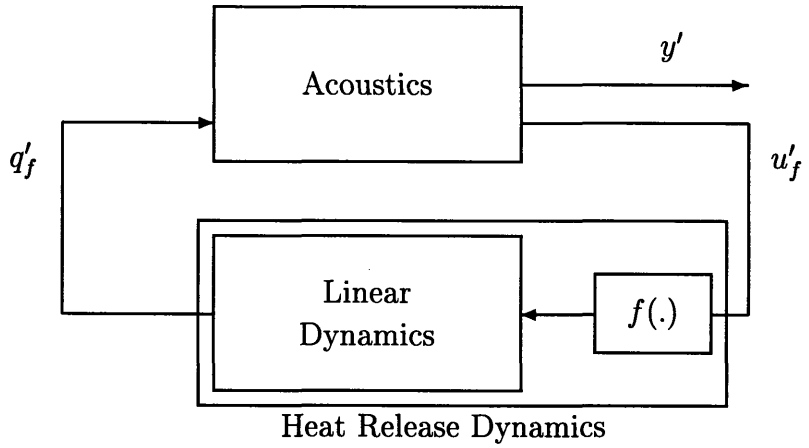

Figure 5-1: Low Order Nonlinear Model of Thermoacoustic Instability

are presented in this chapter that capture these mechanisms. In each of these models, a nonlinear component is added between the unsteady velocity component and the unsteady heat release rate as shown in Figure 5-1.

The complete nonlinear model can be described by the equations

$$\begin{aligned} \ddot{\eta}_i + 2\zeta\omega_i \dot{\eta}_i + \omega_i^2 \eta_i &= b_i \dot{q}'_f + b_{c_i} \dot{v}_a \\ \tilde{u}'_f &= \sum_{i=1}^{n} (c_i \dot{\eta}_i) + \alpha_r v_a \\ \dot{q}'_f + b_f q'_f &= \omega_f g_f f(\tilde{u}'_f) \end{aligned} \tag{5.1}$$

and more compactly, in operator form, as

$$\begin{aligned} \tilde{u}'_f &= G(s)[u'_n] \\ u'_n &= -f(\tilde{u}'_f) \end{aligned} \tag{5.2}$$

where $b_f = \omega_f(1 - \theta a_0 g_f)$, and $\tilde{u}_f = u_f$ with $\theta = 0$ and can be considered as the equivalent flow velocity at x_f. The goal is to evaluate the conditions on f under which the nonlinear model in (5.2) generates limit-cycles.

Broadly speaking, the limit-cycle behavior can occur in a feedback system as in (5.2) due to one of two mechanisms. The first concerns a change in the phase between $\tilde{u}'_f$ and q'_f, while the second is a change in the gain between these two quantities. Of

the three models presented in the sections to follow, the first and the second pertain to limit-cycle dynamics due to the change in the phase and in the gain, respectively. The third model shows the limit-cycle behavior that ensues from a combination of both gain and phase change. All three models are analyzed using the describing function method and are shown to result in a limit-cycle behavior.

In order to verify the predictive ability of limit-cycles in the numerical studies of the proposed models, the 1 kW bench-top combustor rig used for the experimental work in Chapter 4 is chosen as a basis for the model. The linear model was simulated using information from the bench-top combustor rig considering the first two acoustic modes and the following parameters:

$$\begin{aligned} L = 0.62m,\ \ \gamma = 1.4,\ \ \bar{p} = 1atm,\ \ \bar{c}_1 = 347m/s,\ \ \bar{c}_2 = 485, \bar{M} = 3.612 \times 10^{-4}, \\ \rho_u = 1.163kg/m^3,\ \ \Delta q_r = 2.26 \times 10^6 J/kg,\ \ \phi = 0.74,\ \ S_u = 0.3m/s \\ \theta = 0.5,\ \ \epsilon = 2.0,\ \ d_p = 1.5 \times 10^{-3}m,\ \ D = 0.053m,\ \ n_f = 80. \end{aligned} \tag{5.3}$$

The choice of these values follows directly from the geometry and fuel properties.

The goal is to carry out a comparison with the nonlinear model in (5.1) and the experimental results. As shall be shown in the following sections, the model in (5.1) with different nonlinear mechanisms in f is capable of producing limit-cycles. Numerical simulations are also carried out by replacing the linear finite-dimensional acoustic model in (2.9) and (2.10) with the linear PDE model of the combustor acoustics as in (2.4) and (2.5) and the flame model in (2.6).

5.1.1 Nonlinear Model 1: Phase Change Mechanisms

Suppose the nonlinearity $f = f_1$ where

$$f_1(u) = c_1 u - c_2 u^3 \tag{5.4}$$

where c_1 and c_2 are positive. The describing function method can be used as an approximate tool for analyzing the resulting feedback system in (5.2) [28]. For f_1 in

(5.4), the describing function is of the form

$$N_{f_1}(A) = c_1 - \frac{3}{4}c_2 A^2 \tag{5.5}$$

where A is the amplitude of the sine wave entering the nonlinear block. Noting that the describing function analysis predicts the limit-cycle behavior when $G(j\omega) = -1/(N(A))$, where $G(j\omega)$ is the linear plant transfer function, the form of (5.5) suggests that for any unstable G, if $c_1 \leq 1$, then there is always an amplitude A at which the limit-cycle will occur. This is because the Nyquist plot of $G(j\omega)$ intersects the negative real axis to the left of $(-1, 0)$. Numerical simulations of the nonlinear model in (5.4) with the linear parameters as in (5.3), and setting $\zeta = 0.008$, $c_1 = 1$, and $c_2 = 10$, led to a Nyquist diagram and describing function as shown in Figure 5-2 and a limit-cycle in the pressure oscillations as shown in Figure 5-3, which is similar to the response obtained experimentally shown in Figure 4-3(ii). As can be observed in these two figures, the growth rate and amplitude of the pressure at the limit-cycle were similar, although the time taken to reach the limit-cycle was slightly longer in simulation than that observed experimentally. It was observed that the limit-cycle occurred for all values of ζ, $c_1 \leq 1$, and c_2. For example, increasing ζ resulted in a decrease in the amplitude of the pressure at the limit-cycle and an increased time to reach the limit-cycle, decreasing c_1 led to a decreased amplitude at the limit-cycle and an increased time to reach the limit-cycle, and increases in c_2 led to a decreased amplitude at the limit-cycle and a decrease in the time required to reach the limit-cycle. It is interesting to note that the describing function analysis is quite accurate in predicting the amplitude of the limit-cycle. The limit-cycle amplitude of the signal entering the nonlinear block can be computed from the value where the Nyquist plot and describing function intersect and was found to be 0.225 for the chosen nonlinearity. The actual amplitude of this signal at the limit-cycle in the simulations was 0.255.

A qualitative explanation for the generation of limit-cycle behavior with f can be given using the "gain" and "phase" characteristics of f near the unstable frequency

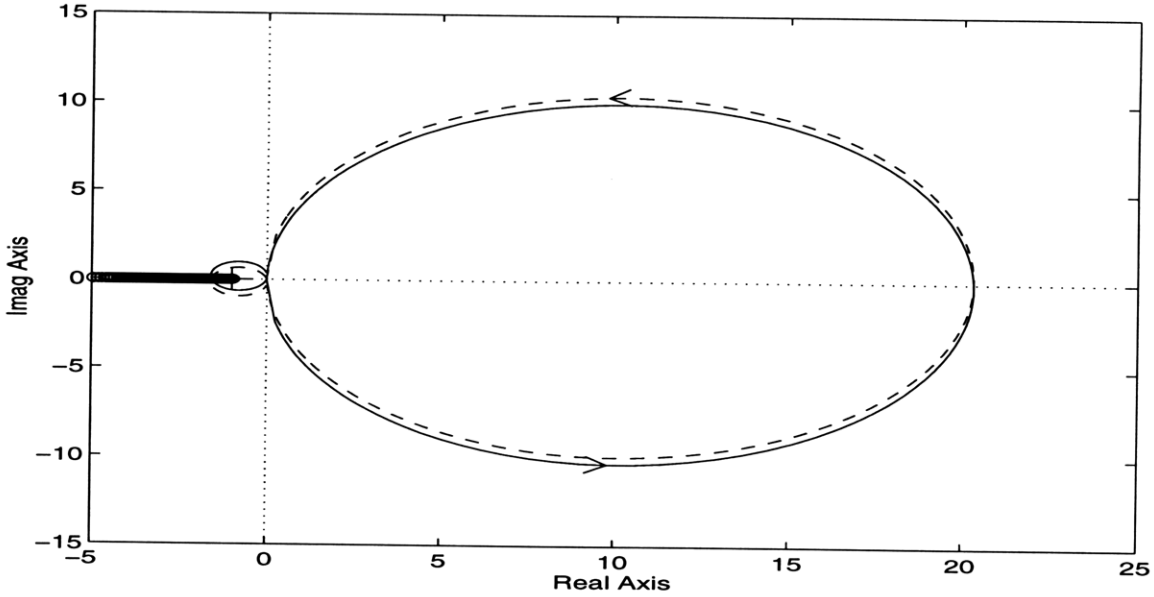

Figure 5-2: Nyquist diagram and describing function of combustor with f_1 (thin-line, dash - linear system Nyquist diagram; thick-line - describing function).

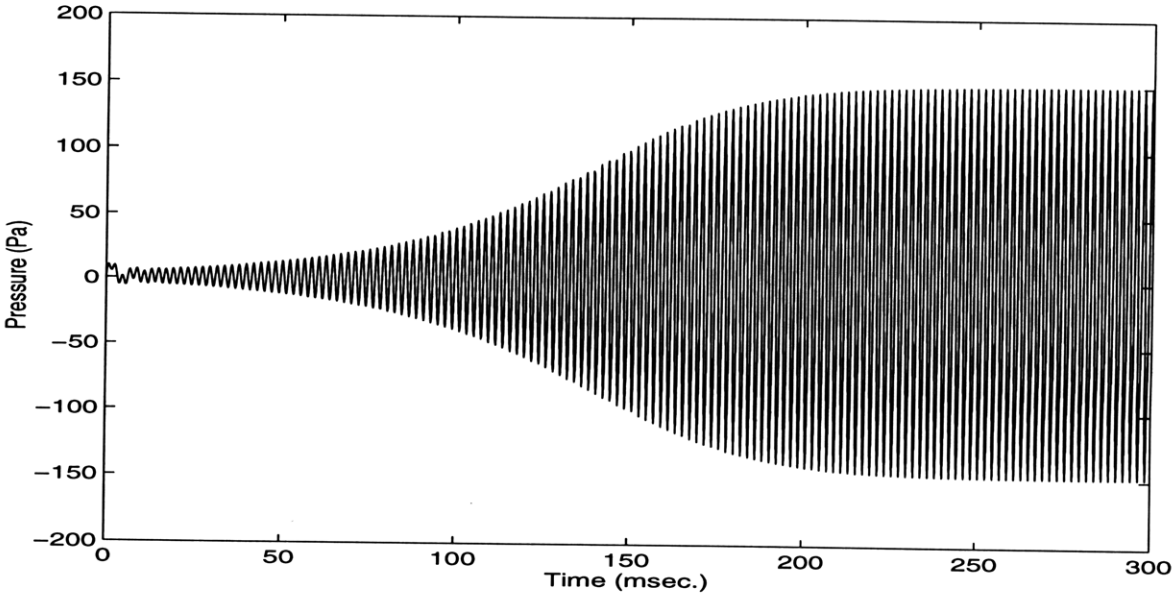

Figure 5-3: Pressure response for the simulation of the system with nonlinear component f_1.

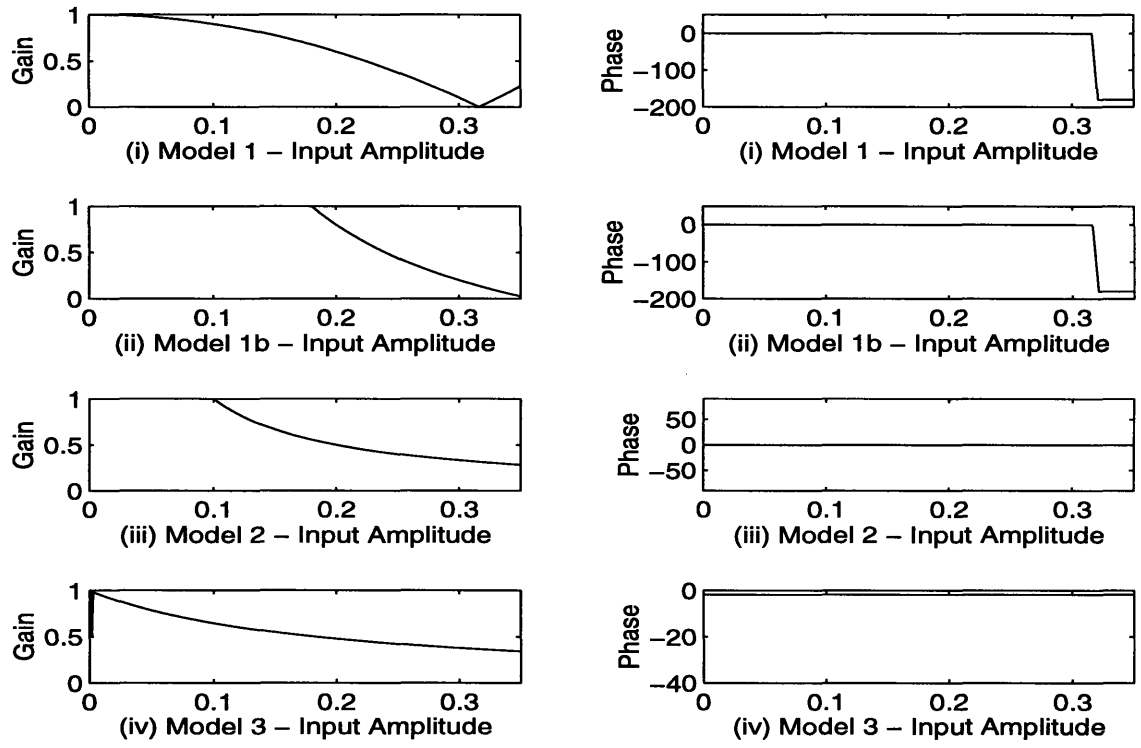

Figure 5-4: Gain (γ_o) and phase (ϕ_o) versus velocity amplitude for nonlinear models (i)f_1, (ii)f_{1b}, (iii)f_2, and (iv)f_3.

ω_u. Denoting $\gamma_o(f(u))$ and $\phi_o(f(u))$ as the "gain" and "phase" of f for $u = sin(\omega t)$, and defining

$$\gamma_o(f(u)) = \left|\frac{f(u)}{u}\right| \quad and \quad \phi_o(f(u)) = \left[\frac{\left|\frac{f(u)}{u}\right| - \frac{f(u)}{u}}{2\frac{f(u)}{u}}\right] 180^\circ \tag{5.6}$$

The plot of $\gamma_o(f_1(u))$ and $\phi_o(f_1(u))$ are shown in Figure 5-4. Suppose f in (5.2) is such that γ_o is a constant for all u and $\phi_o = 0^\circ$ for $|u| \leq u_o$ and $\phi_o = -180^\circ$ for $|u| > u_o$. Then, for all velocities with amplitudes less than u_0, the nonlinear transformation reduces to a positive constant c_1. That is, for amplitudes less than u_0, the model in (5.1) is linear and has unstable solutions, with the pressure p' and q'_f such that

$$\frac{1}{T}\int_0^T p'q'_f dt \;>\; 0 \tag{5.7}$$

For velocities with amplitudes greater than u_0, the value of $\phi_o(f_1)$ changes by -180° implying that at the same frequency, the heat release q'_f is equal and opposite to the values at small amplitudes of u'_f. That is, the Rayleigh criterion changes to

$$\frac{1}{T}\int_0^T p'q'_f dt \;<\; 0 \tag{5.8}$$

leading to "stability" of the closed-loop system thereby tending to reduce the amplitudes of all variables in the feedback loop. As the amplitude decreases, since $\phi_o(f_1)$ increases again to 0°, the overall system continues to toggle between an unstable and a stable mode, which can manifest as a limit-cycle. The above conclusions can be drawn even when $\gamma_o(f_1)$ changes slightly as a function of the amplitude of the input to f_1. Noting that the $\gamma_o - \phi_o$ characteristics of f_1 are as shown in Figure 5-4(i), it can be argued that it is the phase change mechanism in f_1 that is responsible for a limit-cycle behavior.

Other nonlinear functions exist which are similar to f_1 in that the limit-cycle

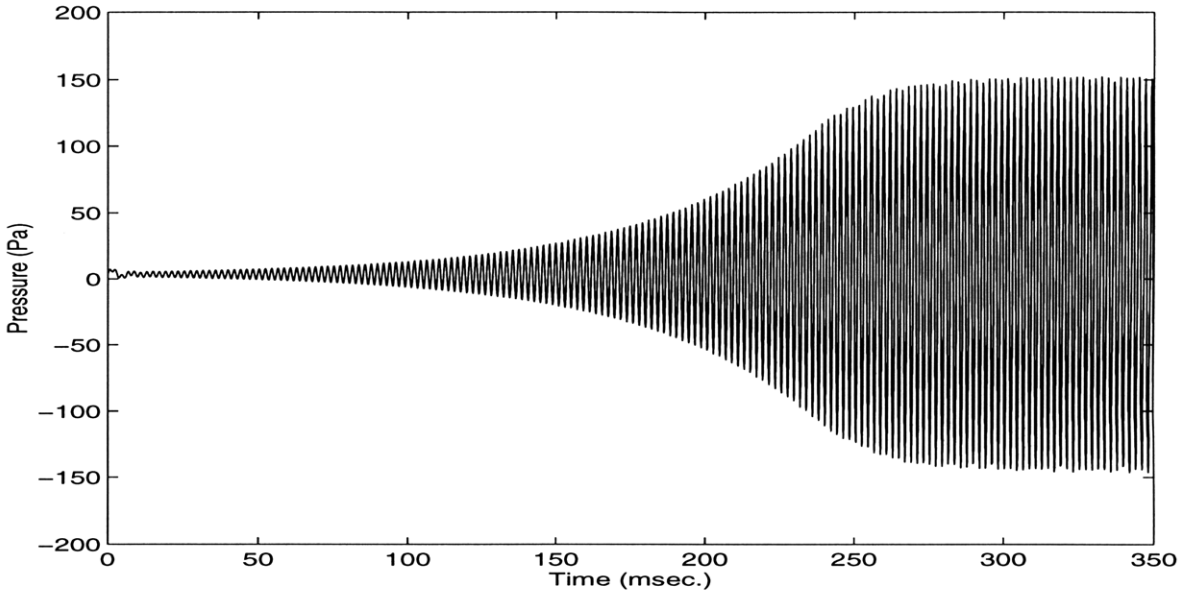

Figure 5-5: Pressure response for the simulation of the system with nonlinear component f_{1b}.

behavior is due to a change in phase. One such example is the nonlinearity f_{1b} where

$$\begin{aligned} f_{1b}(u) &= k_1 u && \text{if } |u| \leq u_0 \\ &= (k_1 + k_2)\, u_0 - k_2 u && \text{if } |u| > u_0 \end{aligned}$$

where k_1, k_2, and u_0 are positive. An analysis similar to that for f_1 can be carried out for this nonlinearity. The resulting pressure response with $\zeta = 0.01$ and $k_1 = 1$, $k_2 = 1$ and $u_o = 0.18$ is shown in Figure 5-5. The limit-cycle amplitude agrees with that observed experimentally, but the growth rate is somewhat smaller and hence it takes a longer time for the limit-cycle to be reached. The functions $\gamma_o(f_{1b})$ and $\phi_o(f_{1b})$ can be calculated as in (5.6) and shown in Figure 5-4(ii). The change in $\phi_o(f_{1b})$ from $0°$ to $-180°$ again occurs when the velocity reaches a certain level. As the velocity increases and decreases, $\phi_o(f_{1b})$ will toggle between $0°$ and $-180°$, resulting in the limit-cycle. Once again, perturbations in ζ, k_1 and k_2 resulted in the limit-cycle with similar trends to that for f_1.

The question that arises is whether phase change mechanisms similar to those exhibited in f_1 exist in premixed combustors. In [20], a physically-based nonlinear

PDE model of premixed laminar combustors was presented and was shown to result in a limit-cycle behavior. It was observed that this was achievable even with a linear acoustic model, and the nonlinearity, which was associated with the heat release dynamics, was such that the phase between u' and q'_f changed from $0°$ to $-180°$ for large amplitudes of q'_f. This change in phase is due to the fact that at small amplitudes the low velocity levels result in heat release which is dominated by propagation, while at higher amplitudes, the high velocity leads to a heat release which is dominated by advection. This suggests that such phase change mechanisms could represent one class of nonlinearities that generates a limit-cycle.

5.1.2 Nonlinear Model 2: Gain Change Mechanisms

Consider a nonlinearity of the form $f = f_2$ where

$$\begin{aligned} f_2(u) &= u \quad \text{if } |u| \leq u_0 \\ &= u_0 \quad \text{if } |u| > u_0 \end{aligned} \tag{5.9}$$

which introduces a saturation in the velocity. The describing function for this case is of the form

$$N(A) = \frac{2}{\pi}\left[sin^{-1}\left(\frac{u_0}{A}\right) + \frac{u_0}{A}\sqrt{1-\frac{u_0^2}{A^2}}\right]. \tag{5.10}$$

For similar reasons to those described for f_1, the nonlinearity in (5.9) can also be shown to lead to a limit-cycle for the model in (5.2) because for any value of u_o, $-1/N(A)$ intersects $G(j\omega)$ for some A. Numerical simulations of the nonlinear model in (5.9) with the linear parameters as in (5.3), $\zeta = 0.008$ and $u_o = 0.1$ led to a Nyquist diagram and describing function which was similar to that shown in Figure 5-2 and a limit-cycle in the pressure oscillations as shown in Figure 5-6. The growth rate for f_2 is less than that observed experimentally, and the time taken to reach the limit-cycle increases somewhat. Decreasing passive damping in f_2, however, led to an even larger discrepancy between simulation and experiment. It should be noted that

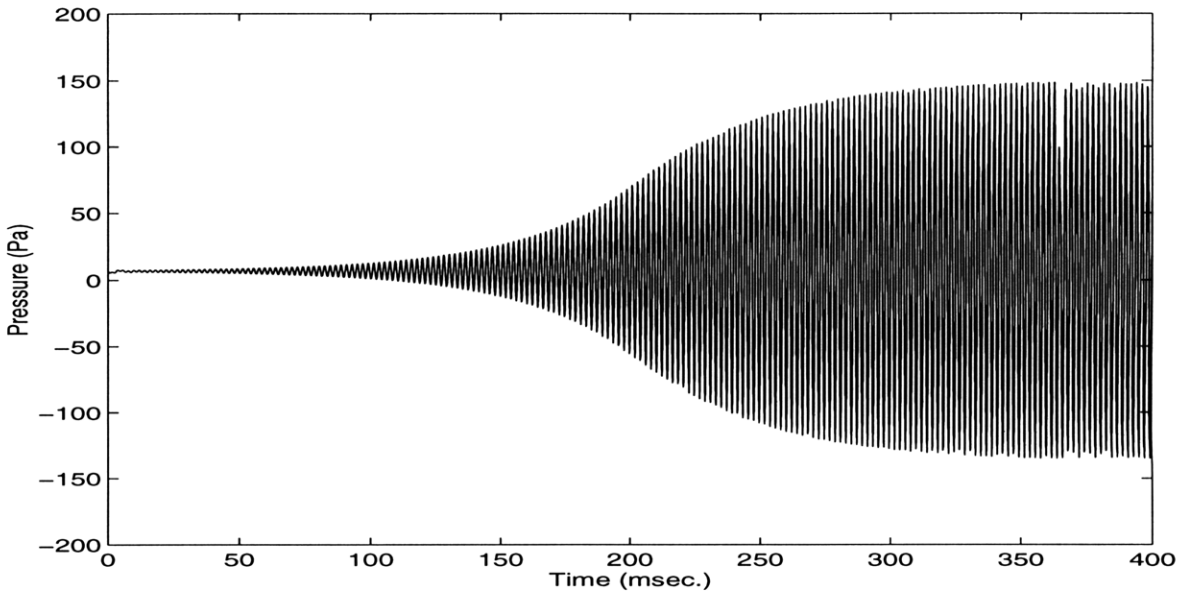

Figure 5-6: Pressure response for the simulation of the system with nonlinear component f_2.

the limit-cycle occurred for all values of ζ and u_o. Increasing ζ resulted in a decrease in the amplitude at the limit-cycle and an increase in the time taken to reach the limit-cycle. Decreasing ζ below a certain value, however, also resulted in a longer time to reach the limit-cycle, although the amplitude increased. Increasing u_o led to an increase in the amplitude of the limit-cycle and a slight increase in the time taken to reach the limit-cycle. Asymmetric saturation in f_2 was also observed to lead to limit-cycles.

Qualitatively, the limit-cycle can be explained using $\gamma_o(f_1)$ and $\phi_o(f_2)$ as in Section 5.1.1. For amplitudes smaller than u_0, the behavior of the nonlinear system (5.1) is identical to that of the linear system. At amplitudes larger than u_0, the fact that $\gamma_o(f_2)$ is smaller than unity implies that the nonlinear mechanism attenuates the signal; as u_0 increases, the attenuation becomes even stronger. This implies that at some amplitude larger than u_0, the amplification due to the linear instability mechanism is offset by the attenuation by a sufficient amount so as to prevent any further increase in the system variables. In particular, $\gamma_o(f_2) = 1.0$ for $|u| \leq u_o$, but decreases towards zero as $|u|$ becomes larger than u_o. It is this gain that results in the change

in the Raleigh criterion from a positive value to a negative value as in Section 5.1.1 and leads to the limit-cycle. The value of ϕ_o, on the other hand, remains constant at $0°$ for all values of u. The values of γ_o and ϕ_o for f_2 are shown in Figure 5-4(iii).

The physical basis for the presence of such a gain changing mechanism has been presented in [22] by Dowling, where the limit-cycle is attributed to a "saturation" effect in the heat release. In particular, it is argued that the lower saturation limit may occur due to the fact that the heat release rate is constrained to remain positive as the velocity becomes more negative; the upper saturation limit may be due to entrainment effects on the flame area. As mentioned earlier, the actual values of these two limits could differ and yet produce limit-cycles.

5.1.3 Nonlinear Model 3: Gain and Phase Change Mechanisms

Suppose that the nonlinear mechanism is such that both the gain and the phase of f changed with the amplitude of u, for example, for $f = f_3$, where

$$f_3\left(u(t)\right) = \frac{u\left(t-\tau\right)}{1+\epsilon|u\left(t-\tau\right)|}. \tag{5.11}$$

The corresponding describing function is such that the curve $-1/N(A)$ still intersects $G(j\omega)$ from right to left, and hence leads to the conclusion that there is a stable limit-cycle. Numerical simulations of the resulting nonlinear model in (5.11) with linear parameters as in (5.3), $\zeta = 0.008$, $\epsilon = 5.5$ and $\tau = 1.0 \times 10^{-5}$, resulted once again in a limit-cycle in the pressure oscillations as shown in Figure 5-7, which is again similar to the response in Figure 4-3(ii). Increasing ζ for f_3 had a similar effect as for f_1. Increasing ϵ decreased the amplitude of the pressure at the limit-cycle and resulted in a slight increase in the time taken to reach the limit-cycle. Modifying τ changed the amplitude of the limit-cycle and the time taken to reach the limit-cycle in some cases, while for other values it did not result in the limit-cycle behavior.

A combined set of arguments presented in Sections 5.1.1 and 5.1.2 can be given to justify the generation of limit-cycles. For this model, while the definition of $\gamma_o\left(f_3\left(u\right)\right)$

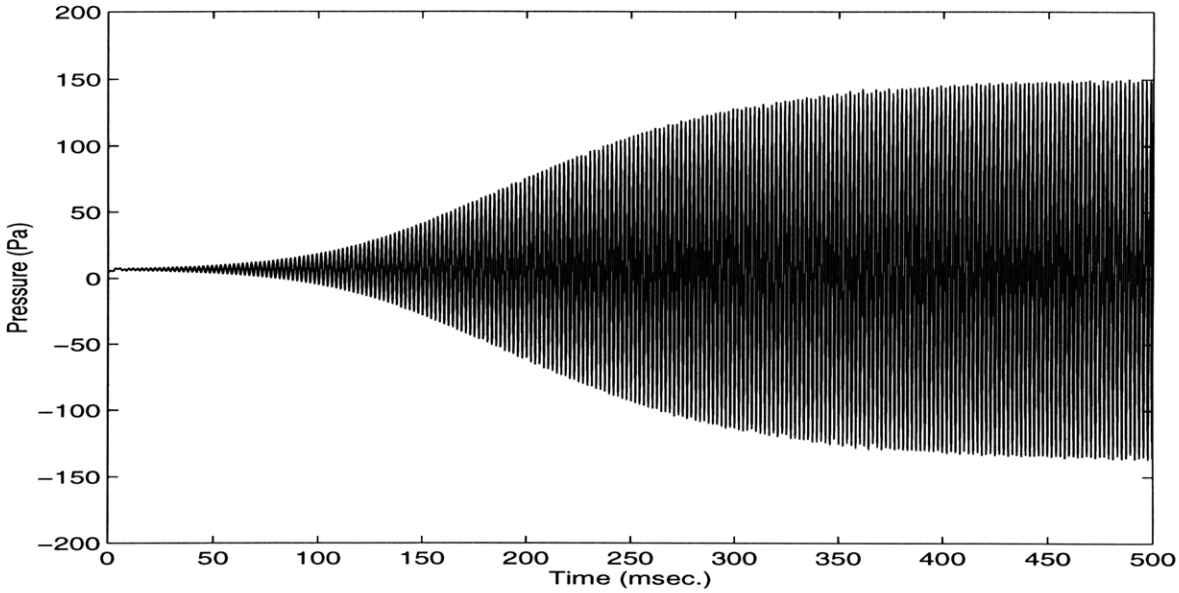

Figure 5-7: Pressure response for the simulation of the system with nonlinear component f_3.

remains the same as in (5.6), $\phi_o(f_3(u))$ is defined as

$$\phi_o(f_3(u)) = \left(\frac{\tau}{\omega}\right)(-360°) \tag{5.12}$$

to account for the presence of the time delay. For this model, both the value of $\phi_o(f_3)$ and the attenuation of $\gamma_o(f_3)$ introduce a stabilizing component at large amplitudes of the velocity. These changes can be seen in Figure 5-4(iv). As with f_1 and f_2, a qualitative explanation of why f_3 causes a limit-cycle to occur can be given in terms of the Raleigh criterion, which switches from positive to negative value when $|u| \geq u_0$.

The physical basis for this type of nonlinearity has been proposed in [29] in the context of a lean premixed gas turbine, where the nonlinearity is attributed to the mixing effects at the injection nozzle and the time-delay to convection. The algebraic nonlinearity in u introduces a smooth saturation effect whereas the time-delay introduces a phase change mechanism. It is well known that this type of nonlinearity will produce bands of τ's for which the limit-cycle occurs. In the simulation of f_3 it was found that the first and second bands of τ which gave the limit-cycle were $\tau \in (0, 4.3 \times 10^{-4})$ and $\tau \in (1.32 \times 10^{-3}, 5.64 \times 10^{-3})$, respectively. These bands

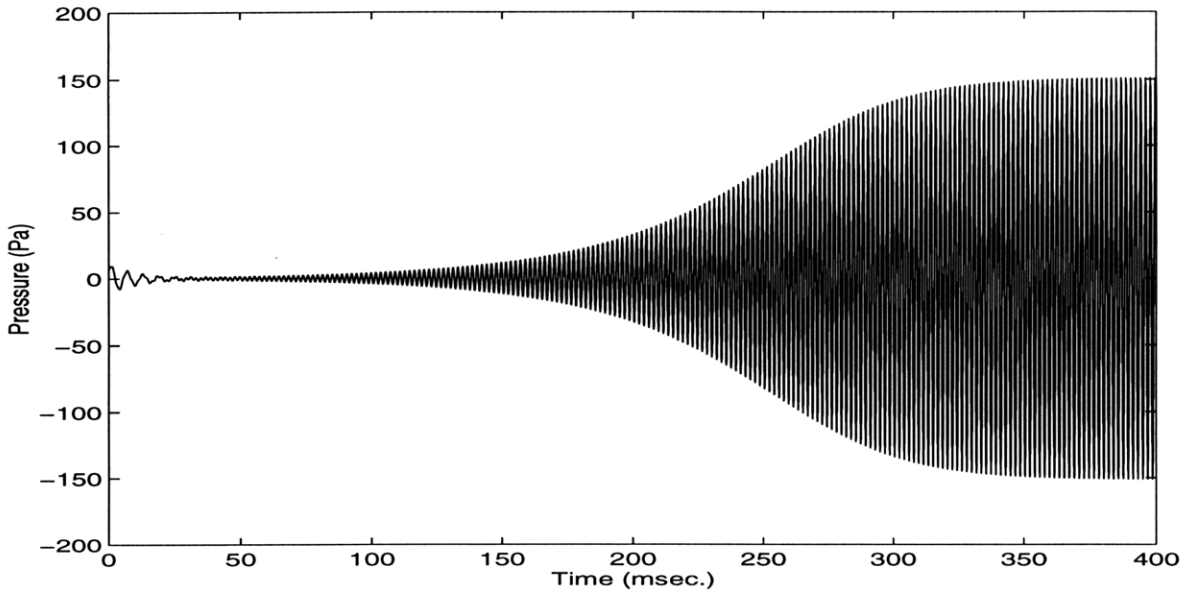

Figure 5-8: Pressure response for the PDE simulation of the system with nonlinear component f_1.

would continue as τ increased. Whether or not this type of nonlinear mechanism is responsible for the limit-cycle depends on if such a sensitivity to τ is supported by the experimental observations as well. It is also worth noting that such a sensitivity to τ implies that f_3 is not as robust as f_1, f_{1b}, and f_2, which produced a limit-cycle for all parameter perturbations.

Finally, it was noted that all of the above three nonlinearities gave rise to a similar limit-cycle behavior in simulation studies with the acoustic relations in (2.9) and (2.10) replaced by their linear PDE counterparts. The pressure plots for the PDE models including the nonlinearities f_1, f_2, and f_3 are shown in Figures 5-8-5-10, respectively.

5.2 Impact of Nonlinearities on Linear Model-Based Control

The motivation behind developing a dynamic model to represent the continuous combustion process was not only to understand thermoacoustic instability, but also to

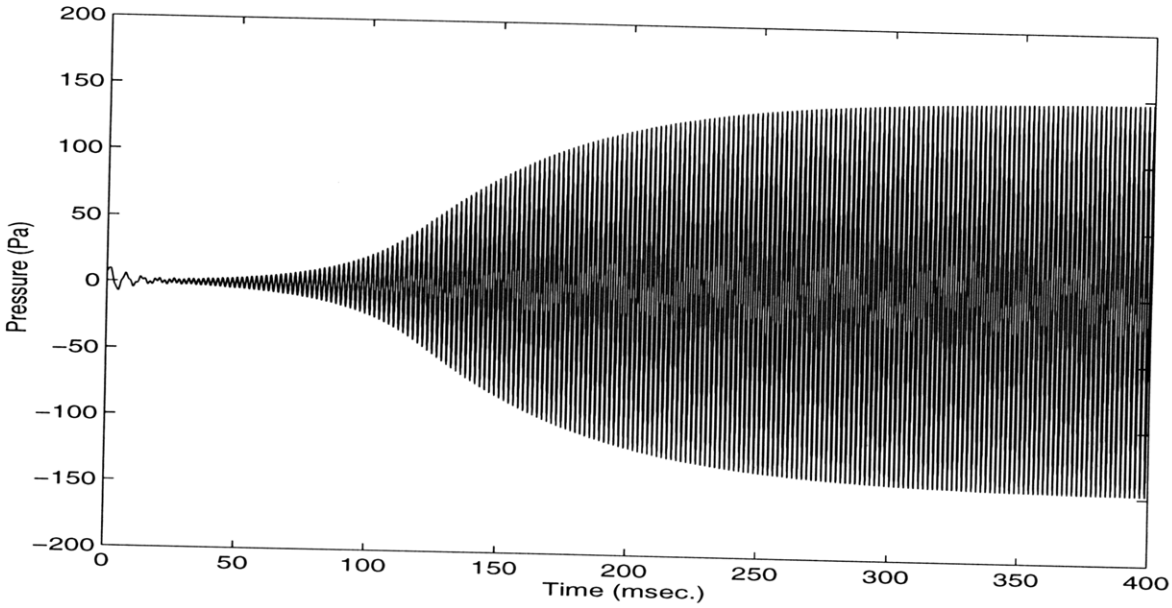

Figure 5-9: Pressure response for the PDE simulation of the system with nonlinear component f_2.

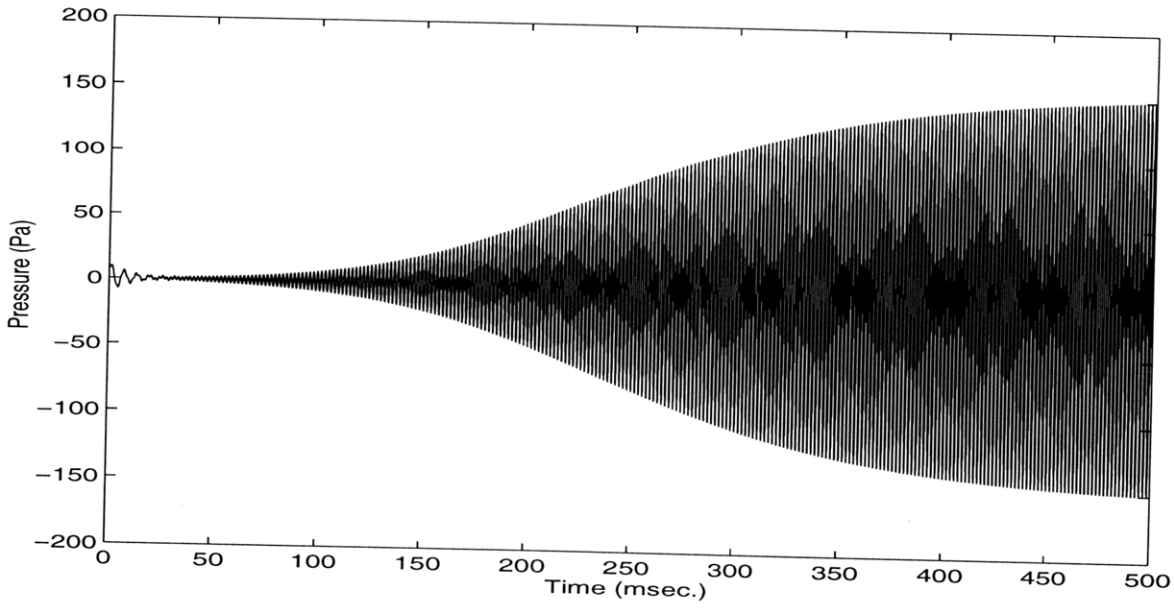

Figure 5-10: Pressure response for the PDE simulation of the system with nonlinear component f_3.

obtain an optimal active controller based on this model to suppress the instability. In Sections 5.1.1 - 5.1.3 a nonlinear model was developed by adding a nonlinear component f to the linear model proposed in [24]. Three different types of nonlinearities in f that correspond to a change in phase, gain, and a combination of phase and gain, were shown to result in limit-cycles. It was also shown in these sections that combustion processes can possess mechanisms that exhibit more than one such nonlinearity. In practice, therefore, the nonlinear phenomenon responsible for the limit-cycle behavior may be uncertain. This implies that if a controller design relies on the structure of f, then the accuracy of the controller and the resulting closed-loop performance can be directly compromised by the lack of fidelity in the model. In such cases, it may be more advantageous to use a linear controller which is designed by entirely neglecting the nonlinearity and using the linear model only.

In Chapter 4 the ability of the linear model-based LQG controller to suppress the thermoacoustic instability was demonstrated. Figure (5-11) shows the thermoacoustic instability growing to the limit-cycle and the LQG controller being turned on at 300 milliseconds for the experiment. The controller suppresses the instability in 23 milliseconds, similar to linear model simulation predictions, despite the nonlinearities.

In addition to the above result, almost all of the experimental results pertaining to active control of thermoacoustic instability reported are essentially based on linear control strategies. That is, the phase added by the controller (whether at a particular frequency or over a large range), does not change with the amplitudes of the system variables. This brings up the question of why such linear strategies are successful and what their limitations are. An answer to this question in the context of the premixed laminar combustors using the nonlinear model will be proposed in this section.

To evaluate the performance of the linear strategies in the presence of nonlinearities in the combustor dynamics, the behavior of such an LQG controller in conjunction with the nonlinear model in (5.1) in a closed-loop is evaluated. Expressing the nonlinear function f as

$$f(u) = u - g(u),$$

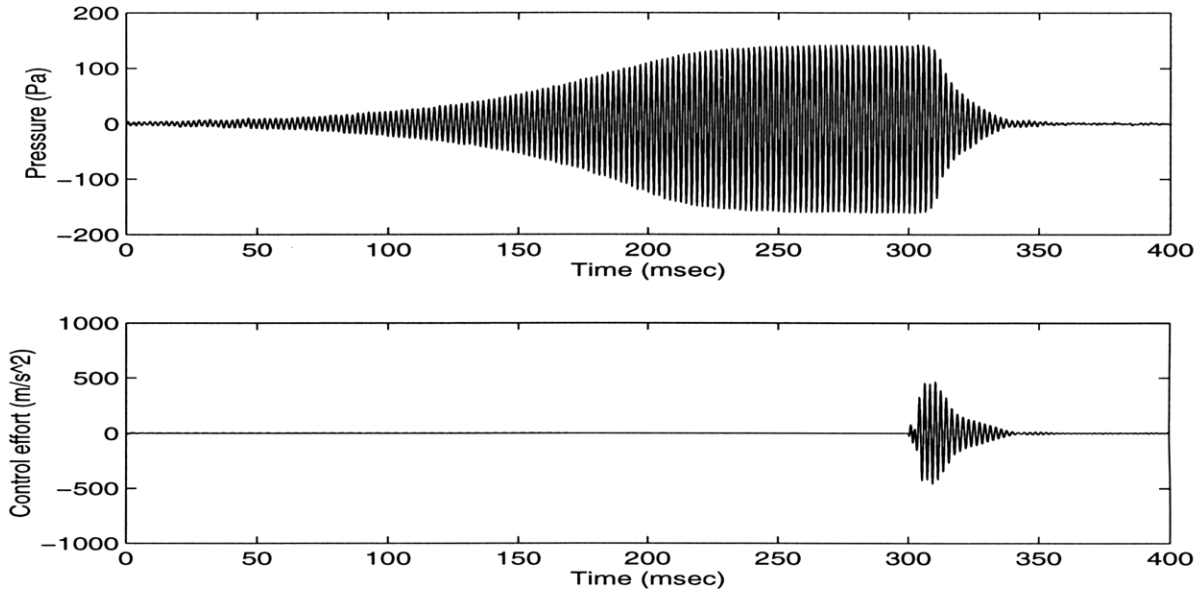

Figure 5-11: Pressure response and control input for a side-mounted loudspeaker with D/D configuration from initial stable operating point to limit-cycle and stabilization by the model-based LQG controller turned on at 300 milliseconds: Experimental results with controller designed using the two-mode model.

setting b_3 to zero (since b_3 is much smaller than the acoustic frequencies for premixed laminar flows), and assuming that the unsteady pressure is a function of the unstable mode only (since the contribution of the unstable mode is significantly more than that of the first acoustic mode), the resulting closed-loop system with two acoustic modes can be described as (see Figure 5-12)

$$\widetilde{u}_f = W_{cl}(s)\left[-g\left(\widetilde{u}'_f\right)\right] \tag{5.13}$$

where

$$W_{cl}(s) = \frac{\sum_{i=0}^{12} n_i s^i}{s^{13} + \sum_{i=0}^{12} d_i s^i} \tag{5.14}$$

$W_{cl}(s)$ represents the stabilized closed-loop system with the linear controller, whereas $g(\cdot)$ represents the deviation in f from linearity.

Under certain conditions on $W_{cl}(s)$ and $g(\cdot)$, it can be shown that the closed-loop system will be stable. The following theorem summarizes these conditions:

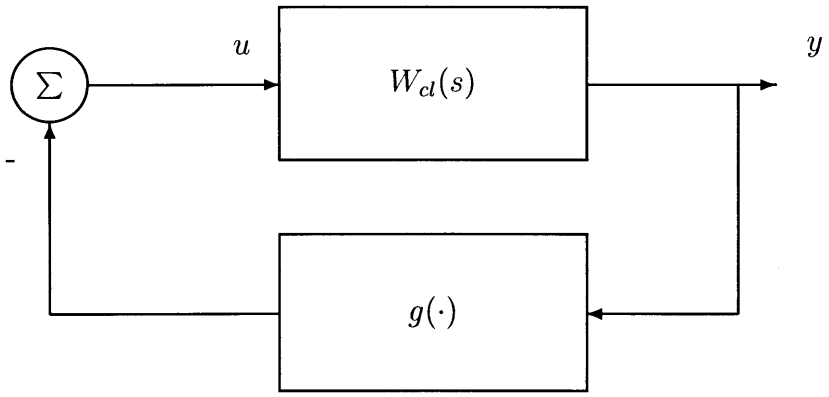

Figure 5-12: Stable nonlinear feedback systems

Theorem 1: If the components in the closed-loop system in Figure 5-12 are such that

$$\begin{array}{lllll} (i) & W_{cl}(s) & & \text{is strictly positive real,} \\ (ii) & g(x)\,x & > 0 & \text{for all x} \neq 0 \\ & g(0) & = 0 & \end{array}$$

Then the closed-loop system is globally asymptotically stable.

Proof: The closed-loop system stability follows in a straightforward manner by showing that $V = x^T P x$ is a Lyapunov function where x is the state vector of the linear system corresponding to $W_{cl}(s)$, i.e.

$$\begin{aligned} \dot{x} &= Ax + bu, \\ y &= c^T x \end{aligned}$$

where $c^T (sI - A)^{-1} b = W_{cl}(s)$ and P is the solution of the equations

$$\begin{aligned} A^T P + PA &= -Q \\ Pb &= c \end{aligned}$$

where Q is a positive-definite symmetric matrix.

When the nonlinear models of thermoacoustic instability together with a linear controller are expressed in the form of (5.13), conditions (i) and (ii) in Theorem 1 are indeed met for the given system for all actuator and sensor locations, which is discussed below. As seen in Eq. (5.14), $W_{cl}(s)$ has a relative degree of 1, with stable poles. W_{cl} was found to be minimum-phase for all actuator and sensor locations as well. The locations of the poles and zeros are shown in Figure 5-13 with the parameters in the model chosen as in (5.3), and the C/D actuator-sensor configuration. The frequency response of $W_{cl}(s)$ (shown in Figure 5-14) is such that the phase is between $-90°$ and $90°$ (or $-450°$ and $-270°$) for all frequencies except 940 rad/sec to 1400 rad/sec. Since near the unstable frequency (3066 rad/sec) the phase is between $-90°$ and $90°$, this implies that condition (i) is satisfied. The frequency response was similar to that shown in Figure 5-14 for all actuator-sensor configurations. It was, in fact, observed that condition (i) holds even when the parameters were perturbed by 20% from their values chosen in (5.3). It is easily shown that for all nonlinearities in f discussed in Section 5.1, the corresponding nonlinear functions g lie in the first and third quadrant, implying that (ii) is also true. Therefore, it follows from Theorem 1 that the closed-loop nonlinear system in (5.13) is asymptotically stable. That is, the nonlinear model in (5.1) can be globally stabilized by the linear controller when $f = f_1$, f_{1b}, f_2, or f_3.

To verify Theorem 1 numerically, the performance of the closed-loop system with the LQG controller and each of the nonlinear models was evaluated through simulations. The result is shown in Figure 5-15 for f_1, showing the similarities between the simulation of the linear controller on the nonlinear model and the experimental results of the same linear controller on the combustor rig. In the simulation, the controller was turned on at 300 milliseconds, and the linear controller is able to suppress the thermoacoustic instability in 30 milliseconds Simulations corresponding to models f_{1b} and f_2 showed similar results as seen in Figures 5-16-5-17, where the controller was turned on at 400 milliseconds, as well as for f_3, where the controller was turned on at 500 milliseconds The controller could be turned on at any time and still successfully

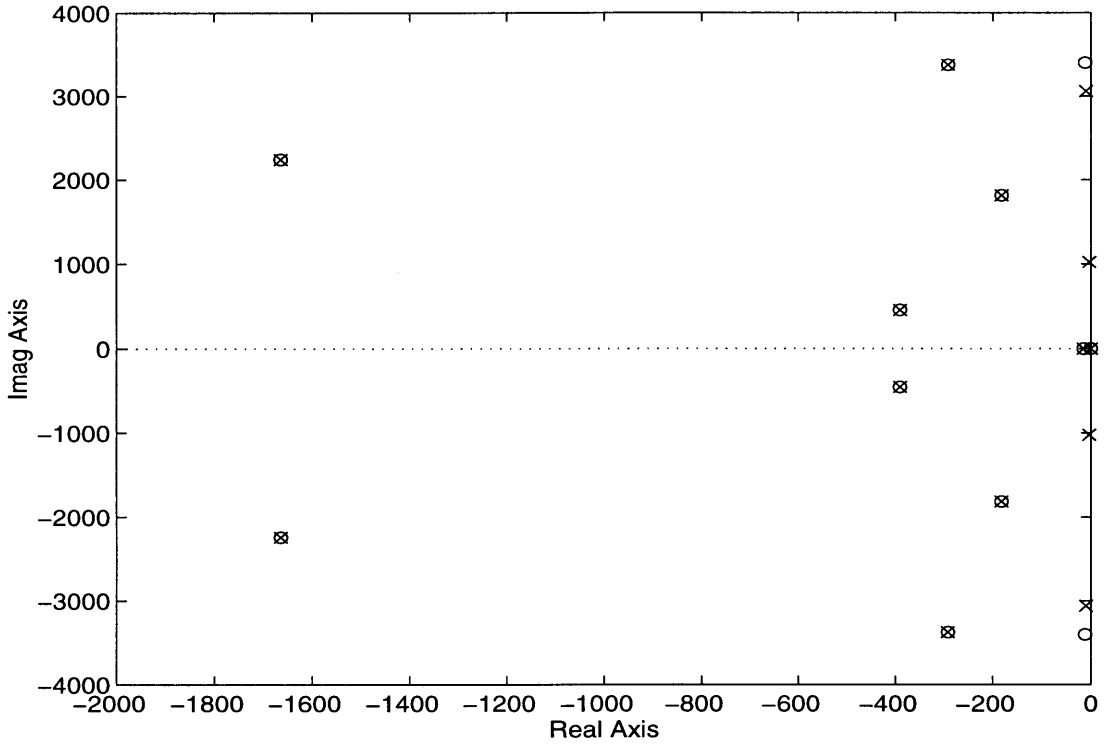

Figure 5-13: Pole and zero locations of $W_{cl}(s)$ with C/D actuator-sensor configuration.

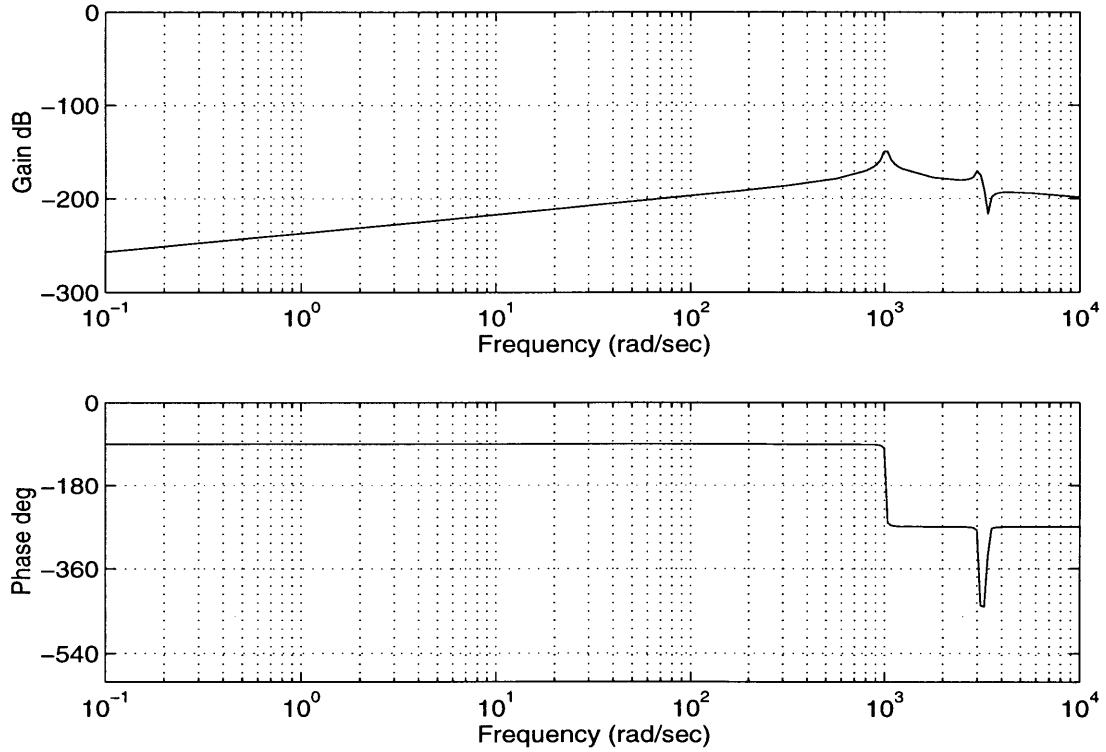

Figure 5-14: Gain and phase characteristics of $W_{cl}(s)$ with C/D actuator-sensor configuration.

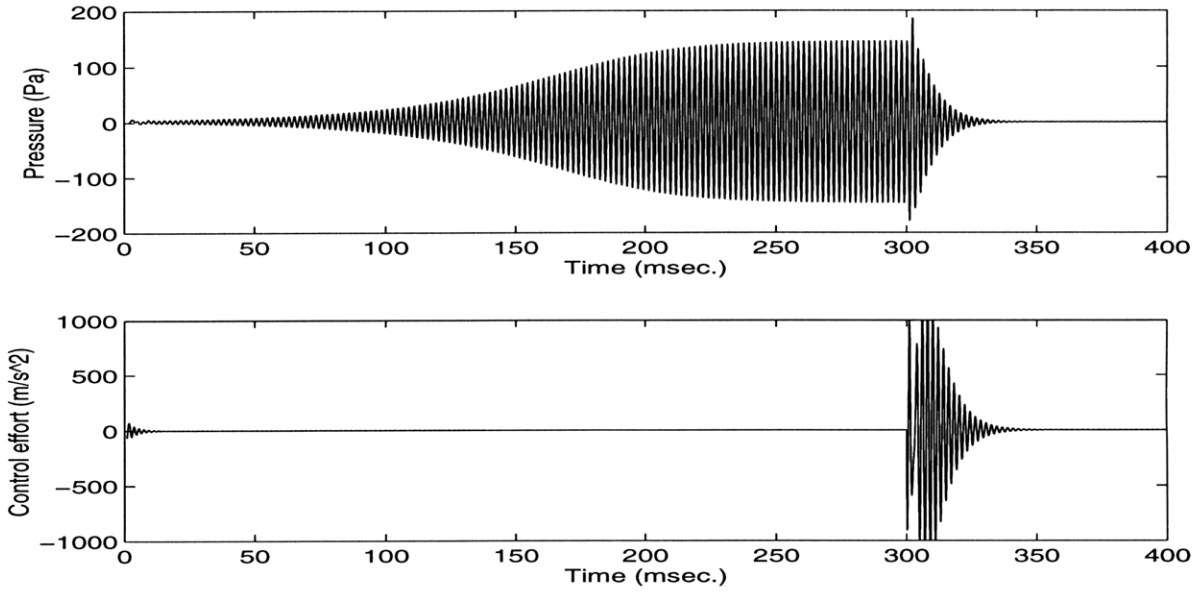

Figure 5-15: Pressure response and control input for a side-mounted loudspeaker with D/D configuration from initial stable operating point to limit-cycle and stabilization by the model-based LQG controller turned on at 300 milliseconds: Simulation results using the two-mode nonlinear model f_1.

suppress the instability. For example, in Models 2 and 3, the controller could be turned on at 250 milliseconds, even though the limit-cycle had not been reached, or at a later time after the limit-cycle was present, and still eliminate the instability. Simulations were also carried out with the PDE of the combustion system and yielded similar results.

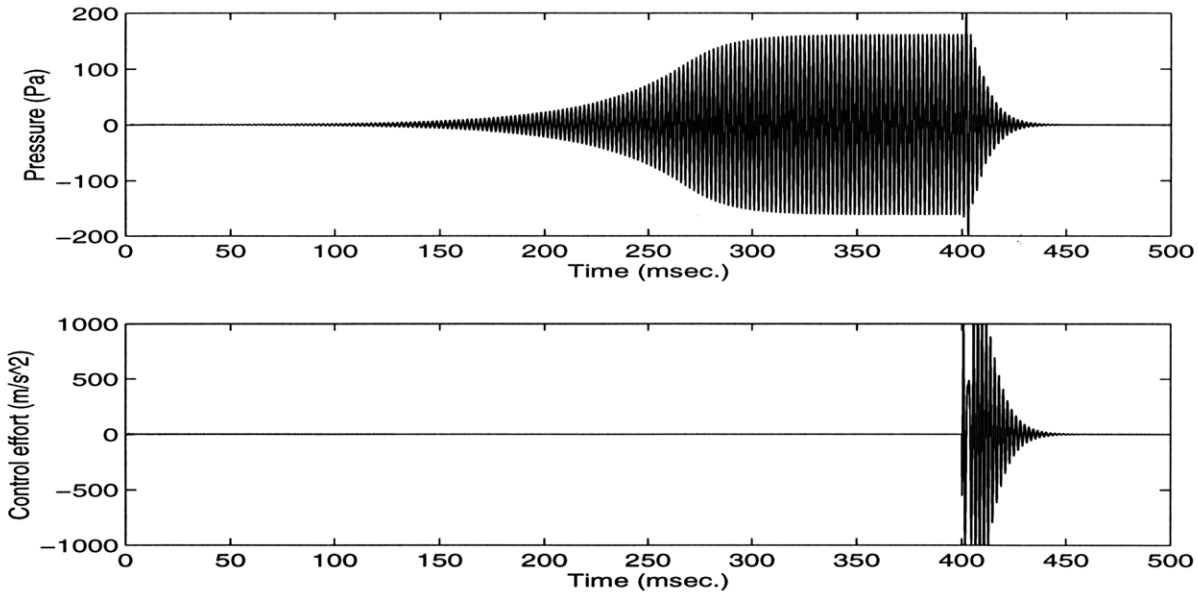

Figure 5-16: Pressure response and control input for a side-mounted loudspeaker with D/D configuration from initial stable operating point to limit-cycle and stabilization by the model-based LQG controller turned on at 400 milliseconds: Simulation results using the two-mode nonlinear model f_{1b}.

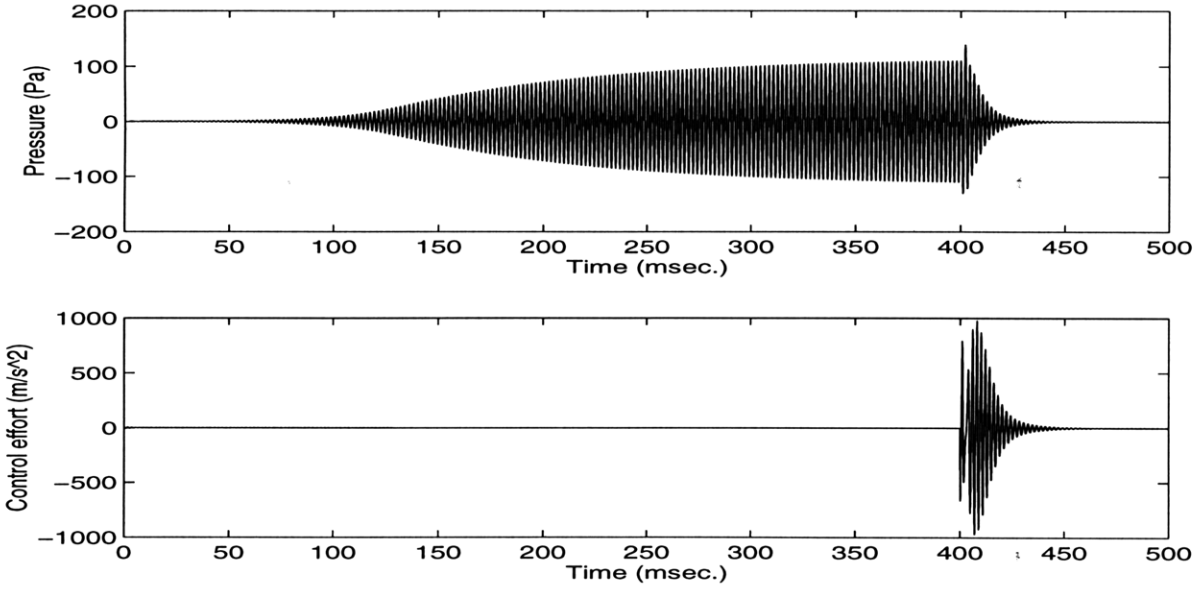

Figure 5-17: Pressure response and control input for a side-mounted loudspeaker with D/D configuration from initial stable operating point to limit-cycle and stabilization by the model-based LQG controller turned on at 400 milliseconds: Simulation results using the two-mode nonlinear model f_2.

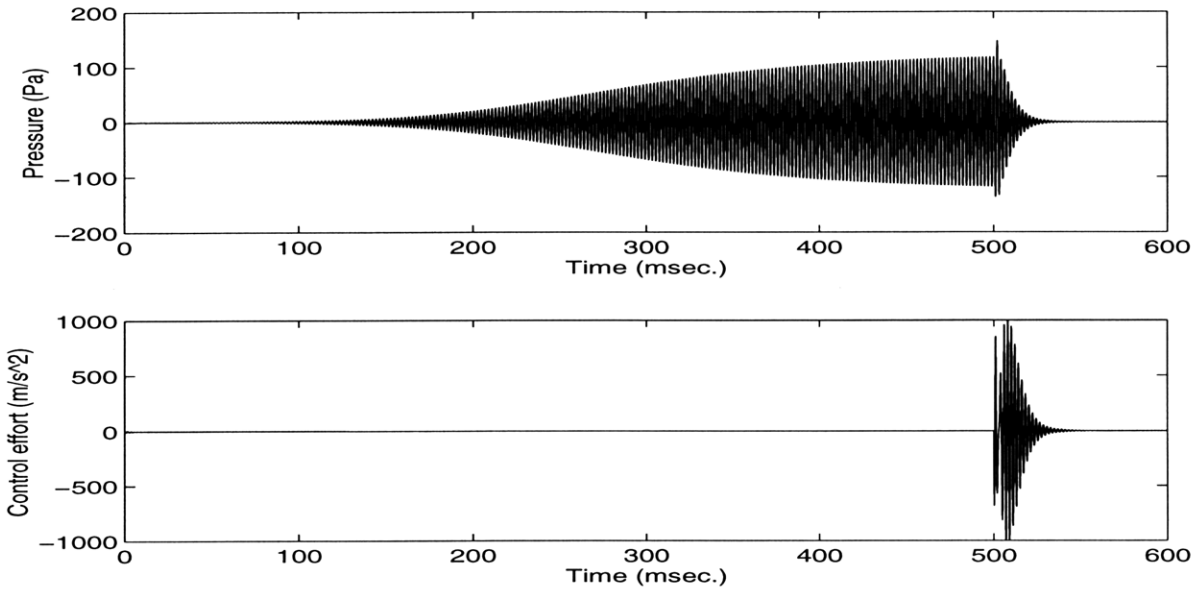

Figure 5-18: Pressure response and control input for a side-mounted loudspeaker with D/D configuration from initial stable operating point to limit-cycle and stabilization by the model-based LQG controller turned on at 400 milliseconds: Simulation results using the two-mode nonlinear model f_3.

Chapter 6

Discussion and Conclusions

Active control of thermoacoustic instability will be a critical part of successful low-emission continuous combustors in the future. A reliable method of control design is needed to ensure that these instabilities can be suppressed over a variety of operating conditions without the excitation of new frequencies and with minimal power from the actuator.

Experimental studies outlined in this thesis illustrate the viability of model-based active control for the elimination of thermoacoustic instabilities. A combustion system model which includes the first two acoustic modes, a first order model of the heat release dynamics, and the actuator and sensor dynamics has been successfully used to develop control strategies which suppress the thermoacoustic instability on a 1 kW bench-top combustor. The unstable frequency and growth rate predicted by the model were both in close agreement with that observed experimentally. An optimal control design, in this case an LQG controller, allows excellent performance to be achieved with minimal control effort. Using the LQG controller, the unsteady pressure can be reduced from 210 Pa to blower noise, a reduction of 44 dB.

Studies of the robustness of the model-based LQG controller to parametric uncertainties and structural variations in the model indicate the degree of accurateness required in the model for the controller to be successful. The LQG was robust to 20% parameter perturbations, as discussed in Chapter 4.4.3. The most critical parameter was the average temperature in the hot section, which can be measured with a fair

degree of accuracy by using a thermocouple to make measurements at a variety of locations in the hot section and averaging them. In cases where this temperature cannot be measured with a reasonable degree of accuracy, an adaptive control strategy may be needed. Structurally, it was found that the inclusion of the unstable acoustic mode and subharmonics as well as acoustic mode coupling were critical to the success of the LQG controller. Neglecting the first acoustic mode in the model of the bench-top combustor rig results in an LQG controller which has a significant deterioration in performance. For certain actuator-sensor configurations and controller parameters, the LQG controller designed based on only the unstable mode results in the excitation of a new frequency in the combustor. The absence of acoustic mode coupling in the model has a similar effect. The LQG controller designed based on the model which neglects this coupling has an increased settling time when tested experimentally. Depending on the actuator-sensor configuration and controller parameters, the LQG controller could result in a system which cannot suppress the unstable frequency. Two factors may contribute to the performance of the LQG controller in the face of modeling errors. These are (1) if the actuator and sensor are collocated or not and (2) how nonminimum phase the uncontrolled combustor zeros are. The robustness improves for a collocated actuator and sensor configuration and as the uncontroller system zeros become less nonminimum phase.

The experimental results reported in this thesis represent the first of its kind where a model-based controller was used for combustion control. Almost all earlier experimental results have adopted an empirical approach where control parameters were determined by trial and error. The results in Chapter 4 demonstrate that the model-based approach is quite effective for a range of equivalence ratios (0.68-0.74) and flow rates (267mL/s-400mL/s), and confirms model predictions. The inability to suppress the instability beyond $\phi = 0.74$ is due to nonlinearities in both the loudspeaker and microphone. By using an actuator and sensor with a larger linear range, the equivalence ratios for which control is successful should easily be extended. Combustor rigs of comparable power densities have been experimentally investigated in [8] and [4]. The results in this thesis illustrate that a significantly faster settling

time of 23 milliseconds can be realized, which is almost a quarter of what was reported in [4]. It is worth noting that the proposed control method does not generate any secondary peaks while that in [8], the controller gave rise to resonances at 240Hz and 550Hz. This perhaps suggests that a model-based approach can be accomplished in a more efficient manner and may lead to faster settling time and reduced controlled effort. It should also be noted that the model-based control design enabled pressure suppression from levels of 210 Pa with a 0.2W loudspeaker, compared to a 10W loudspeaker used in [4] and a 30W loudspeaker used in [8].

A model which will be successful for control design will include enough detail that good controller performance can be achieved, but not so much detail that model development and control design become overly tedious tasks. It is also important that the model and the controller designed based on this model be robust to parametric uncertainties which will invariable exist in the system. The model proposed in this thesis has the ability to meet all of these requirements for a one-dimensional, laminar, premixed combustor. By modifying and refining the model, it can be easily extended to combustion systems with more power, different actuators and sensors or more complex combustion processes.

For the combustion system under consideration, linear controllers were successful in suppressing the instability, despite the nonlinearities in the system. The low-order nonlinear models described in Chapter 5 indicate that simple nonlinear components can be added to the linear model between the velocity and the heat release rate to create the limit-cycle behavior which is observed experimentally. Nonlinearities which corresponded to changes in gain, phase, and a combination of the two were all shown to result in a limit-cycle. For each of the nonlinearities proposed, the resulting system with the inclusion of the LQG controller is asymptotically stable.

The nonlinear models proposed in this thesis have a simple structure (as shown in Figure 5-1) with a single algebraic nonlinearity, which may not be justifiable by actual heat release dynamics. It has been observed in [20], in fact, that multiple dynamic nonlinearities are present in the heat release dynamics leading to a limit-cycle behavior. Suppose one assumes that the nonlinearities are such that the closed-

loop system is of the form of (5.13), then Theorem 1 presents the set of conditions that a combustion process has to satisfy under which a stabilizing linear controller can be found. In practice, these conditions may not be satisfied or may not be easily verifiable. In such cases, a nonlinear controller that can cope with the presence of multiple dynamic nonlinearities may be required. The resulting controller may need to include "smart" elements in that the structure of the nonlinearity may have to be learned and adapted to on-line, which will lead to improved performance over the linear controller for all possible models of the limit-cycle behavior.

All of the results presented in this thesis indicate the clear advantage of utilizing a model-based control strategy for suppressing thermoacoustic instability. The next step in developing this method is to expand the model to represent more complex flow in the combustor. For higher power combustors, an actuator with more capability than a loudspeaker will be needed. Modeling the effect of other actuators, such a fuel injectors, on the combustion system and also developing a dynamic model for the actuator itself will be necessary. The conditions under which the nonlinear dynamics in the system are important in control design must also be studied. Careful expansion of the model and method illustrated in this thesis will lead to the success of model-based control design on commercial combustion systems in the future.

Appendix A

C Code for Implementing LQG Control Experimentally

```
/*****************************************************************/
/*  This program is used to acquire data using das1800 board,    */
/*  and is used to control the thermoacoustic instability in     */
/*  a model combustor.                                           */
/*  - Compile using compact memeory model                        */
/*                                                               */
/*  Edited in 1/12.                                              */
/*  Edited 1/22 - Incorporate LQG Controller                     */
/*  Edited 2/4 - Fixed Problems                                  */
/*  Edited 2/13 - Incorporate multiple Sampling Rates            */
/*  Edited 8/25 - Modified for limited control input, C/D config., */
/*  Edited 2/19/98 - add lh = .09, lc = .06m, Th = 550,          */
/*  rho = .01, mu = .001                                         */
/*                                                               */
/*****************************************************************/

/* C INCLUDE FILES */
```

```
#include <stdio.h>
#include <stdlib.h>
#include <conio.h>
#include <string.h>
#include <math.h>
#include <alloc.h>
#include <process.h>

#include "dasio.h"

#define MAX 7500

/* DEFINE GLOBAL VARIABLES TO BE USED IN ISR */

int points,spoint;   /* NUMBER OF DATA POINTS TO ACQUIRE */
float AD_BitValue;              /* A/D BIT VALUE */
float DA_BitValue;              /* D/A BIT VALUE */
float Samp_Rate;                /* Sampling rate in KHz*/
unsigned cont1, cont2;          /* Variable used for setting clock */
/* Pressure measurement and output to loudspeaker */
float press[MAX], current[MAX];

/* LQG Control Algorithm Variables */
float K1, x1, x2, x3, x4, x5, x6, x7;
float x1_n, x2_n, x3_n, x4_n, x5_n, x6_n, x7_n;
float a11, a12, a13, a14, a15, a16, a17, a21, a22, a23, a24, a25;
float a26, a27, a31, a32, a33, a34, a35, a36, a37, a41, a42, a43;
float a44, a45, a46, a47, a51, a52, a53, a54, a55, a56, a57, a61;
float a62, a63, a64, a65, a66, a67, a71, a72, a73, a74, a75, a76;
float a77, b1, b2, b3, b4, b5, b6, b7;
```

```
float c1, c2, c3, c4, c5, c6, c7, d;

void main (void)
{
COUNTS Counts;

clrscr();
/* Calculate A/D and D/A Bit Values */
AD_BitValue = (float)(10.0/4096);
DA_BitValue = (float)(20.0/4096);

/* Prompt user for desired test conditions */
gotoxy (14,2);
printf("Control of Thermoacoustic Instability\n");
gotoxy (2,4);
printf("Please Enter The Sampling Rate in KHz  -->  ");
scanf("%f", &Samp_Rate);
Counts.byte = long (500/Samp_Rate);
cont1 = Counts.bits.count1;
cont2 = Counts.bits.count2;
gotoxy (2,8);
printf("Enter The Number of Samples to be Taken -->  ");
scanf("%d", &points);
fflush(stdin);
set_time();
set_up_AD();
set_up_DA();
GO();
reset();
```

```
}

void set_up_AD(void)
{
CONT_REG_C_REG cont_reg_c_reg;

outp(AD_STATUS_REG, 0x00);

/* Initialization of QRAM for A/D reading(Ch0 and 1)   */
outp(AD_SELECT_REG,0X01);      /* Set Data Select to QRAM  */
outp(QRAM_ADDR, 0X00);         /* Initialize QRAM for CH0   */
outpw(QRAM_DATA,0X0000);       /* Set the CH0 gain to 1   */
outp(QRAM_ADDR, 0X00);         /* Reinitialize QRAM    */

 /* SET UP A/D CONVERSIONS IN INTERUPT MODE */
     /* SET UP AS BIPOLAR, DIFFERENTIAL, DISABLE BURST MODE */
         /* SET UP AS INTERNAL PACER CLOCK */
cont_reg_c_reg.bits.UB = 0;
cont_reg_c_reg.bits.SD = 0;
cont_reg_c_reg.bits.UQEN = 1;
cont_reg_c_reg.bits.CMEN = 0;
cont_reg_c_reg.bits.BMDE = 0;
cont_reg_c_reg.bits.S0 = 0;
cont_reg_c_reg.bits.S1 = 0;
outp(CONT_REG_C, cont_reg_c_reg.byte);

/* Set Control Register B for interupt when FIFO Not Empty */
outp(CONT_REG_B, 0x40);

outp(CONT_REG_A,0X03);        /* Enable A/D FIFO  */
```

```
  outp(AD_SELECT_REG,0x00);

  outp(AD_STATUS_REG, 0x80);   /* Enable A/D Conversions */

outp(CONT_REG_B, 0xc0);

outp(CONT_REG_A,0X05);
}

void set_up_DA(void)
{
  DA_CONT_C_REG da_cont_c_reg;
DA_SELECT_REGS da_select_regs;

  /* Reset D/A */
  outp(DA_CONT_A, 0x00);

/* Set up operation: Gain of 1, internal Software Clock */
  da_cont_c_reg.bits.GN0 = 1;
  da_cont_c_reg.bits.S1 = 0;
  da_cont_c_reg.bits.S0 = 0;
  outp(DA_CONT_C, da_cont_c_reg.byte);

  /* Enable D/A FIFO */
  outp(DA_CONT_A, 0x01);

  /* Select DAC 0 for output */
  da_select_regs.bits.DSL1 = 0;
  da_select_regs.bits.DSL0 = 0;
```

```
  outp(DA_SELECT_REG, da_select_regs.byte);

    /* Enable D/A Conversions */
  outp(DA_STATUS_REG, 0x80);

/* PRELOAD ZEROS TO CHANNEL 0 */
outp(DA_SELECT_REG, 0x00);      /* CHOOSE DA CHANNEL 0 */
outpw(DA_OUT, 0x0000);          /* LOAD ZEROS */
}


void set_time (void)
{

    /* SET CLOCK FOR DESIRED SAMPLING RATE */

outp(CONT_REG_A, 0x00);
outp(COUNTER_CLR, 0xb4);
outp(COUNTER_2, cont1);
outp(COUNTER_2, cont2);
outp(COUNTER_CLR, 0x74);
outp(COUNTER_1, 0x0a);
outp(COUNTER_1, 0x00);
outp(CONT_REG_A, 0x04);
outp(CONT_REG_B, 0x80);
}


void reset(void)
{
```

```
/* RESET OUTPUT TO 0 */

outpw(DA_OUT, 0x0000);
outp(DA_STATUS_REG, 0x60);
outpw(DA_OUT, 0x0000);
outp(DA_STATUS_REG, 0x60);
outp(AD_STATUS_REG, 0x00);      /* DISABLE A/D CONVERSION */
outp(CONT_REG_A, 0x00);         /* DISABLE A/D FIFO */
outp(DA_STATUS_REG, 0x00);      /* DISABLE D/A CONVERSION */
outp(DA_CONT_A, 0x00);          /* RESET D/A FIFO */
}


 void GO (void)
{
int inp1, outda;
unsigned long i;
float time;
float pres, cur;
char string[20];
FILE *out_file;
AD_STATUS_REGS Ad_status_regs;

/* INITIALIZE CONTROLLER VARIABLES */
K1 = .47;
x1 = 0;
x2 = 0;
x3 = 0;
x4 = 0;
```

```
x5 = 0;
x6 = 0;
x7 = 0;
/* DEPENDENT ON SAMPLING RATE */
if (Samp_Rate == 10) {
a11 = 9.9870e-001;
a12 = 1.4957e+001;
a13 = -6.6134e+003;
a14 = 1.3168e+004;
a15 = -3.8726e+005;
a16 = 3.6471e+003;
a17 = -1.2002e+006;
a21 = 3.4144e-006;
a22 = 1.3296e+000;
a23 = -1.7516e+002;
a24 = 2.1026e+002;
a25 = 2.5116e+004;
a26 = 6.8144e+000;
a27 = 2.8241e+005;
a31 = 8.3046e-009;
a32 = 1.3636e-003;
a33 = 4.9637e-001;
a34 = 4.5497e-001;
a35 = -5.2042e+002;
a36 = 8.9667e-002;
a37 = 1.0828e+003;
a41 = 3.5691e-009;
a42 = 1.7955e-004;
a43 = 5.6625e-003;
a44 = 8.8894e-001;
```

```
a45 = -4.4186e+002;
a46 = 4.8798e-002;
a47 = 4.6997e+002;
a51 = 7.4821e-013;
a52 = 3.1312e-008;
a53 = -6.4371e-006;
a54 = 1.6885e-004;
a55 = 1.0379e+000;
a56 = -4.4281e-006;
a57 = -9.9438e-002;
a61 = 4.9344e-009;
a62 = 1.8677e-004;
a63 = -8.1219e-002;
a64 = 1.0819e-001;
a65 = 3.4780e+002;
a66 = 9.3023e-001;
a67 = -6.9300e+002;
a71 = 2.2379e-013;
a72 = 8.7952e-009;
a73 = -3.7907e-006;
a74 = 4.6095e-006;
a75 = 1.5863e-002;
a76 = 8.4509e-005;
a77 = 7.2210e-001;
b1 = 1.2629e+001;
b2 = -3.0273e+000;
b3 = -8.4162e-003;
b4 = -2.2687e-003;
b5 = 7.5480e-007;
b6 = 3.0989e-003;
```

```
b7 = 2.7590e-006;
c1 = -5.4074e-005;
c2 = -2.2996e+000;
c3 = 9.6775e+002;
c4 = -9.4836e+002;
c5 = 6.5773e+005;
c6 = -2.1398e+002;
c7 = -5.5000e+004;
d = 0;
}

else {
printf("Invalid Sampling Rate.\n");
printf("Hit any key to quit program.\n");
getch();
exit(1);
}


/* SET UP LOOP TO TAKE DESIRED NUMBER OF SAMPLES */
gotoxy (2,12);
printf("To start control press any key     ");
getch();
for (i = 0; i < points; i++) {
outpw(AD_IN,0X0000);                /* Initiate A/D for CH0 */
while(!(inp(AD_STATUS_REG)&0x40) ); /* Wait Till FIFO Not Empty */
inp1 = inpw(AD_IN);

/* CONVERT SIGNAL TO VOLTS AND STORE IN ARRAY */
press[i] = float(inp1) * AD_BitValue;
```

```
x1_n = a11*x1+a12*x2+a13*x3+a14*x4+a15*x5+a16*x6+a17*x7+b1*press[i];
x2_n = a21*x1+a22*x2+a23*x3+a24*x4+a25*x5+a26*x6+a27*x7+b2*press[i];
x3_n = a31*x1+a32*x2+a33*x3+a34*x4+a35*x5+a36*x6+a37*x7+b3*press[i];
x4_n = a41*x1+a42*x2+a43*x3+a44*x4+a45*x5+a46*x6+a47*x7+b4*press[i];
x5_n = a51*x1+a52*x2+a53*x3+a54*x4+a55*x5+a56*x6+a57*x7+b5*press[i];
x6_n = a61*x1+a62*x2+a63*x3+a64*x4+a65*x5+a66*x6+a67*x7+b6*press[i];
x7_n = a71*x1+a72*x2+a73*x3+a74*x4+a75*x5+a76*x6+a77*x7+b7*press[i];

/* CALCULATE OUTPUT TO LOUDSPEAKER */
current[i] = K1*(c1*x1+c2*x2+c3*x3+c4*x4+c5*x5+c6*x6+c7*x7+d*press[i]);
x1 = x1_n;
x2 = x2_n;
x3 = x3_n;
x4 = x4_n;
x5 = x5_n;
x6 = x6_n;
x7 = x7_n;


/* CONVERTS THE DESIRED OUTPUT TO COUNTS */
outda = (int)(current[i] / DA_BitValue);
/* CHECK LIMITS OF  OUTPUT */
if (outda < -2048) {
outda = -2048;
}
else if (outda > 2047) {
outda = 2047;
}
current[i] = outda*DA_BitValue;
outpw(DA_OUT, outda);       /* OUTPUT CURRENT */
```

```
/* Initiate D/A Conversion */
outp(DA_STATUS_REG, 0x60);
while (!(inp(AD_STATUS_REG)&0x04) );
Ad_status_regs.bits.C2TC = 0;
outp(AD_STATUS_REG, Ad_status_regs.byte);

}

gotoxy (2,14);
printf("Do you want to save data (y/n) ?");
if (getch () == 'y') {
gotoxy (2,16);
printf("Enter the file name :  ");
scanf("%s", string);
gotoxy (2,18);
printf("Enter the number of samples to be saved:  ");
scanf("%i", &spoint);
out_file = fopen(string,"w");

for(i = 0; i < spoint; i++)
{
pres = press[i];
cur = current[i];
time = (float (i))/float (Samp_Rate);
fprintf(out_file, "%f  %f  %f\n",time,pres,cur );
}
fclose(out_file);
}
}
```

Appendix B

Matlab Code for Uncontrolled Combustor

```
% Program to simulate 2 mode case of continuous combustion system
% Paramters model experimental system
% Loudspeaker included in model


% Mean flow, mean heat

% Acoustic parameters

gamma = 1.4;                    % Specific heat ratio
Tc=300;                         % Temperature in the cold section
Th=550;                         % Temperature in the hot section
c=sqrt(gamma*287*Tc)            % Speed of sound in cold section
ch=sqrt(gamma*30);              % Speed of sound in hot section
pbar = 1E+05;                   % Static pressure
rho = gamma*pbar/c^2;           % Density
lh = 0.09;                      % Length correction for hot section
lc = 0.06;                      % Length correction for cold section
```

```
L = .47+lh+lc;                    % Total acoustic length
x0 = 0.26+lc;                     % Flame location
Leff = (.47+lh+lc)-(1-c/ch)*(L-x0); % Effective length with mean heat
a0 = (gamma-1)/(gamma*pbar);      % Acoustic constant

% Flame parameters

eps2 = 2;                         % Correction factor for flame radius
theta = 0.5;                      % Correction factor for velocity
phi = 0.74;                       % equivalence ratio
dhr = 50000*1000*phi/(phi+15.6); % Heat of reaction for Propane
su = .3;                          % Laminar burning velocity
D = .053;                         % Diameter of combustion tube
df = eps2*1.5E-03;                % Diameter of flame
nfl = 80;                         % Number of holes in flame holder

% Constants to simplify flame equations

b1 = 4*su/df;
b2 = b1*rho*dhr*nfl*df^2/(D^2);
b3 = b1-theta*a0*b2;

% Mach number - average of cold & hot section mach number

M1 = 4.727E-4;
M2 = 2.497E-4;
Mb = (M1+M2)/2;

% Loudspeaker Parameters
```

```
wl = 1822;                          % Natural frequency
zeta = .1;                          % Damping ratio
b = 2*zeta*wl;
kl = 35.6;                          % Loudspeaker gain
Ksen = 45.3;                        % Sensor gain
kl = kl/Ksen;

ubar = .16404;                      % Average velocity

% Actuator sensor locations

% D/D Configuration
%disp('D/D')
%xs = .062+lc;
%xa = .062+lc;
% C/D Configuration
disp('D/C')
xs = .062+lc+.125;
xa = .062+lc;

Ar = .55;                   % Area ratio between loudspeaker/combustor

% Assumed modes solution - Close-Open Case

k1 = pi/(2*Leff);                   % Wave number for 1st acoustic mode
w1 = c*k1;                          % Frequency of 1st acoustic mode
k2 = 3*pi/(2*Leff);                 % Wave number for 2nd acoustic mode
w2 = c*k2;                          % Frequency of 2nd acoustic mode
E = L*0.5;                          % Energy in the modes
```

```
zetcl = .0033;                    % Passive damping in system

% Flame Feedback
bt1 = gamma*a0/E*cos(k1*x0);
bt2 = gamma*a0/E*cos(k2*x0);
ct1 = (1/gamma)*(-sin(k1*x0)/k1);
ct2 = (1/gamma)*(-sin(k2*x0)/k2);

% Actuators and sensors
bct1 = gamma*Ar/E*cos(k1*xa);
bct2 = gamma*Ar/E*cos(k2*xa);
cct1 = cos(k1*xs);
cct2 = cos(k2*xs);
but1 = gamma*a0/E*ubar*(-k1*sin(k1*x0));
but2 = gamma*a0/E*ubar*(-k2*sin(k2*x0));
cut1 = 1/gamma*ubar*cos(k1*x0);
cut2 = 1/gamma*ubar*cos(k2*x0);
z1 = ((cos(k1*Leff)^2) - (cos(k1*0)^2))/(k1*E);
z2 = ((cos(k2*Leff)^2) - (cos(k2*0)^2))/(k2*E);

% Write out in state-space format
% v## just used to write out each term before combining
% States are: x1 - eta1, x2 - eta2, x3 - eta1dot, x4 - eta2dot,
%             x5 - qfprime, x6 = va (loudspeaker velocity),
%             x7  - y2 where y2 = vadot - Kl*w^2*i
%                      (i is input to loudspeaker)


v11 = -(w1^2 + bt1*b2*cut1);
v12 = -bt1*b2*cut2;
```

```
v13 = bt1*b2*ct1 - Mb*z1*w1 - 2*zetcl*w1;
v14 = bt1*b2*ct2;
v15 = -(but1 + bt1*b3);
v16 = bt1*b2*Ar;
v21 = -bt2*b2*cut1;
v22 = -(w2^2 + bt2*b2*cut2);
v23 = bt2*b2*ct1;
v24 = bt2*b2*ct2 - Mb*z2*w2 - 2*zetcl*w2;
v25 = -(but2 + bt2*b3);
v26 = bt2*b2*Ar;
v31 = -b2*cut1;
v32 = -b2*cut2;
v33 = b2*ct1;
v34 = b2*ct2;
v35 = -b3;
v36 = b2*Ar;

Ap = [ zeros(2,2) eye(2)    zeros(2,1) zeros(2,1) zeros(2,1);
      v11   v12   v13   v14   v15   v16 bct1 ;
      v21   v22   v23   v24   v25   v26 bct2 ;
      v31   v32   v33   v34   v35   v36 0;
      zeros(1,6) 1;
      zeros(1,5) -wl^2 -b];
Bp = [zeros(2,1);
       kl*bct1;
       kl*bct2;
       0;
       kl;
       -kl*b];
```

```
% Output in Pascals (Pressure)
Cp = pbar*[cct1 cct2 zeros(1,5)];
Dp = 0;

% Get rid of unobservable mode (diaphram velocity)
[Apo,Bpo,Cpo,Dpo] = minreal(Ap,Bp,Cp,Dp,.0001);

% Set Initial Conditions
% Unstable mode only

disp('unst. mode only')
fi1 = pi/4;
eta1 = 0;
eta1d = 0;
eta2 = 10*sin(fi1)/(pbar*cos(k2*xs));
eta2d = -10*w2*cos(fi1)/(pbar*cos(k2*xs));
xpo = [eta1 eta2 eta1d eta2d 0 0 0];

eig(Ap)

% Simulate Uncompensated System
tu=[0:.00001:.2];

% Initial Condition Response, Convert output back to Pa
[y,x,tu]=initial(Ap,Bp,Cp,Dp,xpo/5,tu);

figure(1)
plot(tu*1000,y,'b:');
ylabel('Pressure (Pa)')
xlabel('Time (msec)')
```

```
title('I.C. Response of System')

figure(2)
pzmap(Ap,Bp,Cp,Dp)
```

Appendix C

Matlab Code for LQG Control Design

```
% Program to calculate LQG Controller

% Observer design
mu=.001;
Qo=Bpo*Bpo';
Sigma=are(Apo',Cpo'*Cpo/mu,Qo);
H=1/mu*Sigma*Cpo';

% Controller Design
rho=.01;
Qo=Cpo'*Cpo;
P=are(Apo,1/rho*Bpo*Bpo',Qo);
G=1/rho*Bpo'*P;

% Model based compensator
Ac_lqg=Apo-Bpo*G-H*Cpo;
Bc_lqg=H;
Cc_lqg= G;
```

```
Dc_lqg=0;

% Loop
Al_lqg=[Ap Bp*Cc_lqg;
        zeros(length(Ac_lqg),length(Ap)) Ac_lqg];
Bl_lqg=[Bp*Dc_lqg;Bc_lqg];
Cl_lqg=[Cp zeros(1,length(Ac_lqg))];

% Complementary Sensitivity
At_lqg=Al_lqg-Bl_lqg*Cl_lqg;
Bt_lqg=Bl_lqg;
Ct_lqg=Cl_lqg;

% Time response
tstep=0.0017/50;
t_lqg=0:tstep:0.1;                  % Time for simulation
xpo = [0 .0016 0 3.62 0 0 0];       % Initial conditions
Cout_lqg=[Ct_lqg;
          -Dc_lqg*Cp Cc_lqg];

% Initial Condition Response, Convert output back to Pa
[y2,x2,t2] =
initial(At_lqg,Bt_lqg,Cout_lqg,[0;0],[xpo zeros(1,length(Ac_lqg))],t_lqg);
yp_lqg=y2(:,1);



figure(1)
% Plot pressure and control effort versus time
up_lqg=y2(:,2);
```

```
subplot(2,1,1)
plot(t2*1000,yp_lqg,'c:')
xlabel('Time (msec)')
ylabel('Pressure (Pa)')
axis([0 100 -150 150])
title('LQG Controller')

subplot(2,1,2)
plot(t2*1000,up_lqg,'c:')
xlabel('Time (msec)')
ylabel('Control Effort (m/sec^2)')
axis([0 100 -1000 1000])

figure(2)
% Plot poles and zeros of controller
pzmap(Ac_lqg,Bc_lqg,Cc_lqg,Dc_lqg)
```

Bibliography

[1] J.W.S. Rayleigh. *The Theory of Sound*, volume 2. Dover, New York, 1945.

[2] K.R. McManus, T. Poinsot, and S.M. Candel. "A review of active control of combustion instabilities. 1992.

[3] J. Rumsey, M. Fleifil, A.M. Annaswamy, J.P. Hathout, and A.F. Ghoniem. "The role of active control in suppressing thermoacoustic instability". In *Proceedings of the American Control Conference*, Albuquerque, New Mexico, June 1997.

[4] W. Lang, T. Poinsot, and S. Candel. Active control of combustion instability. *Combustion and Flame*, 70:281–289, 1987.

[5] G.J. Bloxsidge, A.P. Dowling, N. Hooper, and P.J. Langhorne. "Active control of an acoustically driven combustion instability". *Journal of Theoretical and Applied Mechanics*, supplement to vol. 6, 1987.

[6] T. Poinsot, F. Bourienne, S. Candel, and E. Esposito. "Suppression of combustion instabilities by active control". *Journal of Propulsion and Power*, 5(1):14–20, 1989.

[7] A. Gulati and R. Mani. "Active control of unsteady combustion-induced oscillations". In *28th Aerospace Sciences Meeting*, pages AIAA–90–0270, Washington, D.C., January 1990. American Institute of Aeronautics and Astronautics.

[8] A. Gulati and R. Mani. Active control of unsteady combustion-induced oscillations. *Journal of Propulsion and Power*, 8(5):1109–1115, 1992.

[9] G. Billoud, M.A. Galland, C. Huynh Huu, and S. Candel. Adaptive active control of combustion instabilities. *Combust. Sci. and Tech.*, 81:257–283, 1992.

[10] K.R. McManus, U. Vandsburger, and C.T. Bowman. "Combustor performance enhancement through direct shear layer excitation". *Combustion and Flame*, 82:75–92, 1990.

[11] M. Fleifil, A.M. Annaswamy, J.P. Hathout, and A.F. Ghoniem. A model-based active control design for thermoacoustic instability. Technical report, Adaptive Control Laboratory, MIT, Cambridge, MA, 1996.

[12] J.E. Tierno and J.C. Doyle. "Multidmode active stabilization of a Rijke tube ". In *DSC-Vol. 38.* ASME Winter Annual Meeting, 1992.

[13] Y.-T. Fung, V. Yang, and A. Sinha. Active control of combustion instabilities with distributed actuators. *Combust. Sci. and Tech.*, 78:217–245, 1991.

[14] Y-T. Fung and V. Yang. Active control of nonlinear pressure oscillations in combustion chambers. *Journal of Propulsion and Power*, Vol. 8, No. 6:1282–1289, 1992.

[15] V. Yang, A. Sinha, and Y.-T. Fung. "State feedback control of longitudinal combustion instabilities". *Journal of Propulsion and Power*, 8, 1992.

[16] A.M. Annaswamy, M. Fleifil, J.P. Hathout, and A.F. Ghoniem. "Impact of linear coupling on the design of active controllers for thermoacoustic instability ". *Combustion Science and Technology*, 128:131–180, December 1997.

[17] M. Fleifil, A.M. Annaswamy, Z. Ghoniem, and A.F. Ghoniem. "Response of a laminar premixed flame to flow oscillations: A kinematic model and thermoacoustic instability result". *Combustion and Flame*, 106:487–510, 1996.

[18] J.P. Hathout, A.M. Annaswamy, M. Fleifil, and A.F. Ghoniem. "A model-based active control design for thermoacoustic instability". In *ASME International Mechanical Engineering Congress and Exposition, (to appear)*, Dallas, Texas, November 1997.

[19] M. Fleifil, A.M. Annaswamy, J.P. Hathout, and A.F. Ghoniem. "The origin of secondary peaks with active control of thermoacoustic instability". *Submitted to Combustion, Science, and Technology*, March 1997.

[20] M. Fleifil, A.F. Ghoniem, and A.M. Annaswamy. A nonlinear model for the unsteady heat release from a class of laminar premixed flames. In *Twenty-seventh International Symposium on Combustion*, Boulder, CO, (submitted), December 1997.

[21] F.E.C. Culick. "Nonlinear behavior of acoustic waves in combustion chambers". *Acta Astronautica*, 3:715–756, 1976.

[22] A.P. Dowling. Nonlinear acoustically-coupled combustion oscillations. In *AIAA Aeroacoustics Conference*, State College, PA, 1996.

[23] A.A. Peracchio and W. Proscia. Nonlinear heat release/acoustic model for thermoacoustic instability in lean premixed combustors. In *ASME Gas Turbine and Aerospace Congress*, Sweden, 1998.

[24] A.M. Annaswamy, M. Fleifil, J. Rumsey, J.P. Hathout, and A.F. Ghoniem. An input-output model of thermoacoustic instability and active control design. Technical Report 9705, Adaptive Control Laboratory, Department of Mechanical Engineering, M.I.T. (submitted to IEEE Control Systems Technology), July 1997.

[25] A.E. Bryson, Jr., and Y.C. Ho. *Applied Optimal Control.* Blaisdell Publishing Company, Waltham, Massachusetts, 1969.

[26] G. Stein and M. Athans. The LQG/LTR procedure for multivariable feedback control design. *IEEE Transactions on Automatic Control*, 32:105–114, February 1987.

[27] Karl J. Astrom and Bjorn Wittenmark. *Computer-Controlled Systems: Theory and Design.* Prentice-Hall, Inc., New Jersey, 1997.

[28] J.-J. E. Slotine and W. Li. *Applied Nonlinear Control.* Prentice Hall, Englewood Cliffs, NJ, 1991.

[29] R.M. Murray, C.A. Jacobson, R. Casas, A.I. Khibnik, C.R. Johnson Jr., R. Bitmead, A.A. Peracchio, and W.M. Proscia. "System identification for limit cycling systems: A case study for combustion instabilities". In *American Control Conference*, Philadelphia, PA, 1998.